© 2013 Nathaniel Adams

COUPLING TOUGH2 AND SEAWAT VARIABLE-DENSITY MODELS TO UNDERSTAND POTENTIAL GEOLOGIC CARBON SEQUESTRATION IMPACTS ON GROUNDWATER RESOURCES

BY

NATHANIEL ADAMS

THESIS

Submitted in partial fulfillment of the requirements
for the degree of Master of Science in Civil Engineering
in the Graduate College of the
University of Illinois at Urbana-Champaign, 2013

Urbana, Illinois

Adviser:

Professor Albert J. Valocchi

ABSTRACT

The Mt. Simon Formation, the basal sandstone reservoir in the Illinois Basin, is the storage reservoir for a geologic carbon sequestration (GCS) project in central Illinois (USA). The Mt. Simon is a highly saline reservoir at the injection location (Macon County), but its salinity decreases to the north, becoming a source of drinking water in Wisconsin. In the current study, an improved understanding of the possible effects of potential future commercial-scale GCS projects in the south on underground drinking water sources in the Illinois Basin is sought by coupling two codes. TOUGH2 is suitable for simulating multiphase and variable density flow problems such as GCS, while SEAWAT is suitable for variable density, groundwater flow problems. Rather than using a single TOUGH2 model, coupling SEAWAT and TOUGH2 lowers the computational cost of modeling this system, allowing the impacts of the GCS project (increasing formation pressure) and groundwater pumping (reducing formation pressure) to be analyzed more efficiently. The use of the SEAWAT model also allows us to incorporate current and projected freshwater pumping data developed for a calibrated MODFLOW model. The migration of native brine and its impact on freshwater drinking sources is investigated by passing pressure and salt concentration data between the models at specific time steps. Results show the method to be successful with pressure impacts of the simulated GCS activity reaching the Chicago, IL region, but rather limited brine migration. Results indicate that no impacts on the Mt. Simon aquifer at the Illinois-Wisconsin border should be expected at the injection rates examined in this work.

ACKNOWLEDGMENTS

I would like to thank Dr. Yu-Feng Lin, Professor Albert Valocchi, and Dr. Edward Mehnert for their guidance, patience, and input throughout this work. I would also like to thank Scott Meyer of the Illinois State Water Survey for providing historic pumping well data and estimates of future pumping rates for the regional MODFLOW model.

I gratefully acknowledge my Graduate Research Assistantship from the Illinois State Geological Survey. This assistantship was funded by the U.S. Environmental Protection Agency, Office of Research and Development, National Center for Environmental Research through US EPA Funding Opportunity EPA-G2008-STAR-H1 (EPA RD-83438201). Barbara Klieforth and Angela D. Page served as Project Officers for the USEPA.

TABLE OF CONTENTS

CHAPTER 1

INTRODUCTION

1.1 Background

Geologic carbon sequestration (GCS) has been identified as a key transitional technology in the mitigation of climate change [1]. GCS involves the injection of supercritical carbon dioxide (CO_2) into geologic formations that have sufficient porosity to sequester large amounts of CO_2 and are, otherwise, generally unusable, such as saline reservoirs and depleted oil reservoirs. These formations must have some mechanism to prevent the movement of CO_2 back to the surface. Main trapping mechanisms include structural trapping, residual trapping, solubility trapping, and mineral trapping [2]. Structural trapping is the trapping of CO_2 in geologic features such as domes. Residual trapping is the trapping of CO_2 in pore spaces due to the wetting characteristics of the CO_2 relative to the resident fluid. Solubility trapping is the dissolution of CO_2 into the resident fluid, which occurs at the interfaces between the two fluids. Mineral trapping occurs when CO_2 reacts with the rock matrix and fluid to produce minerals. Typically, the initial main mechanism is a low permeability caprock that overlies the injection formation and prevents the upward movement of the more buoyant CO_2, with zones of lower permeability rock acting as secondary seals.

One such GCS site is the Illinois Basin Decatur Project (IBDP) located in Decatur, IL, on the property of Archer Daniels Midland (ADM). The site is operated in conjunction with the Midwest Geological Sequestration Consortium (MGSC). At this site, CO_2 from an on-site ethanol plant is injected into the Mt. Simon Formation, a sandstone reservoir covering most of Illinois and extending into parts of Indiana, Kentucky, Wisconsin, and Minnesota. This

formation is overlain by a cap rock called the Eau Claire and underlain by Precambrian bedrock. Apart from the northern extremity of the basin, the Mt. Simon is ubiquitous, ranging in thickness from about 300 feet to over 2,000 feet at its depocenter in Northeastern Illinois [3]. The Mt. Simon Formation slopes upward to the north, becoming a shallow formation that is used as a drinking water source in areas of southern Wisconsin and Minnesota. It has been estimated that the formation has a storage capacity of anywhere from 11 to 150 billion metric tonnes [4]. However, the current federal permit issued by the state of Illinois (Class I) for the site allows for a total injection of 1 million metric tonnes of CO_2. At the time of writing, CO_2 injection had been taking place for nearly two years at an average daily rate of about 870 metric tonnes, with supercritical CO_2 being detected at a monitoring well located about 1,000 ft from the injection well after just under one year.

This injection process results in pressure buildups that may emanate tens of kilometers from the injection wells and have magnitudes in the megapascals range as the native fluids are displaced by the injected CO_2. As this pressure is dissipated throughout the injection formation, the native fluids migrate. This could possibly result in the fluids simply being pushed outward to the other regions of the reservoir or potentially out of the reservoir and into overlying or underlying formations. In the case of the Mt. Simon reservoir, it is underlain by Precambrian bedrock, so there is no concern over migration of some brine into this formation. However, the potential for brine to reach the freshwater sources in the north, the industrial sources in Northeastern Illinois, or to be forced through the caprock into overlying aquifers must be further examined to reduce uncertainties associated with potential future commercial scale injection.

Because there exists the possibility of the contamination of water resources as a result of the brine migration induced by injection in the Mt. Simon, numerical models of the system must be built to give system behavior predictions that can aid decision-makers. As the freshwater sources in southern Wisconsin are located a great distance away from the injection site, a

large domain must be used to simulate the reaction of the groundwater system to injection. Because of the complexity of solving the multi-phase, variable density groundwater flow equations that describe the behavior of such as system, modeling the entire basin using a code designed for this purpose would be computationally intensive. However, because the CO_2 plume is not expected to reach the northern portion of the basin, it is not necessary to solve the more complex multi-phase groundwater flow equations in this area of the domain. Therefore a more efficient kind of model may be used in this region, one that is not capable of solving multi-phase flow in porous media. While analytical solutions such as those presented by Celia [5] could be used to obtain an estimate of the size and shape of the plume and the pressure front, the heterogeneous geology and complex boundary conditions require that a numerical model be used. Additionally, as monitoring data and other data related to the relevant geologic parameters is obtained, numerical models updated with this information should give increasingly accurate predictions of the plume and pressure fronts.

1.2 Scope of Thesis

This thesis applies the previously mentioned approach to modeling GCS in the Mt Simon Formation. In this work, two models are built and coupled to simulate system response to CO_2 injection, with their physical domains having an overlapping region. A TOUGH2 [6] model is created in the southern portion of the Illinois basin to model the CO_2 injection, while a SEAWAT2000 [7] model is adapted from a MODFLOW2000 [8] model covering the northern portion of the basin in order to model induced brine flow in this region. Pressure and concentration data are passed between the two models in the overlapping region in order to simulate the induced pressure front as well as the migration of the resident brine in both the injection formation (Mt. Simon) and the overlying caprock (Eau Claire). A thorough description of the nature of the coupling may be found in Chapter 3. While the geological model used in this work is fairly simple, the work has been done with the anticipation that more spatially varied rock parameters will be incorporated into the model during future

work. It should be noted that this work does not attempt to imitate the setup at the ADM site, but rather lays the groundwork for computationally efficient simulations of GCS in the Mt Simon system with the eventual goal of simulating system response under commercial injection rates.

A script in the object-oriented programming language, Python, is also written to automate the coupling of TOUGH2 and SEAWAT. The results of this work will give decision-makers information that can be used to guide data collection efforts and/or set limits on injection rates into the Mt. Simon. Results will also indicate what modeling efforts should be made to improve the usefulness of and confidence in the modeling results.

1.3 Literature Review

While coupling of hydrologic models is not uncommon, a search of the available literature produces nothing concerning the coupling of SEAWAT and TOUGH2. In fact, only in a select few instances are SEAWAT and TOUGH2 even used to model the same formations. Karsten et al. [9] simulated aquifer responses to perturbations of multiple uses in southeastern Australia. Their modeled formation, the Gippsland Basin, is a sedimentary basin on the Australian coast that is used as a freshwater drinking source onshore and is an oil and gas reservoir offshore. Karsten et al. used SEAWAT for basin-scale simulations of the impacts of various basin uses on the flow of formation water. The pending results will be compared to completed TOUGH2 simulations of the same basin and perturbations. Baidariko and Pozdniakov [10] also used SEAWAT and TOUGH2 to perform comparative simulations of an aquifer. In their case, a waste fluid that is lighter than resident brine was injected into a formation for storage. The lighter brine ascended as it spreads, akin to the behavior of injected supercritical CO_2. They concluded that the results from the comparative simulations are similar enough that SEAWAT can be used to model ascending migration.

There does exist a growing literature concerning the coupling of MODFLOW or SEAWAT with surface hydrology models, typically SWAT. Sophocleous and Perkins [11] use such a combination to model the Lower Republican River basin in northeastern Kansas. A MODFLOW model and a SWAT model are coupled in time by running a SWAT simulation for a certain length of time and passing the time averaged results from into MODFLOW as recharge and evapotranspiration rates. A MODFLOW run is then performed over that same simulation length. Successive runs can be undertaken if the resulting evapotranspiration values differ from the values given by SWAT by more than a specified tolerance, at which point the MODFLOW results would be passed back into SWAT as input for a successive run. Kim et al. [12] take a similar approach in modeling the Musimcheon Basin in Korea, following the lead of Sophocleous. Loops of a SWAT run followed by a MODFLOW run are made on a daily basis, with SWAT results of recharge rates and river stage serving as input data for the subsequent MODFLOW run. The stream gain or stream loss and the evapotranspiration values computed by MODFLOW are used in SWAT's simulation of the next day. Galbiati et al. [13] also couple SWAT and MODFLOW in time to model the Bonello watershed in Italy, but include MT3DMS as well. After each SWAT run, recharge values, including water and solute, are passed into MODFLOW as inputs, while SWAT's stream-flow routing package serves as the basis for MODFLOW's river stage values. A MODFLOW run with these boundary conditions is then performed and the calculated stream-aquifer fluxes are passed back into SWAT to be accounted for in the stream-flow routing calculations. Similar to Galbiati et al., Conan et al. take the SWAT-MODFLOW coupling of Perkins and Sophocleous and expand it to include MT3DMS. SWAT results from each simulation, including stream-aquifer flux, recharge rates, and maximum evaporation rates from shallow groundwater are used as inputs to the corresponding MODFLOW simulation. While the paper does not make clear what input from MODFLOW is used in the subsequent SWAT simulation, it is likely the simulated head distribution.

Although no attempts to couple TOUGH2 and SEAWAT have been found, there is a clear

precedent of temporally coupling MODFLOW with another hydrologic model, providing guidance and examples for linking MODFLOW models with other hydrologic models. All efforts mentioned here have focused on running series of simulations in which results from one model's simulation are taken as some form of boundary conditions in the other model's simulation.

1.4 Organization

Chapter 1 of this thesis has given a background of the problem as well as a brief review of the literature pertaining to linking two hydrologic models, and the thesis' scope. Chapter 2 presents a sensitivity analysis of the MODFLOW model from which the SEAWAT model used in this work is adapted. Chapter 3 gives a brief explanation of the modeling software as well as a more thorough justification for the coupled use of two different models. It also covers the setup of both models as well as the manner in which they are coupled. Chapter 4 gives and discusses the model results. Conclusions drawn from the work are given in Chapter 5 and ideas for continued work are presented. Chapters 6 and 7 contain all figures and tables respectively.

CHAPTER 2

SENSITIVITY ANALYSIS OF MODFLOW MODEL

2.1 Objectives

This Chapter will quantify the relative importance of several different model parameters of a MODFLOW model on the model's head results. This is accomplished through the use of the optimization software PEST. An overview of the software will be given along with a brief description of the mathematics behind the software. The sensitivity analysis runs themselves will then be explained along with a presentation and discussion of the results.

2.2 Pest - Parameter Estimation Software

2.2.1 Overview of PEST

PEST is a model-independent parameter estimation optimizer. While the parameter optimization portion of the software is not used in this work, an essential part of optimization is creating a matrix of sensitivity values for the parameters to be optimized. Because of this, and the fact that PEST has been interfaced with some of the software used in developing the original MODFLOW model (Groundwater Vistas [14]), PEST is used to obtain the sensitivities of the examined parameters in this study.

In an effort to reduce computational time, a parallel version of PEST is run, with four different CPUs utilized. The section describing the setup of the sensitivity run discusses this further.

2.2.2 Mathematics of PEST

Although the main thrust of PEST is optimization, this work does not use this portion of the software, so the mathematics behind it will not be explained here. In fact, the minimum number of optimization iterations that PEST is permitted to perform was set to one for this sensitivity analysis, so as to prevent any time from being spent on optimization.

A parameter's sensitivity value with respect to a certain model output is an indication of how much the value of the output changes for a given change in the value of the parameter. Thus sensitivity values are calculated as derivatives (Equation 2.1).

$$S_j = \left(\frac{\delta y_i'}{\delta b_j} \right) \Big|_b \tag{2.1}$$

In Equation 2.1, S is the sensitivity values, $y_i^{'}$ is the vector of model results, and b_j is the jth parameter, and b is the vector of parameter values at which the derivative is evaluated [15].

Different finite difference methods may be used to calculate these values. PEST gives the user the option to calculate them with a forward difference approximation, a central difference approximation, or a combination of the two. In the last option, PEST will use forward differences until 'the relative reduction in the objective function between optimisation iterations' falls below a user specified tolerance, at which point, PEST switches to using central differences [16]. Because sensitivities are all that are sought in this work, the objective function is not minimized. This still requires changes in the objective function to be evaluated, however, so an objective function (the sum of the squares of the errors between model output and targets) is used, with values of zero input for all targets. For this work, a central difference scheme is used. Three options for calculating sensitivities are given by PEST. The first option is to ignore the interior point and obtain a sensitivity from the slope calculated from

the outside points (Equation 2.2). Here Δb_j is the perturbation in the parameter vector and is specified by the user.

$$\left(\frac{\delta y_i'}{\delta b_j}\right)\Big|_b \approx \frac{y_i'(b+\Delta b) - y_i'(b-\Delta b)}{2\Delta b_j} \tag{2.2}$$

The second option is to use all three points fit a line through them using least squares. The slope of this line would then be the sensitivity. The third option, which is what is used here, has PEST fit a parabola to the three points and evaluate it at the center node to obtain the sensitivity value. In Figure 6.1, the black line is the parabola constructed from the three data points, *i-1* and *i+1* are the outer points and i is the point at which the parabola's derivative is evaluated (shown in green). A two-point derivative approximation is shown in red. While using the parabola method does incur the cost of an extra model run over the first two methods, the method does have a higher accuracy. Given that these runs are performed in parallel however, the improved accuracy is considered here to be worth the extra computational cost.

Of course, these sensitivity values are not the final values output by PEST. The resulting sensitivities, referred to as composite sensitivities, are calculated by Equation 2.3 [16].

$$S_i = \frac{(J^t Q J)_{ii}^{\frac{1}{2}}}{m} \tag{2.3}$$

In Equation 2.3, J is the Jacobian matrix, Q is the cofactor matrix, and m is the number of observations. In this case, the Jacobian matrix is a matrix in which the first row of entries are partial derivatives, one with respect to each node, of the equation describing the head value at the first node. Each subsequent row is the same set of partial derivatives, but of the equation describing the head value at the subsequent node. So, the Jacobian in this case is an n by n matrix, where n is the number of nodes in the model. The cofactor matrix is a diagonal matrix with its entries being the squares of the observation weights.

Relative sensitivities are also calculated and output by PEST. These are obtained by multiplying the composite sensitivities by the magnitudes of their respective parameter values.

These sensitivities, however, are reported as they are input. That is to say, if a parameter is input as the log-transformation of its original value, the composite and relative sensitivities reported by PEST will be the sensitivities of the log of that parameter.

2.2.3 Setup of Sensitivity Runs

Two sensitivity analyses are performed, differing in the targets used as well as the length of the simulation. Each analysis is examined separately. The first run is created using head targets set a long the Illinois-Wisconsin border for all four Mt. Simon layers of the MODFLOW model (Figure 6.2). For the second run, a grid of head targets, covering a more representative area of the model domain is utilized (Figure 6.3). The targets in this second simulation are also placed in all four layers of the Mt. Simon Formation. Simulations 1 and 2 are run for 40 years and 500 years with the observation values taken at 40 years and 500 years respectively.

Six different parameters, as seen in Table 2.1, are included in each of the sensitivity analyses. The four hydraulic conductivity zones mentioned earlier and the two parameters (*rch1* and *rch2*), ratios by which the original constant head values at the southern boundary are multiplied, are considered. The two zones are at the southern boundary of the model - one zone for the constant head boundary values in the Mt. Simon and one for those in the caprock, the Eau Claire. Their values are obtained by multiplying the initial heads at these locations by a factor of 1.5 to place them in a range suggested by preliminary TOUGH2 simulations. So, the values of each of the individual constant head values in zones 1 and 2 are multiplied by *rch1* and *rch2* respectively to obtain the boundary conditions for model runs used to calculate sensitivities.

As each of the observations in the first run is of the same type (head) and there is no reason to believe one to be more important than another, the same weights are applied to each

Table 2.1: Sensitivity Values from Run 1

Parameter	**Sensitivity**	**Relative Sensitivity**
Kx (zone 43)	2.617E-03	1.120E-03
Kx (zone 45)	2.382E-03	1.010E-02
Kx (zone 42)	0.000E+00	0.000E+00
Kx (zone 47)	5.634E-04	3.854E-06
Rch1	0.000E+00	0.000E+00
Rch2	0.000E+00	0.000E+00

observation. As this value is chosen to be one, all targets in the first run will contribute equally to the composite sensitivity value given by PEST. This also means that the cofactor matrix, Q, explained above, will simply be the identity matrix.

As will be seen in the results section of this chapter, not all parameters cause changes in the target values, resulting in sensitivity values of zero. For this reason a second run is conducted, in which a more spatially diverse set of targets (still all head targets) is used. However, they are still considered to have equal importance in determining the sensitivities of the parameters, as in order for brine to reach drinking water sources in Wisconsin and/or Minnesota, the pressure pulse must travel through the entire zone covered by the targets. With their values chosen as one again, the cofactor matrix is the identity matrix.

As mentioned before, PEST is run in parallel to reduce computing time. This is an option provided by PEST, introduced in the 5th Edition of the User's Manual as follows: 'In the course of optimising parameters for a model or of undertaking predictive analysis, PEST runs the model many times. Some model runs are made in order to test a new set of parameters. Others are made with certain parameters temporarily incremented as part of the process of calculating the Jacobian matrix, ie. the matrix of derivatives of observations with respect to parameters (unless derivatives are supplied to PEST directly by the model in accordance with PEST's external derivatives functionality). In calculating the Jacobian matrix, PEST needs to run the model at least as many times as there are adjustable parameters (and

up to twice this number if derivatives for some of the adjustable parameters are calculated using central differences). In most cases by far the bulk of PEST's run time is consumed in running the model. It follows that any time savings that are made in carrying out these model runs will result in dramatic enhancements to overall PEST performance [16].' In this work, two different machines are used, with one hosting the master and two slaves, while the other hosts two slaves. While the master is responsible for making decisions and sending out modified input to the slaves, the slaves are the ones to perform the MODFLOW runs.

2.2.4 Results

Results from the first run, in which targets are located at the Illinois-Wisconsin border are summarized in Table 2.1. These sensitivities result are calculated based on observations after 40 years. Neither of the constant head ratios (*rch1* and *rch2*) had any effect on the values of the head targets. This is also true of the hydraulic conductivity of zone 42 which lies in the Eau Claire Formation.

A mass balance report from a representative model run is summarized in Table 2.2. Head values from each stress period are used to calculate the mass flux in and out of the model. The discrepancy between inflows and outflows is what is tabulated. Lower values indicate more valid model solutions.

Figure 6.4 shows the head contours at the conclusion of a model run using the hydraulic conductivity values given in Table 2.3 and values of 1.0 for *rch1* and *rch2*. The head contours at the southern end of the domain are difficult to see as they are spaced so tightly. They descend from the constant head boundary condition values of approximately 1000 feet to around 730 feet, which is where the contours begin to break off from the cluster. Of course, this is a contrived situation as such a sharp pressure front would not develop as a result of GCS, but it serves to illustrate the relative impact of certain parameters on model output.

Table 2.2: Mass Balance Summary for Representative Run (Run 1)

Stress Period	**Cumulative Mass Balance Percent Discrepancy**
1	1.35
2	0.88
3	0.83
4	0.92
5	0.90
6	0.85
7	0.84
8	0.84

This figure is taken from the top layer of the Mt. Simon, but the contours in the rest of the Mt. Simon are similar.

Table 2.3: Hydraulic Conductivity Values

Zone	**Kx=Ky (ft/d)**	**Kz (ft/d)**
43	4.28E-01	2.85E-03
45	4.22E+01	2.83E-02
42	6.84E-03	6.84E-06
47	7.19E-01	1.44E-02

Results from the second run, in which the model domain is more regularly covered with head targets are summarized in Table 2.4. The greater simulation length allows *rch2* and hydraulic conductivity zone 42 to have an effect on the model results. *Rch1*, however, still exhibits no effect on the model output.

A mass balance report from a representative model run is summarized in Table 2.5. This report is of the same nature as that of 2.2.

Figure 6.5 shows the head contours after 500 years of simulation. The contours are marginally different from the contours in Figure 6.4.

Table 2.4: Sensitivity Values from Run 2

Parameter	**Sensitivity**	**Relative Sensitivity**
Kx (zone 43)	2.416E-02	1.034E-02
Kx (zone 45)	3.623E-03	1.536E-02
Kx (zone 42)	1.625E-16	1.112E-18
Kx (zone 47)	3.546E-04	2.550E-04
Rch1	0.000E+00	0.000E+00
Rch2	3.573E-04	3.573E-04

Table 2.5: Mass Balance Summary for Representative Run (Run 2)

Stress Period	**Cumulative Mass Balance Percent Discrepancy**
1	1.58
2	1.03
3	0.99
4	1.09
5	1.07
6	0.98
7	0.95
8	0.95

2.2.5 Discussion

Results from the first run reveal a very limited amount of information. As can be seen from the sensitivity values given in Table 2.1, three parameters, including both constant head multipliers and a hydraulic conductivity zone, have no effect on the observation values. That a change in constant head values has no effect on the observation values indicates that forty years is not sufficient for the pressure pulse effect to have a far reaching effect on the domain. In fact, an unreported run, that has a simulation time of 500 years, also shows these parameters to be insensitive. For the first reported run, the model gives reasonable results upon inspection of the head contours and the mass balance values are low.

While the constant head multipliers explain nothing, the hydraulic conductivities from the first run can be compared to show their relative importance in prediction of the system heads as a response to a pressure pulse at the southern end of the boundary domain. As

seen in Table 2.1, zones 43 and 45 are several orders of magnitude more sensitive than zone 47. Given the location of the observations, this makes sense. All observations come from the Mt. Simon Formation, where zones 45 and 43 are located. Zone 47 lies directly over the majority of the observations , while zone 42 covers only the very eastern portion of the domain which lies a significant distance from any pumping included in the model (partially as a result of lying beneath Lake Michigan).

Comparing the sensitivities of zones 43 and 45 is a bit more difficult. Which parameter is more sensitive depends on whether the composite sensitivity values are reported or the relative sensitivity values are reported. Of course, the difference between their sensitivity values is small regardless. It is worth noting that the composite sensitivities here are reported in terms of the log of the parameters in question. So, because the hydraulic conductivity of zone 45 is a full order of magnitude larger than that of zone 43, it is varied over a greater range of values. However, any further comparison would require knowledge of the accuracy to which each hydraulic conductivity value can be trusted. Assuming that each is accurate to within an order of magnitude, the composite sensitivity values are legitimate and the observations will experience greater changes per a fractional change in the value of zone 45 than of zone 43.

Results from the second reported run tell a bit more about the system in the long term. As this run has a length of 500 years, the pressure front from the elevated constant heads at the southern end of the boundary reach further into the domain. However, it is clear from Figures 6.4 and 6.5 that the head distribution throughout the domain changes little over the course of 450 years. Of course, these runs were performed before an updated storativity value was obtained for the system, so these results do not necessarily indicate that there will be no effect on the heads in the northern portion of the Illinois Basin as a result of GCS. Placing observations closer to the southern boundary allows the sensitivity values of one of the constant head multipliers to become non-zero, indicating that the head distribution does indeed change. The values of the hydraulic conductivities relative to one another change

very little in this second run, with zone 45 still exhibiting slightly more influence on the head distribution than zone 43. The composite sensitivity of zone 45 decreases in relation to zone 43, but this is to be expected as the majority of the observation locations for this run lie within zone 43. Zone 42 also registers having an impact on the observations, but of at least twelve orders of magnitude lower than any other parameters. Again, zone 47 has a sensitivity value of at least an order of magnitude smaller than zones 43 and 45. It has a much lower permeability value than the other Eau Claire zones (42), perhaps allowing it to produce a sharper pressure interface between it and the underlying Mt. Simon, and thus exert more influence on the head distribution than zone 42.

CHAPTER 3

MODEL DESCRIPTION

3.1 Geology

Because of its geologic properties, the Illinois Basin lends itself well to GCS. As mentioned, the geology of concern to GCS projects in the Illinois Basin are the basal sandstone, the Mt. Simon, and an overlying formation, the Eau Claire. Underlying the Mt. Simon is Precambrian bedrock. The extent of the basin is quite large, with the majority of Illinois and Indiana covered as well as portions of Kentucky, Wisconsin and Minnesota. The thickness of the Mt. Simon reservoir throughout the basin can be seen in Figure 6.6. Such lateral coverage means an increased storage capacity and helps to absorb any pressure buildup as a result of carbon injection into the Mt. Simon. As both the Mt. Simon and the Eau Claire Formations dip upward to the north, they become hydraulically connected to surface water features at the basin's northern extremity while becoming increasingly deeper and eventually absent in southern Illinois.

As the Mt. Simon is a saline basin with great spatial variation in its total dissolved solids (TDS) values, its use is also quite varied (Figure 6.7). It should be noted here that Figure 6.7 is not the TDS map used in this work. An improved TDS map of the Mt. Simon is used, but as it is still in press, it cannot be reproduced here. In the southern portion of the Illinois Basin, the reservoir is rarely utilized because of its very high TDS values. Where TDS values are lower (more northern areas of the basin), the Mt. Simon becomes more useful. In northeastern Illinois, the native fluids of the Mt. Simon are used for industrial purposes. The reservoir is even used as an underground source of drinking water (USDW) in areas

of southern Wisconsin and Minnesota [17]. Other uses of the Mt. Simon include natural gas storage facilities. Illinois and Indiana account for 71% of the saline aquifer natural gas storage capacity in the United States, with at least ten storage sites being located in the Mt. Simon [18]. A map of their locations is given in Figure 6.8.

The Mt. Simon is a fine to coarse-grained sandstone generally composed of quartz and small amounts of potassium feldspar and is considered by geochemists at the Illinois State Geological Survey (ISGS) to be fairly unreactive with CO_2. The Eau Claire, being a confining formation, has permeability values orders of magnitude lower than that of the Mt. Simon. For specific values used in simulations, see the 'TOUGH2 Model' and 'SEAWAT Model' sections of this chapter. The formation consists of several different lithologies, including fine to medium-grained sandstone, shale, dolomite, and siltstone. Although the composition varies somewhat from state to state, the formation is continuous across them. Core from the IDBP project shows the Eau Claire to contain potassium feldspar, Fe-illite, and illite-smectite clays with some glauconitic siltstone [19]. Laboratory scale tests of CO_2 and brine with this Eau Claire core by Yoksoulian et al., 2013 show dissolution of Ca, MG, Si, and K from the Eau Claire into the brine. Results also indicate that the Eau Claire becomes more friable as it is exposed to a mixture CO_2 and brine [19].

Hydrogeologic parameters of the Mt. Simon and Eau Claire Formations also make the Illinois Basin a good option for GCS. The Mt. Simon sandstone can conceptually be divided into three layers. The upper two layers were deposited by a braided river system and contain both fluvial and eolian deposits. The deepest layer was deposited under marine settings. In the area surrounding the IBDP, the lower Mt. Simon is a very clean sand, with little cement. Correspondingly, this deepest layer has significantly higher porosity and permeability values than the upper layers. This, of course, is conducive to the sequestration of the more buoyant CO_2. As the CO_2 will tend to migrate upward upon injection, zones of lower permeability overlying zones of higher permeability will increase the lateral spread of CO_2. While the

main seal for any GCS project in the Mt. Simon would be the Eau Claire Formation, there do exist in the Mt. Simon lenses of lower permeability clays that would serve to delay upward movement of and increase secondary trapping of injected CO_2. Porosity estimates vary from approximately 10% at the top of the Mt. Simon (and lower in clay zones) to over 25% near the bottom of the reservoir. The spatial variation of the porosity values are not well known, contributing to the large storage range estimate of 11 to 150 billion metric tons quoted earlier. Much of the core data obtained in the Mt. Simon comes from natural gas storage sites which are strategically placed at structural domes and, as a result, may provide biased values.

3.2 TOUGH2

Overview of Software

TOUGH2, the second version of a simulator developed at the Lawrence Berkeley National Laboratory in the 1980s, is used in this work to simulate the injection of supercritical carbon dioxide into a saline reservoir. TOUGH2 can simulate three dimensional, multi-phase, variable density flow and contaminant transport in porous media using an Integral Finite Difference Method [6]. The equation of state (EOS) implemented with TOUGH2 in this work is the ECO2n EOS. ECO2n is a fluid property module that describes the properties of mixtures of CO_2, NaCl, and H_2O, making it suitable for modeling GCS in saline reservoirs [20].

TOUGH2 Model

The final TOUGH2 model used in this work is composed of eight layers and 66,904 elements. Four of these layers make up the Mt. Simon, while the Eau Claire accounts for three more. The last layer represents the Ironton-Galesville, a Cambrian sandstone. This sandstone is a productive aquifer composed of fine to medium grade sands, but is simply used as a Dirich-

let boundary condition in this model. This decision was based on the anticipation that the underlying low permeability Eau Claire Formation would prevent the upward migration of brine. As this is an assumption, model output must be checked to verify the validity of the assumption. Should no increased brine movement through the Eau Claire caprock be found, this assumption will be taken to be valid. However, if significant increased brine migration occurs through the Eau Claire, a new boundary condition should be used in the next version of the model. Underlying the Mt. Simon is Precambrian bedrock. As this is a very impermeable rock, a no-flow boundary condition is used underneath the model. No-flow boundary conditions are also utilized at the eastern, western, and southern boundaries of the model. These boundaries are located at great physical distances from the simulated injection location and thus, are not expected to experience pressure changes due to activity at the wells. The last boundary, in the north, is another Dirichlet boundary condition. This is chosen because of the manner in which the TOUGH2 model is coupled with the SEAWAT model. Although the pressure values at the northern Dirichlet boundary interface changes from stress period to stress period, within each stress period, the values are held constant. A thorough explanation of the manner in which the two models are coupled is given in a section of this chapter entitled 'Coupling.'

In this work, locations were chosen for potential future GCS sites within the Mt. Simon reservoir. These locations were chosen based on the depth of the Mt. Simon, its thickness, and the absence of other uses (these locations are not actual future injection well locations). Thicker portions of the Mt. Simon were chosen based on an isopach map obtained from the ISGS (personal communication, Hannes Leetaru, February 2013). In the thicker portions of the Mt. Simon, the bottom layer, which has the highest porosity and permeability values in the reservoir, is present and is thicker, allowing for a thicker injection zone. As drilling to such depths is quite costly, a location that minimizes depth, while avoiding natural gas storage facilities is also desired. Thus, a location approximately 50 km to the north of the IBDP was chosen to place potential future commercial scale projects. The resulting well

locations can be seen in Figure 6.9. Well placement also comes into play when considering the geography of the model domains and the proximity of the interface of the TOUGH2 and SEAWAT models to the injections wells. As SEAWAT cannot simulate multi-phase flow (for a description of SEAWAT, see the 'SEAWAT' section of this chapter), it is necessary to place the interface far enough from the wells that no supercritical CO_2 enters the SEAWAT domain. However, as one of the purposes of developing this methodology is to examine the pressure front propagation in the domain of a sequentially coupled SEAWAT model, it is necessary to place the interface close enough to the wells that pressure changes resulting from the potential GCS projects are observed in the SEAWAT domain. To that end, simple radial simulations of GCS injection are performed and a range of locations identified based on the distance between the edge of the CO_2 plume and the location of appreciable pressure buildup in the reservoir.

Initial conditions for the TOUGH2 model are developed through several different sources of data at the ISGS. The initial head values in the domain are a result of creating a TOUGH2 run with the pressure values at the northern Dirichlet interface mentioned above equal to the pressures taken from the SEAWAT nodes at this interface. All other boundaries for this TOUGH2 run were set to no-flow boundaries. The resulting pressure distribution was taken to be at steady state as model output indicated nearly no change in pressure values toward the end of the run (approximately 1000 years). The pressures in the Ironton-Galesville sandstone were then converted to Dirichlet values under the previously stated assumption that the Eau Claire confining Formation would prevent upward migration of brine. Initial salt concentration in the Mt. Simon was taken from a ISGS TDS map of the reservoir [21]. A second map, taken from an Illinois State Water Survey (ISWS) publication was used to create the salt concentration initial conditions in the Ironton-Galesville [22]. As little data is available on the spatial distribution of salt concentration data in the Eau Claire, a linear distribution of the salt concentration between the Mt. Simon and Ironton-Galesville sandstones was assumed. Initial temperatures for the model were calculated using

the geothermal gradient in Equation 3.1.

$$T = 55.0 + \frac{depth}{100ft} \tag{3.1}$$

This is a general equation for formation temperature in Fahrenheit in Illinois.

Rock parameter data used in the TOUGH2 domain is an upscaling of the parameters used in Zhou, 2010 [23]. Consistent with the description above, four different sets of parameters were used for the Mt. Simon, one for each layer, with each layer being homogeneous. The Eau Claire caprock is also homogeneous with distinct values from those of any of the Mt. Simon layers. Although data is available from a variety of locations within the basin and has been collected by the ISGS, there is not unanimity in the interpretation of the data and so, it was not used in this work.

Tables 3.1 through 3.3 give the rock parameter data used in the TOUGH2 domain for each layer of the Mt. Simon as well as for the Eau Claire. As was discussed in the geology subsection of the present section, the porosity and permeability values (both horizontal and vertical) of the lowermost two Mt. Simon layers (composing the bottom layer of the previously discussed conceptual division) are higher than their counterparts in overlying layers of the same hydrogeologic formation. The values for these parameters are lowest in the Eau Claire. Values for other relevant rock properties, including rock grain density, heat conductivity, rock grain specific heat, and pore compressibility are also given in Table 3.1. Van Genuchten parameters for the relative permeability function are given in Table 3.2 and the Van Genuchten parameters for the capillary pressure function are given in Table 3.3. The Van Genuchten functions can be found in Van Genuchten, 1980 [24]. All values are in standard SI units.

Table 3.1: Rock Parameter Values for TOUGH2

	Eau Claire	**Mt. Simon Layer 1**	**Mt. Simon Layer 2**	**Mt. Simon Layer 3**	**Mt. Simon Layer 4**
Rock Grain Density (kg/m^3)	2600.0	2600.0	2600.0	2600.0	2600.0
Porosity	0.176	0.100	0.112	0.176	0.176
Horizontal Permeability (m^2)	2.57E-20	1.01E-14	1.25E-15	3.86E-14	3.86E-14
Vertical Permeability (m^2)	1.00E-20	2.85E-15	3.06E-16	1.97E-15	1.97E-15
Heat Conductivity ($W/m^\circ C$)	2.51	2.51	2.51	2.51	2.51
Rock Grain Specific Heat ($J/kg^\circ C$)	920.0	920.0	920.0	920.0	920.0
Pore Compressibility (Pa^{-1})	7.42E-10	3.71E-10	3.71E-10	3.71E-10	3.71E-10

Table 3.2: Van Genuchten Parameters - Relative Permeability Function

	Eau Claire	**Mt. Simon Layer 1**	**Mt. Simon Layer 2**	**Mt. Simon Layer 3**	**Mt. Simon Layer 4**
h	0.412	0.412	0.412	0.412	0.412
$\mathbf{S_{lr}}$	0.40	0.30	0.00	0.00	0.00
$\mathbf{S_{ls}}$	1.00	1.00	1.00	1.00	1.00
$\mathbf{S_{gr}}$	0.30	0.25	0.25	0.25	0.25

Table 3.3: Van Genuchten Parameters - Capillary Pressure Function

	Eau Claire	**Mt. Simon Layer 1**	**Mt. Simon Layer 2**	**Mt. Simon Layer 3**	**Mt. Simon Layer 4**
h	0.412	0.412	0.412	0.412	0.412
$\mathbf{S_{lr}}$	0.03	0.03	0.03	0.03	0.03
$\mathbf{1/P_0}$	2.00E-07	5.00E-05	1.50E-04	1.30E-04	1.30E-04
$\mathbf{P_{max}}$	1.00E+09	5.00E+05	5.00E+05	5.00E+05	5.00E+05
$\mathbf{S_{ls}}$	0.999	0.999	0.999	0.999	0.999

3.3 SEAWAT

Overview of Software

For this work, SEAWAT2000 was used to simulate flow in the northern portion of the Illinois Basin deep system. SEAWAT2000, groundwater modeling software produced by the United States Geological Survey (USGS), is a three dimensional finite difference code that can simulate variable density flow and solute transport in porous media [8]. The code is a coupling of two previously distributed USGS codes, MODFLOW2000, which simulates constant density groundwater flow, and MT3DMS, which simulates the transport of multiple solutes, in this case, based on MODFLOW's solution of the flow field. In SEAWAT, the governing equations from MODFLOW are derived again, but account for variable density by putting them in terms of fluid mass and retaining all the density terms that were dropped in the original MODFLOW derivation. The program also assumes a single liquid phase with a small compressibility, isothermal conditions, and complete water saturation of the porous media [7].

SEAWAT Model

The SEAWAT model in this work is a modified version of a MODFLOW model documented in Meyer et al. 2009 [25]. This original model was composed of 20 layers and included both aquitards and aquifers from the Precambrian bedrock to land surface. Hydrogeologic parameters were taken from literature and are documented in Meyer et al. 2009 [25]. Horizontal and vertical hydraulic conductivity values for all layers can be seen in Figures 6.10, 6.11, and 6.12 through 6.22. The final SEAWAT model contains the deep system of the original model, but also has initial salt concentration values input in the model. As the concentration gradients are rather shallow (Figure 6.33) and the advection is relatively small (this can be seen in Chapter 4), it is expected that grid refinement, while desirable, will not change

model results significantly. Dispersion values are set to zero as the size of the cells of the numerical grid will cause numerical dispersion. Densities in the model vary solely with salt concentration.

The division of layers in the SEAWAT model is the same as that of the TOUGH2 model described earlier, so as to provide continuity between the two models. There are, again, eight layers, with the bottom four being four divisions of the Mt. Simon and the three layers above the Mt. Simon composing the Eau Claire Formation. The final, top layer (the Ironton-Galesville) is taken to be a Dirichlet boundary condition as the assumption that the Eau Claire will prevent any upward migration of brine due to GCS pressure build up is made. As in the TOUGH2 model, this assumption will need to be checked and validated with the results. The same method of comparing brine exchange between the overlying Ironton-Galesville sandstone and the Eau Claire Formation before and during GCS activity will be used to assess the validity of the assumption.

Again, the model is underlain by Precambrian bedrock, so a no-flow boundary underneath the model is appropriate. No-flow boundaries are also used along the eastern, western, and northern boundaries of the model. The southern boundary of the model is the taken to be another Dirichlet boundary condition as this is the region in which the SEAWAT model is linked to the TOUGH2 model. As discussed previously, within a stress period the head values at this boundary will be kept constant, but the values will change from stress period to stress period. The coupling procedure will be explained in the section of this chapter titled 'Coupling.'

The initial heads for this model were obtained by starting with pre-development conditions in the basin and running a transient simulation from these conditions (1864), using historic pumping record data, up to the year 2010. The pumping data contains daily volume extraction/injection rates for wells located throughout both the state of Illinois and the state

of Wisconsin in the Mt. Simon sandstone, Eau Claire Formation, and Ironton-Galesville Formation (personal communication, Scott Meyer, ISWS, June 2012). For the GCS simulations, projected pumping rates were estimated by Scott Meyer based on county by county water withdrawal predictions taken from Dziegielewski et al. [26]. This data is a prediction of future pumping rates at the previously mentioned wells with a rate given for each well for a block of five years, beginning in 2010 and ending in 2050. For simulation times beyond 2050, pumping rates are assumed to remain at their 2050 rates as projection beyond this date is beyond the scope of this work.

As in the TOUGH2 domain, salt concentration come from the ISGS TDS map of the Mt. Simon [21]. Values in the Ironton-Galesville were taken from the same map used for the TOUGH2 model and values in the Eau Claire were again assumed to vary linearly between the Mt. Simon and the Ironton-Galesville sandstones [22]. All cells located north of the TDS data were assumed to contain fresh water in keeping with the gradient in the basin and the fact that Wisconsin uses the Mt. Simon as a USDW. The effects of temperature were not considered in the SEAWAT model.

3.4 Coupling

When it is said in this work that a TOUGH2 model and a SEAWAT model are coupled, it is meant that they are linked sequentially. The physical domains of the two models must overlap at some border for the two to be linked. For this work, an overlapping region of three rows of cells or nodes were used (Figure 6.23), but other numbers of rows or columns would also work. However, because of how the coupling is done, there must be at least two rows or columns, otherwise, the head and concentration data will always be part of a constant boundary condition and will be unable to change.

All input files for both models must be prepared separately by the user for the first 'stress period' or period of time in which all external stresses on the system are constant. Additionally, the user must create files containing data for all external stresses (pumping/injection wells, recharge, river levels, etc.), one for each stress type and one for the stress period information. In SEAWAT, targets must be placed at the locations of the head and concentration output values needed for boundary value input into TOUGH2 runs. A script written in the Python object-oriented programming language manages model output, converts output to input (explained below), and initiates model runs.

The following is an explanation of the linking process (Numbers in parentheses correspond to those in Figure 6.24, which is a flowchart of the procedure). Grid and boundary node information is read to create boundary node dictionaries before beginning the main loop of the program (1). A TOUGH2 directory is created for the next stress period (2). The TOUGH2 model is run first (3), for a stress period, using the user supplied initial conditions with Dirichlet boundary conditions at the previously mentioned locations. Pressure and salt mass fraction values from the TOUGH2 results are then read from the output files (4). The values at an interior row of TOUGH2 nodes in the overlapping region corresponding to the boundary of the SEAWAT model are saved and converted to head and salt concentration values (5) using the method outlined in Haas, 1976 [27] (Figure 6.25). However, it should be noted that in keeping with the source code for TOUGH2, Equation 10 of Haas, 1976 has been modified slightly. In place of the v_0 in the numerator of the squared term, v_c is used. Equations 7 through 11 from Haas are reproduced here as Equations 3.2 through 3.6. These equations are used in TOUGH2 to obtain the density of the vapor-saturated brine, which is then adjusted for the effects of pressure using another method not detailed here.

$$d = \frac{1000 + xW_2}{1000v_0 + x\phi} \tag{3.2}$$

$$\phi = \phi_* + kx^{0.5} \tag{3.3}$$

$$\phi_* = c_0 + c_1 v_0 + c_2 v_0^2 \tag{3.4}$$

$$k = (c_3 + c_4 v_0)[v_0/(v_c - v_0)]^2 \tag{3.5}$$

$$v_0 = \frac{v_c + c_5\theta^{1/3} + c_6\theta + c_7\theta^4}{1.0 + c_8\theta^{1/3} + c_9\theta} \tag{3.6}$$

where x is the molality of the brine, 'd is the density, W_2 is the molecular weight of sodium chloride, v_0 is the specific volume of H_2O at the critical point, ϕ is the molal volume of NaCl in the solution, and ϕ_* is the limiting apparent molal volume of NaCl as the liquid goes to 0' [27]. The constants in Equations 3.2 to 3.6, along with the equation for θ, are given below.

$$c_0 = -167.219$$

$$c_1 = 448.55$$

$$c_2 = -261.07$$

$$c_3 = -13.644$$

$$c_4 = 13.97$$

$$v_c = 3.1975$$

$$c_5 = -0.315154$$

$$c_6 = -1.203374 \times 10^{-3}$$

$$c_7 = 7.48908 \times 10^{-13}$$

$$c_8 = 0.1342489$$

$$c_9 = -3.946263 \times 10^{-3}$$

$$\theta = 647.27 - T_x$$

where T_x is the temperature (°C) of the brine.

These resulting concentration and head values calculated in this manner are then used to rewrite the appropriate input files (sink and source mixing package and constant head package) for the SEAWAT run of the same stress period (5). All SEAWAT output data files (if

applicable) are moved into a new directory so as not to be overwritten by the next SEAWAT run (6) and all other SEAWAT input files are updated with the user supplied data (7). The SEAWAT run is then launched and the script waits for termination (8). SEAWAT output is then read by running the Groundwater Vistas utility targpest (9). The targets must be in a predetermined order (explained in the pseudocode in the appendix) for the script to work properly. If the final stress period has been run, the SEAWAT head and concentration output is then read by the script (10) and converted back to pressure and salt mass fraction data (11) using the same set of equations as was used to convert TOUGH2 output to SEAWAT boundary condition values. These pressure and salt mass fraction values are then used to rewrite the initial condition file for TOUGH2 (INCON) and data from the user supplied stress period file is used to rewrite the input file (12). This process is continued until all stress periods defined in the stress period file have been run.

CHAPTER 4

RESULTS AND DISCUSSION

4.1 Pressure Pulse

Pressure results obtained from a simulation of continuous injection of CO_2 over 300 years are largely as expected. Figures 6.26 through 6.38 give the initial conditions in each of the models. There is no plot for initial temperature in the SEAWAT model as the model does not include temperature. Figures 6.39 through 6.46 give the change in pressure in the TOUGH2 model between the initial conditions and certain points throughout the simulation. Individual pressure footprints for each of the three wells after 5 years of continuous injection can clearly be seen in Figure 6.39. These footprints grow in both size and magnitude over the next 5 years, but still remain distinct (Figure 6.40). After 20 years of injection however, well interference can be seen (Figure 6.41). Figure 6.42 shows that the easternmost well has the largest footprint, with the largest maximum pressure increase. This stems from the fact that all three wells are injecting at the same rate (150 kg/s), but the thicknesses of the injection intervals at each of the three locations are different. The westernmost well is injecting over an interval of about 188 meters, the center well over 166 meters, and the easternmost well over 118 meters. This results in an increase in both the size and magnitude of the pressure footprint as one moves eastward. It can also be seen that after 50 years of injection the pressure pulse has begun to move into the overlapping region that links the two models. For reference, Figure 6.47 shows the area of the TOUGH2 model that makes up the overlapping region. This pulse is seen to continue growing through the last few plots with pressure changes on the order of megapascals being seen after the full 300 years have been completed (Figure 6.46). Although the simulation was run for over 300 years, the results

past this point have not been evaluated as the no-flow boundary condition in the southern portion of the domain is no longer valid. Pressure increases near the border can be seen, indicating that fluid flow would be induced here and that, as a result, a different boundary condition is required for simulations extending beyond 300 years.

Figures 6.48 through 6.51 show the pressure changes at the top of the Mt. Simon reservoir at certain times throughout the simulation. Plots at early times clearly show distinct footprints from each of the three wells. As in the bottom of the Mt. Simon, these footprints begin to overlap later (Figure 6.50) and show an increase in both size and magnitude in the more eastern wells. All of these results are as expected since none of the relatively thin, lower permeability zones are built into the vertical distribution of the model. Inclusion of these zones would certainly reduce the impact of GCS on pressures higher up in the Mt. Simon. This is important to remember when looking at the impacts on pressure at the top of the Eau Claire (Figures 6.52 through 6.54). Although early times show no change in fluid pressure in this layer, model results do predict some increase in pressures, albeit at much smaller magnitudes than anywhere else in the model. The baffle effect on rising CO_2 produced by the inclusion of lower permeability lenses in the Mt. Simon would reduce, if not eliminate this result altogether.

Another assumption made in the methodology of this work is that the separate supercritical phase would not move from the TOUGH2 domain into the SEAWAT domain. As expected, the supercritical plumes in these simulations remained far from the SEAWAT domain. In fact, over the 300 years of simulated injection, the three plumes grew, but remained separate (Figures 6.55 to 6.57). The plumes also migrated very little in the upward direction, with none of the plumes reaching the top of the Mt. Simon in the first 100 years (Figure 6.58). Even after 300 years of simulation, the plume from the westernmost well never reached the top of the Mt. Simon, with the other two plumes only reaching the top of the reservoir in the immediate vicinities of their respective wells (Figure 6.59). This is a result of the lower

permeability of the middle Mt. Simon which encourages lateral spreading of the CO_2 plume over vertical spreading. Finally, no CO_2 was seen at the top of the Eau Claire after the full 300 simulated years (Figure 6.60). Again, this is as expected, but given that the model represented the caprock to have perfect integrity, efforts should be made in the future to include more detailed and updated data concerning the geological conceptual model and the hydrogeologic properties of the Eau Claire that could be constructed from wire-line logs and limited core from throughout the state of Illinois.

Moving into the SEAWAT domain, simulated head distributions from early times through 300 years are seen in Figures 6.61 through 6.68. Early simulated results show some change in heads as a result of regional groundwater flow and extensive pumping throughout the model, but especially in northeastern Illinois. The effects of the simulated GCS are not seen in these early times (Figures 6.61 through 6.63). Consistent with the results presented from the TOUGH2 domain, the pressure pulse, which is a combination of all three of the wells' footprints 50 years in to the simulation, can be seen in the SEAWAT domain starting in Figure 6.64. Here, the head contour lines begin to turn south, becoming more perpendicular to the southern border. This becomes more pronounced at 100 years (Figures 6.65) and after 150 years, the pressure pulse can be clearly seen in the south-central portion of the domain. It continues to move into the SEAWAT domain in the latter stages of the simulation, but its migration is arrested west of the southern tip of Lake Michigan (Figures 6.67 and 6.68). This behavior seems unnatural at first as there is no discontinuity in hydraulic conductivity in this area of the model. However, looking at the location of pumping wells that are open to the Mt. Simon (Figure 6.69) provides some explanation. There is a contour line in later plots of the bottom of Mt. Simon that begins to flatten and form a straight line East to West. It can be seen that this contour line coincides with the location of the southernmost of the pumping wells in this region. The development of this feature begins at these wells (Figure 6.67), but migrates north over the next 100 years to its location at the end of the simulation (Figure 6.68). Furthermore, examination of mass exchange through the tops of several different

model layers reveals that recharge from above decreases with time. As seen in Figure 6.72, recharge from above the Eau Claire Formation provides water to the model, but this mass flux decreases with time. As pumping after year 40 remains constant and there is a steady decrease in net mass flux through the top of the Eau Claire (Figure 6.72), this pumped fluid must be accounted for by some other means. While some fluid is lost from storage, brine migration through the southern boundary supplies most of this water. Consistent with the timing of the appearance of the pressure pulse in the SEAWAT domain, the sharp downturn in net mass flux through the top of the bottom layer of the Mt. Simon occurs at 50 years. As the only non-constant mass fluxes in and out of this layer are the recharge from above and the Dirichlet boundary condition to the south, any mass not coming out of storage must be accounted for from one of these sources. As mass lost from storage over the last 5 years of the simulation (year 295 to year 300) only amounts to about 73,500 lbm, the difference in the net mass flux through the top of the bottom layer between the early and late five year periods of the simulation, which is on the order of 100,000 lbm, must be accounted for by influx from the Dirichlet boundary condition. The net influx from this boundary condition into the bottom layer is indeed on the order of 100,000 lbm. More specifically, a net mass flux in the vertical direction of the bottom layer of the Mt. Simon is analyzed in the region in question (Figure 6.70). As can be seen in Figure 6.71, the direction of brine movement in this layer reverses from downward at the start of the simulation to upward shortly after the pressure pulse enters the region. So, the GCS induced brine migration feeds the pumping wells in this area, but is not sufficiently large to exceed their demand and propagate all the way to the Illinois-Wisconsin border.

The pressure pulse can also be seen at the top of the Mt. Simon as it moves into the SEAWAT domain. Figures 6.73 through 6.80 show the development of the pulse, with it first becoming apparent after 50 years of simulation. As expected, the pulse is not as strong as it is at the bottom of the formation, where injection occurs. And just as is seen at the bottom of the Mt. Simon, the development of the pulse stops rather abruptly in northeastern Illinois

upon encountering some of the southernmost wells.

As seen in Figures 6.81 to 6.88, heads in the SEAWAT domain remain largely unchanged throughout the 300 years of simulation. Some small pressure increases are seen in the southern portion of the domain, but they are limited to the overlapping region linking the SEAWAT and TOUGH2 models. While injection rates chosen for the simulation are much larger than those of any current project in the Illinois Basin, it should be remembered that the location of potential future injection wells and their injection rates may not coincide with those chosen here. Future modeling efforts would be required to analyze their effects, but a possible methodology for doing so has been presented here.

In all model layers, head contours at the Illinois-Wisconsin border remained unchanged. All of Wisconsin then, is unaffected by the potential GCS projects simulated in this work. Some changes in head contours in northeastern Illinois (very southern portion of the Chicago area) can be seen throughout the Mt. Simon, but they are minimal. Any changes in the salt concentrations here will be discussed in the following section.

4.2 Salt Concentrations

Results concerning salt concentrations are relatively uninteresting in both model domains. Although pressure buildup propagates many miles from the injection wells, the mass flux of the induced brine flow does little to affect the brine distribution. Salt mass fractions after 5 years of injection in the TOUGH2 domain are seen in Figure 6.89. This can be compared to the previously presented initial mass fraction distribution (Figure 6.32). Little to no difference can be seen between the two. Of course, this is not unexpected due to the short time period being examined. When comparing these plots to the calculated salt mass fraction after 300 years, however, there is still very little change in the values. Figure 6.90

shows the results at this later time. Small changes do exist near the wells, but their extent is smaller than that of the pressure pulse and their magnitude less than 2% of the original values. Changes in salt mass fraction do extend into the overlapping region, but again, their magnitude is minimal.

In the SEAWAT domain, the initial salt concentration plots (Figures 6.33 to 6.35) can be compared to plots of the concentration distributions after 5 years of injection in Figures 6.91, 6.94, and 6.97. Again, little to no change can be seen between the two sets of plots. This is expected at early time periods as no GCS induced brine migration has occurred in the domain. Later times are shown in Figures 6.92, 6.95, 6.98 (200 years) and 6.93, 6.96, and 6.99 (300 years). Although there is minimal change in the southern portion of the domain, most of the domain experiences no change whatsoever. The very small changes in values in the overlapping region of the domain are consistent with the results from the TOUGH2 domain. Small changes may also be seen in the Chicago region where concentration values approach zero. This can be attributed to a mix of intensive pumping in the region and brine migration as the concentration changes begin before the pressure pulse reaches the area. And given that the areas through which the pressure pulse passes prior to reaching the Chicago area experience little to no change in salt concentrations, it is likely that pumping is a stronger drive of concentration changes in the Chicago area.

As one objective of this work is to examine the impacts of the potential future GCS projects on USDWs, specifically in southern Wisconsin and Minnesota, results at the IL-WI border should also be examined. At no point throughout the simulations are the pressure or concentration values along this line altered. Although only one injection scenario was evaluated, pumping wells in northeastern Illinois appear to absorb the pressure pulse, indicating that a much larger pressure pulse would be required before GCS activity in the Mt. Simon in central Illinois would affect resources in Wisconsin or Minnesota.

CHAPTER 5

CONCLUSIONS AND FUTURE WORK

5.1 Conclusions

A method to couple two hydrologic models on the basin scale to examine the environmental impacts of geologic carbon sequestration (GCS) activities on water resources was developed in this work. The method utilizes an existing, regional MODFLOW model by converting it to a SEAWAT model so as to take advantage of previous modeling and calibration efforts as well as the model's inclusion of pumping well data. A reduction in computation time was also achieved by modeling only the area near the three simulated injection wells with a TOUGH2-PC (for personal computer) model and linking it with the less computationally costly regional SEAWAT model to create a coupled model of the Illinois Basin. This method will allow for future analysis of proposed GCS projects in which underground sources of drinking water may be affected. The method is simple to use and the only additional software required (Python) is available at no cost.

As shown in Chapter 4, the method is successful in linking the two models. Plots show the pressure pulse forming at the injection wells and migrating from the TOUGH2 domain in the south into the SEAWAT domain in the north. While the changes in salt mass fractions (TOUGH2) and salt concentrations (SEAWAT) were very small, the method did capture these as well. So, future modeling efforts examining larger and/or varying injection rates, more complex geology, different temperature distributions, and/or different time scales may be conducted using this method.

Model results show the pressure pulse to be stronger in the eastern portion of the model. This is due to the geometry of the formation at the locations chosen for the injection wells. The thickness of the Mt. Simon sandstone injection zones decreases to the east, while the injection rate (150 kg/s) remains constant, resulting in a larger maximum pressure change at the well as well as a farther reaching pressure pulse.

The migration of the pressure pulse slows and the pulse 'flattens' as it moves into the region of pumping wells in northeastern Illinois. This, combined with the observation that the vertical direction of flow in the bottom layer of this same area reverses from downward to upward over the course of the simulation and that the recharge from above the Eau Claire, the caprock, declines throughout the simulation, indicates that the pressure pulse supplies brine to the overlying layers, reducing the induced recharge from above the Eau Claire. It is also expected that the pressure pulses of future simulations with larger injection rates would be at least partially absorbed by the same region of pumping wells.

One of the main motivations for this work was to examine the impact of GCS projects on freshwater resources in southern Wisconsin and Minnesota. As discussed, these simulations indicate no effects will be experienced in the aquifer at the Illinois-Wisconsin border, neither in the heads nor the salt concentrations within the 300 simulated years. So, at the simulated injection rates, water resources in the north are expected to remain unaffected by GCS activity. While no change in salt concentrations was seen at the Illinois-Wisconsin border, very little change was seen in any area of the domain. This is a result of the relatively small mass of brine migration compared to the overall storage of the reservoir. Changes in the hydrogeologic parameter set used could potentially result in increased pressure changes as more permeable material allows for pressure to propagate more easily. However, given the effects that the well field south of Chicago had on the pressure pulse in this work, it is expected that changes in hydrogeologic parameters, within reasonable limits, would not change the overall conclusion that the modeled level of GCS activities will not affect water

resources at the Illinois-Wisconsin border.

Model results also indicated that the Dirichlet boundary condition chosen to overlay the model was valid. Minimal pressure increases were seen in the top active layer (immediately below the boundary layer) and even these small increases will decrease as more vertical discretization and lower permeability lenses are introduced into the model. However, good modeling practice should still be followed. Should a thinner section of the Mt. Simon where these lower permeability lenses are not seen be chosen for a future GCS project, a different boundary condition on the top of the model may be necessary.

5.2 Future Work

As it has been shown that the methodology laid out here has worked, future work should focus on developing the individual models, specifically the TOUGH2 model. However, certain aspects of the methodology laid out below should be tested to examine their impacts on overall model results.

As was discussed earlier, at least two overlapping rows of nodes are necessary for the two models to be successfully linked. As three rows were used in this work, other numbers should be tested to examine the impact that the size of the overlapping region has on model results. A related aspect of the methodology is the length of the stress periods used. As TOUGH2 model results show that several stress periods are required for the pressure pulse to move through the overlapping region, it is not expected that model results will change with shorter stress periods. If stress periods are lengthened, head values near the boundaries may be kept artificially low. However, this would also reduce the total number of stress periods required to complete the simulation. Simulations using larger stress periods should be tested to examine if shorter run times can be achieved without affecting model output.

As shown in Chapter 3, the TOUGH2 model used in this work is rather simplistic. A variety of factors have been left out, including faults, spatial variability of porosity and permeability within each layer, better vertical discretization of the geology, and inclusion of thinner layers of lower permeability zones in the Mt. Simon that act as baffles inhibiting upward migration of CO_2.

As better porosity and permeability data sets could be developed from a variety of data that is available from locations throughout the state of Illinois, much of it from natural gas storage sites, and such hydrogeologic parameters control large scale processes such as the development of a pressure pulse, efforts should be made in the future to incorporate this data into new versions of the model. Monitoring data is also available from the Illinois Basin Decatur Project, offering insight into local rock properties and the local geological conceptual model. However, because there is not unanimity in the interpretation of either set of data, future modeling efforts would require analysis of the data and defense of its interpretation before model parameters could be updated. Such data has the potential to change the overall shape and size of the pressure distribution as well as both the overall conclusions regarding impacts on USDWs in both the northern portion of the Illinois Basin and those overlying the Eau Claire caprock. So, efforts to improve this aspect of the model are important to increasing confidence in model results and conclusions.

The model geometry was kept simple in this work. However, geophysical data indicates that lower permeability zones do exist in the Mt. Simon, although they are thinner than the model layers in this work. While the upscaling done in this work may allow for the capture of basin scale processes in the horizontal direction, the usefulness of results in the vertical direction suffers. Therefore, a finer discretization that captures more of the spatial variability of porosity, permeability, and storativity values of the Mt. Simon in the vertical direction should be developed. At locations far from injection wells, vertical flow will be

less significant and the current vertical discretization may remain appropriate. Near the wellheads, however, such improvements would allow for more confidence in local results.

Issues in the SEAWAT model are fewer since the model is calibrated and more is known about the deep system in this region, as it is more accessible than in the south. Yet, as the model is being put to a new use for which it was not originally designed, the grid spacing, especially in the southern region, may be an issue. Refining the grid spacing would reduce the grid peclet number of the model and, as a result, numerical dispersion [28]. At present, this would require refinement across the model resulting in a rather large increase in the number of model nodes, but with new developments in SEAWAT related software, a more local refinement may be possible in the future.

So, while improvements related to the methodology and the SEAWAT model should be undertaken, the first course of action in any further development of this work should first focus on the TOUGH2 model itself. The TOUGH2 related factors laid out above control the major basin-scale processes and thus, have a much greater impact on overall model results.

CHAPTER 6

FIGURES

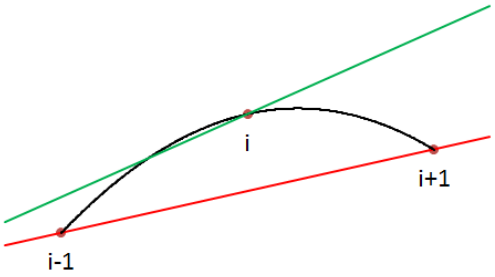

Figure 6.1: Sensitivity Calculation. The black line is a quadratic fitted to the three points (i-1, i, and i+1), the green line is the derivative of the quadratic evaluated at i, and the red is a two-point derivative based on i-1 and i+1. The user may choose the to use slope of either the green line or the red line to obtain sensitivities

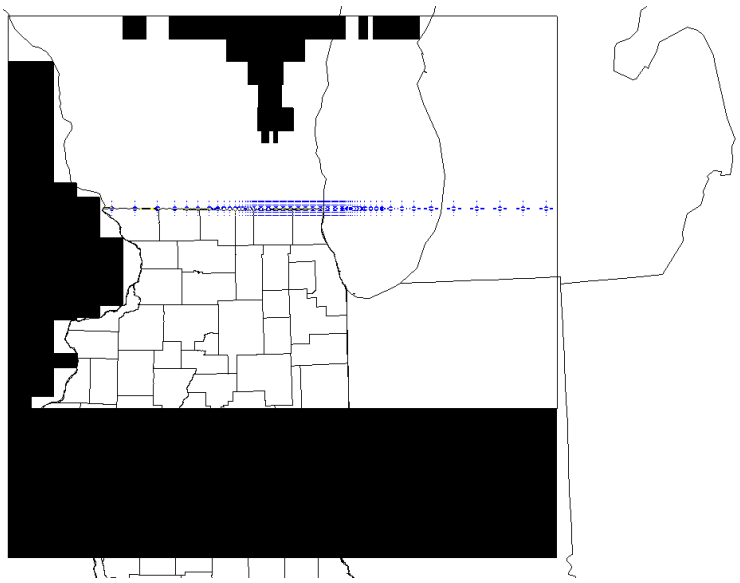

Figure 6.2: Location of Targets in Mt. Simon for Run 1. Base map modified from Meyer et al., 2009

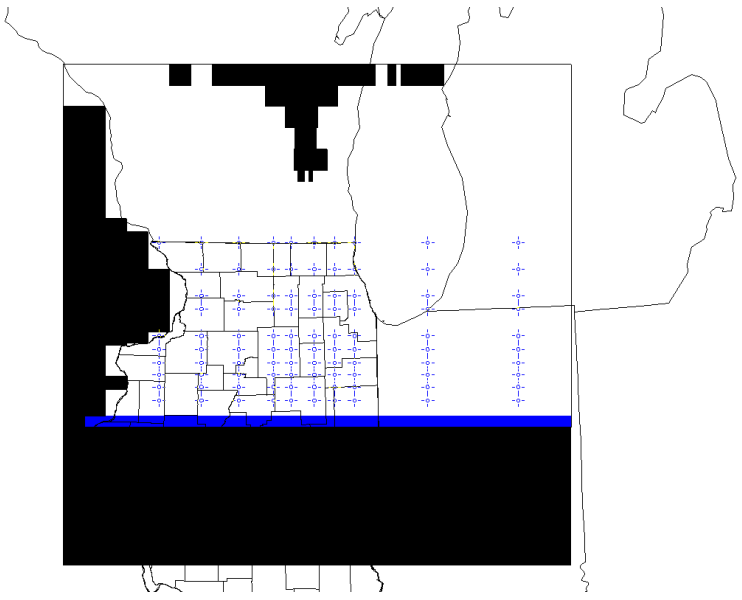

Figure 6.3: Location of Targets in Mt. Simon for Run 2. Base map modified from Meyer et al., 2009

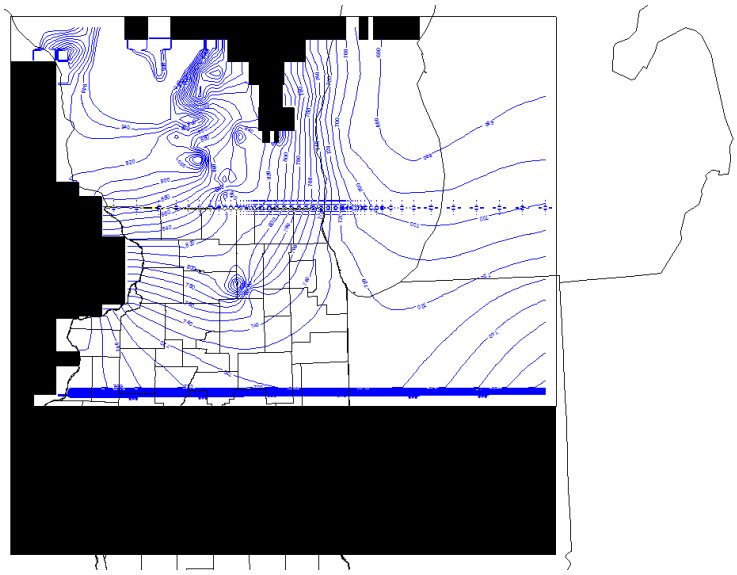

Figure 6.4: Head Contours in the Top of the Mt. Simon After 40 Years of Simulation. Base map modified from Meyer et al., 2009

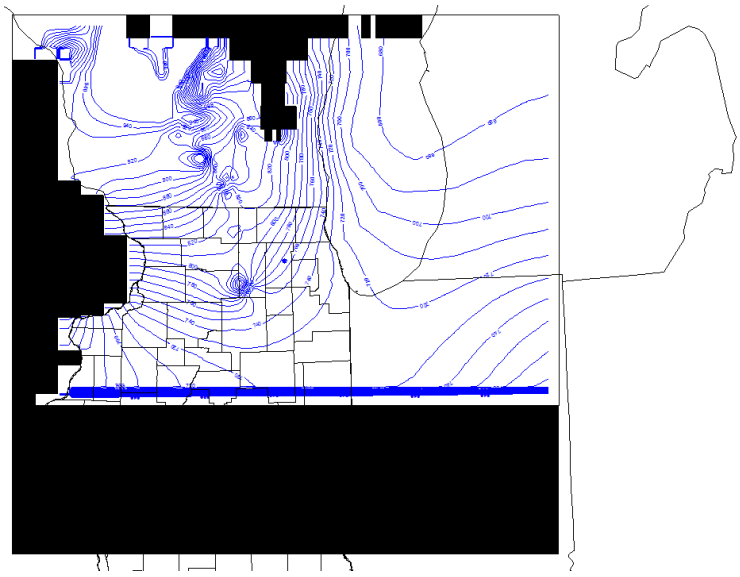

Figure 6.5: Head Contours in the Top of the Mt. Simon After 500 Years of Simulation. Base map modified from Meyer et al., 2009

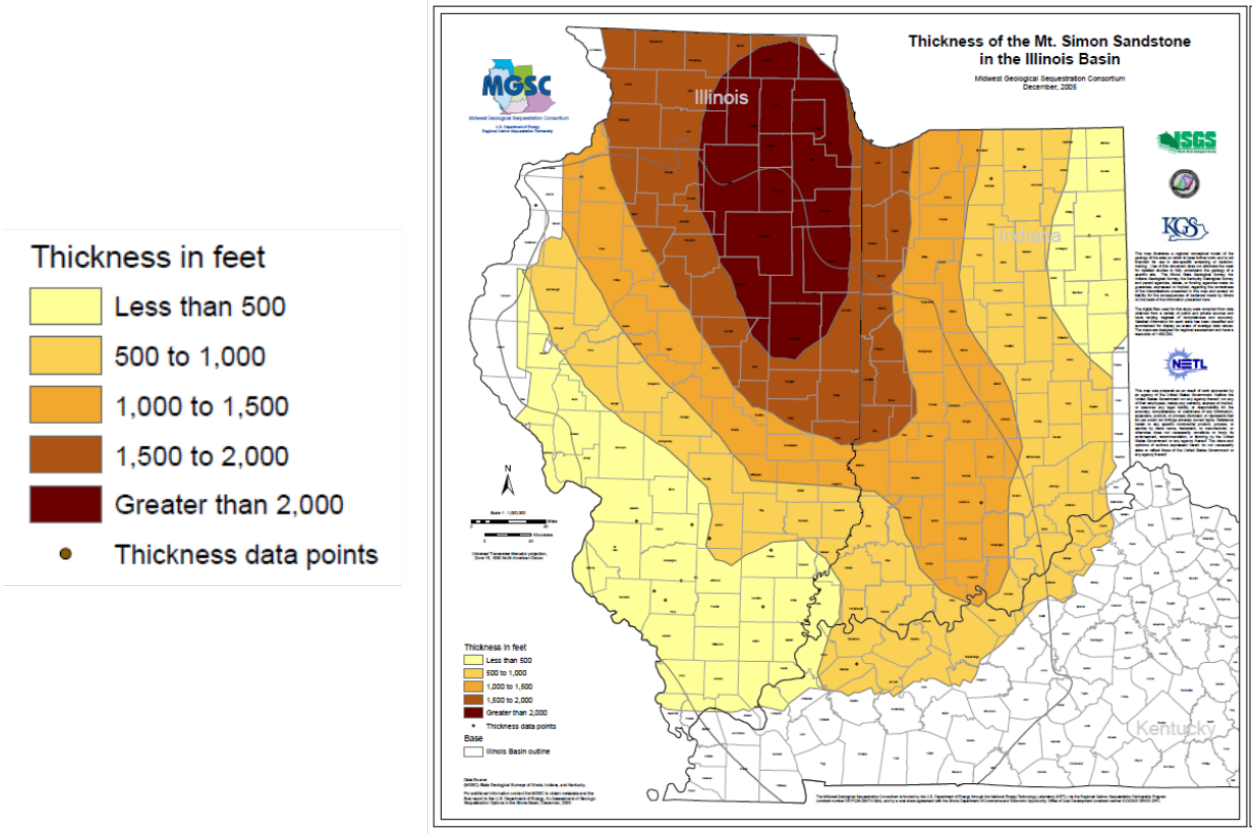

Figure 6.6: Thickness of the Mt. Simon [29]

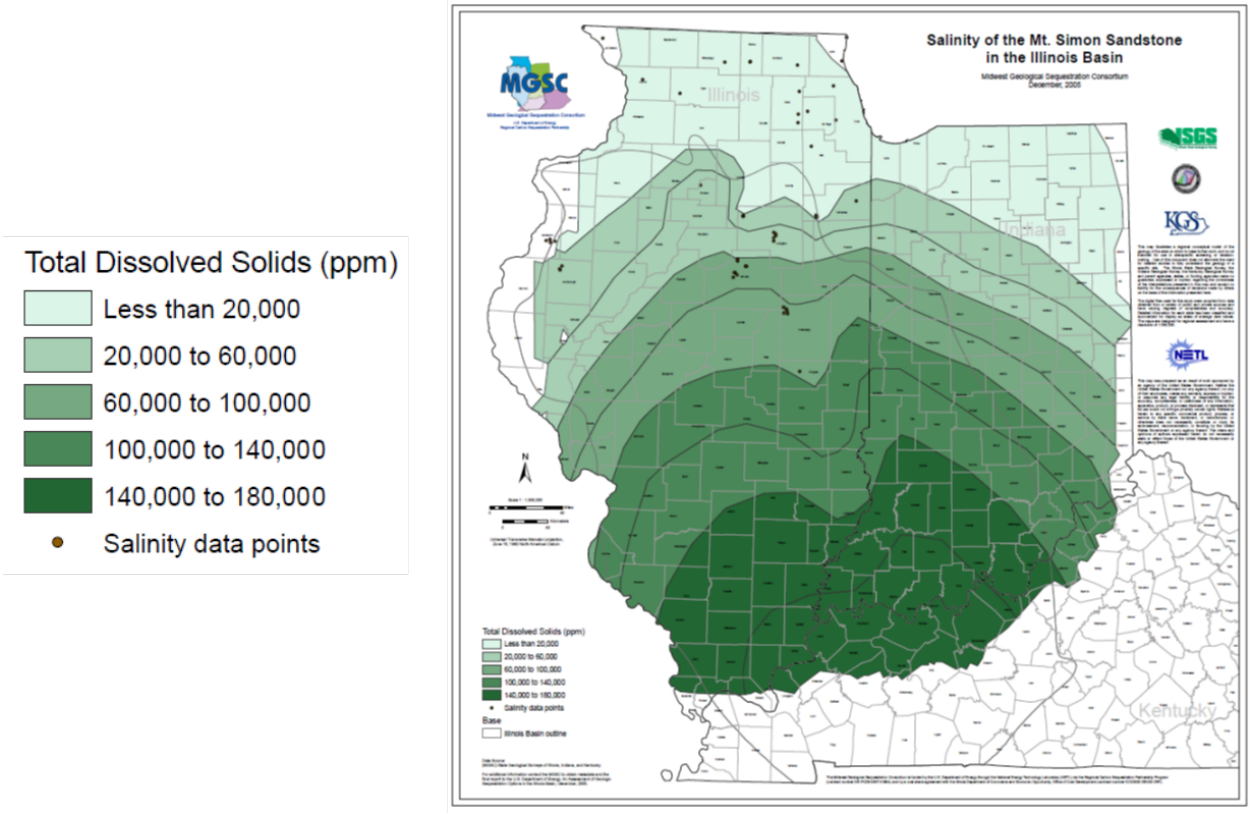

Figure 6.7: Salinity of the Mt. Simon [30]

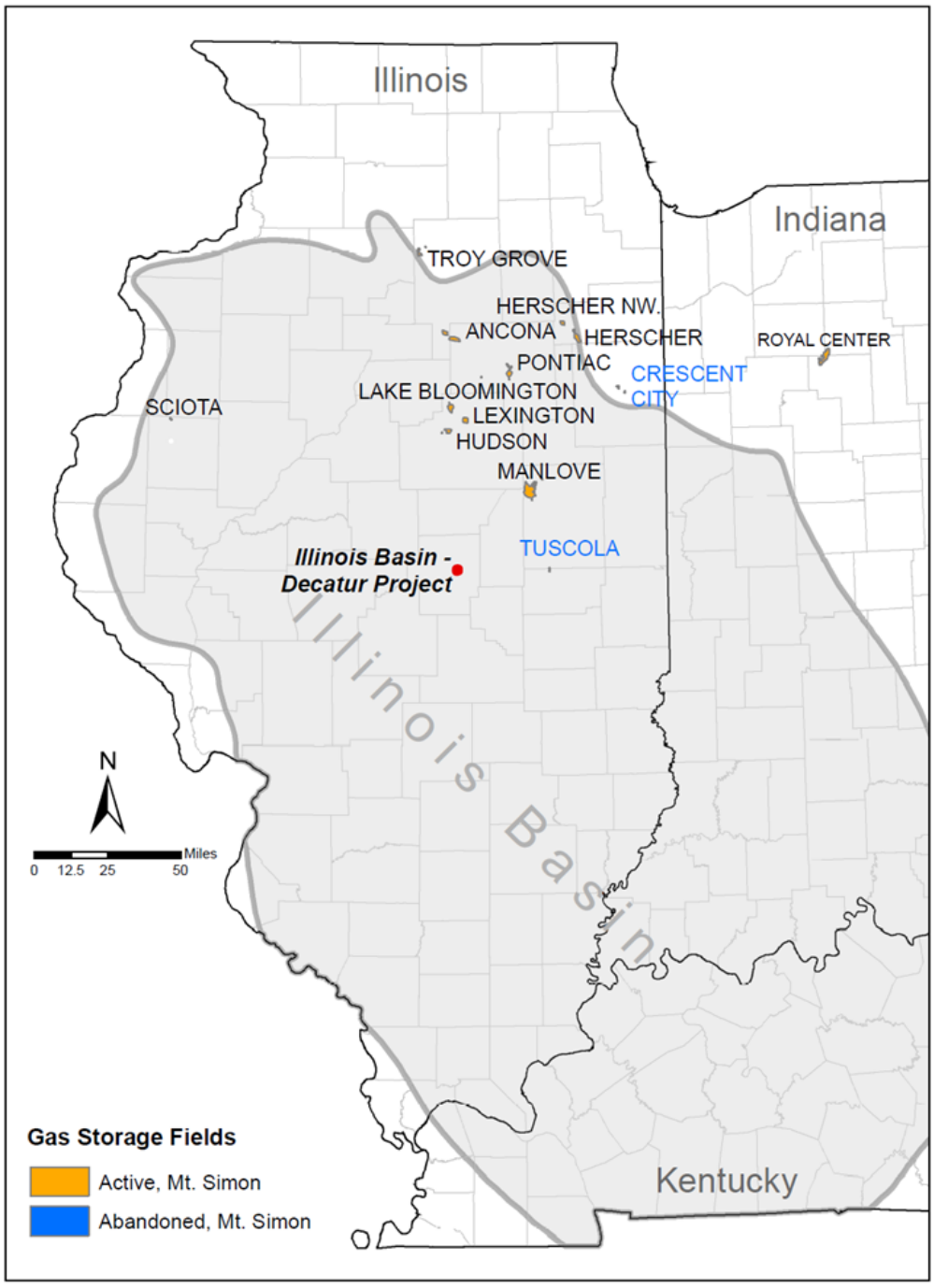

Figure 6.8: Location of the Illinois Basin Decatur Project Sequestration Well and Natural Gas Storage Fields in the Mt. Simon Sandstone. Source: Personal Communication, Chris Korose, ISGS, 2012

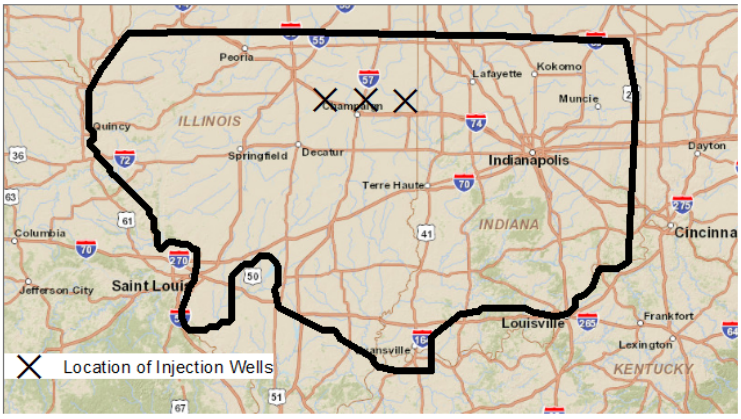

Figure 6.9: Location of Simulated Injection Wells in TOUGH2 Model

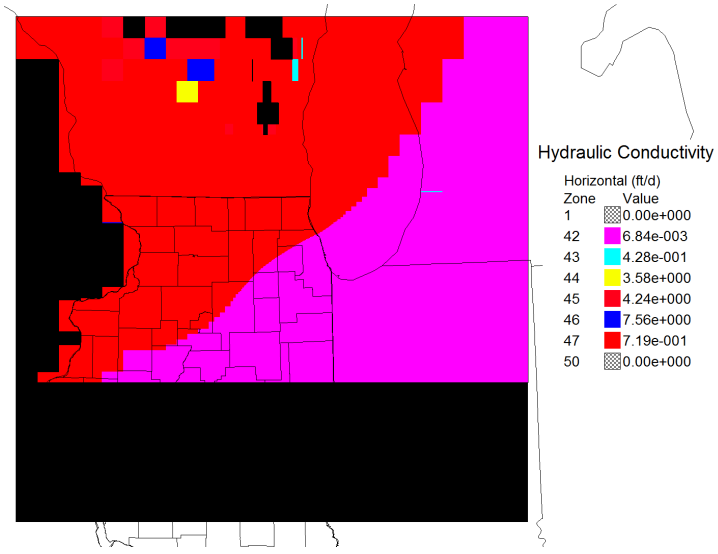

Figure 6.10: Horizontal Conductivity Values at the Top of the Eau Claire (Layer 2). Modified from Meyer et al., 2009

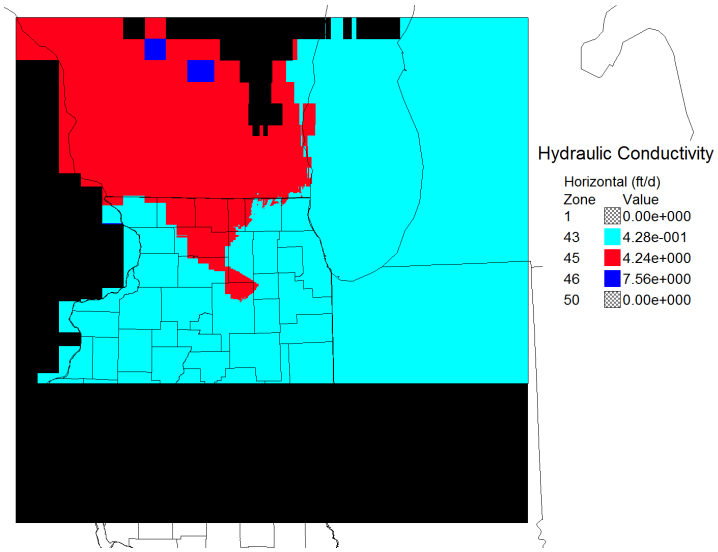

Figure 6.11: Horizontal Conductivity Values at the Top of the Mt. Simon (Layer 5). Modified from Meyer et al., 2009

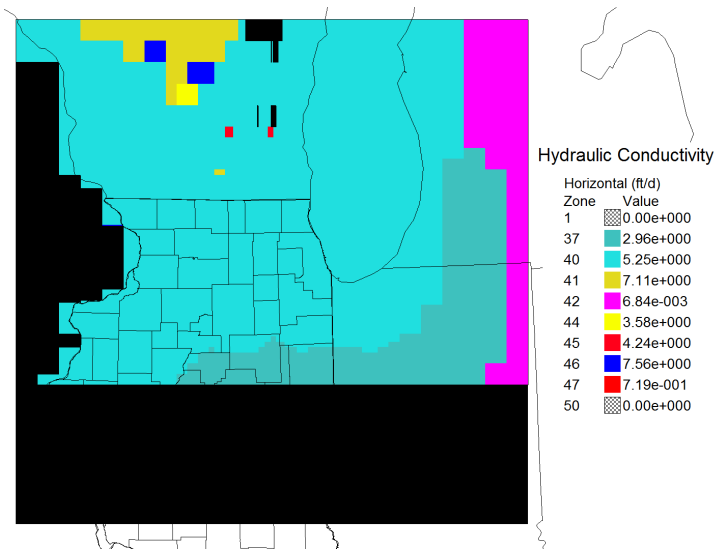

Figure 6.12: Horizontal Hydraulic Conductivity in Layer 1 (Ironton-Galesville). Modified from Meyer et al., 2009

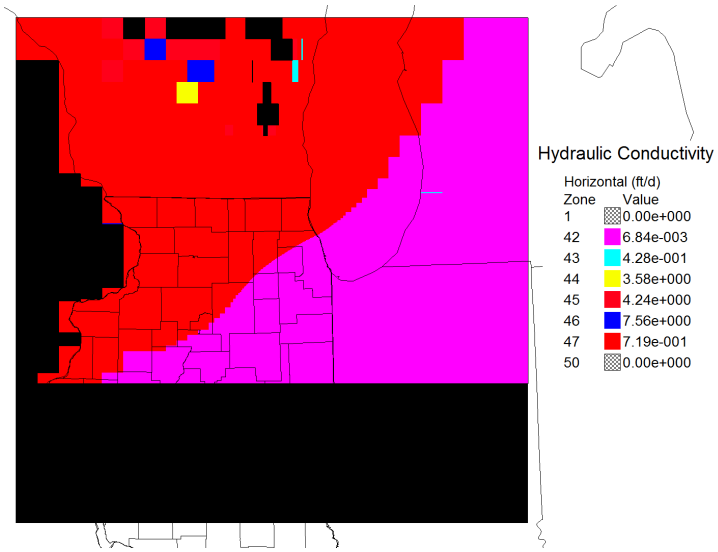

Figure 6.13: Horizontal Hydraulic Conductivity in Layers 2 - 4 (Eau Claire). Modified from Meyer et al., 2009

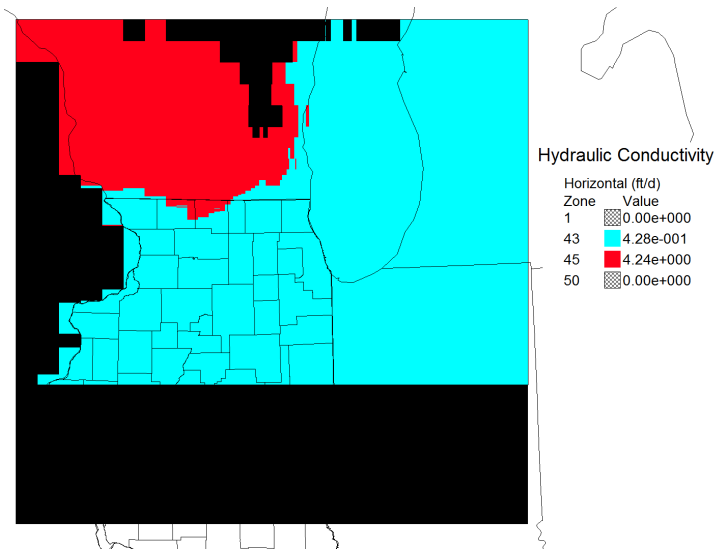

Figure 6.14: Horizontal Hydraulic Conductivity in Layer 6 (Mt. Simon). Modified from Meyer et al., 2009

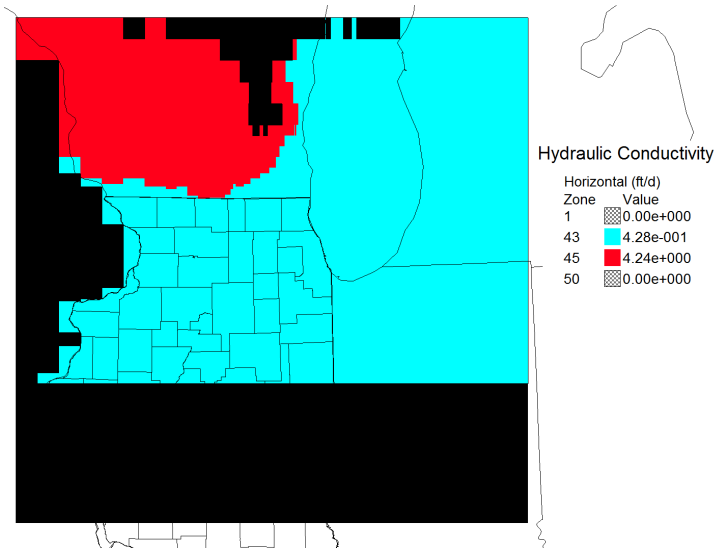

Figure 6.15: Horizontal Hydraulic Conductivity in Layer 7 (Mt. Simon). Modified from Meyer et al., 2009

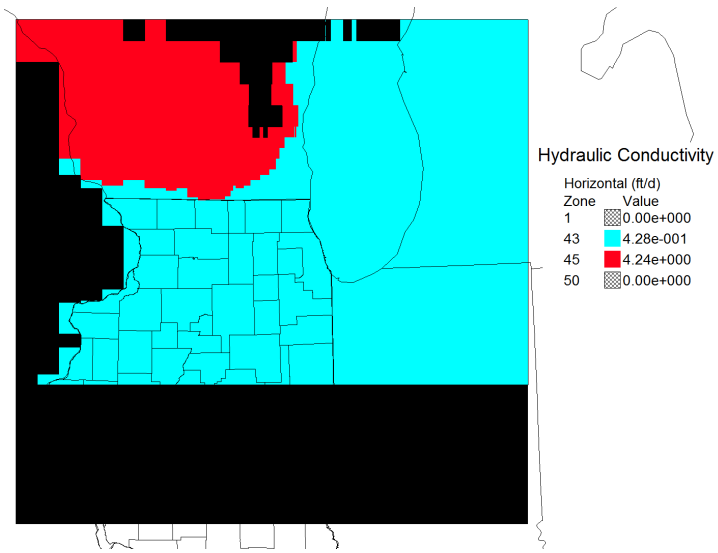

Figure 6.16: Horizontal Hydraulic Conductivity in Layer 8 (Mt. Simon). Modified from Meyer et al., 2009

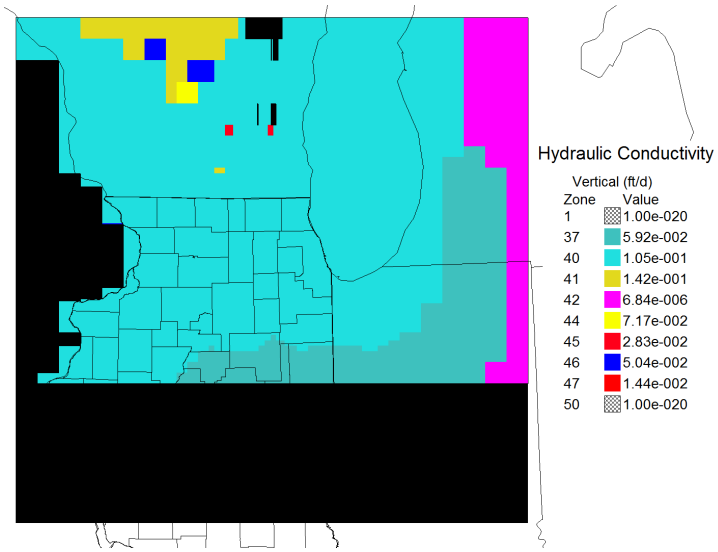

Figure 6.17: Vertical Hydraulic Conductivity in Layer 1 (Ironton-Galesville). Modified from Meyer et al., 2009

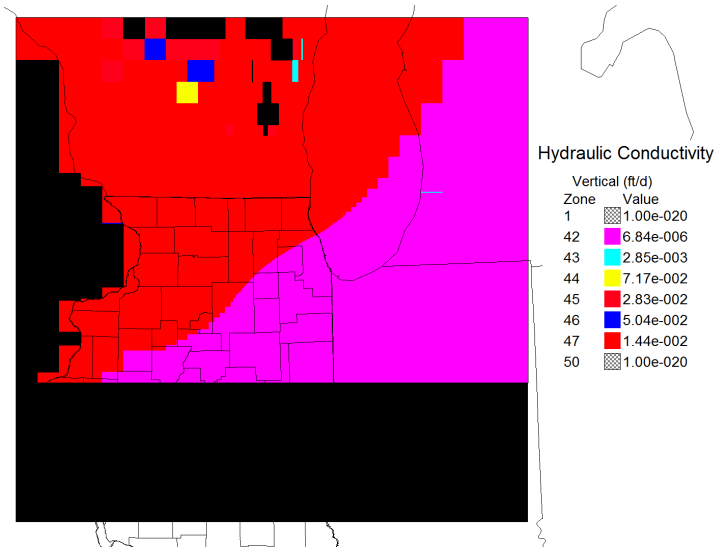

Figure 6.18: Vertical Hydraulic Conductivity in Layers 2 - 4 (Eau Claire). Modified from Meyer et al., 2009

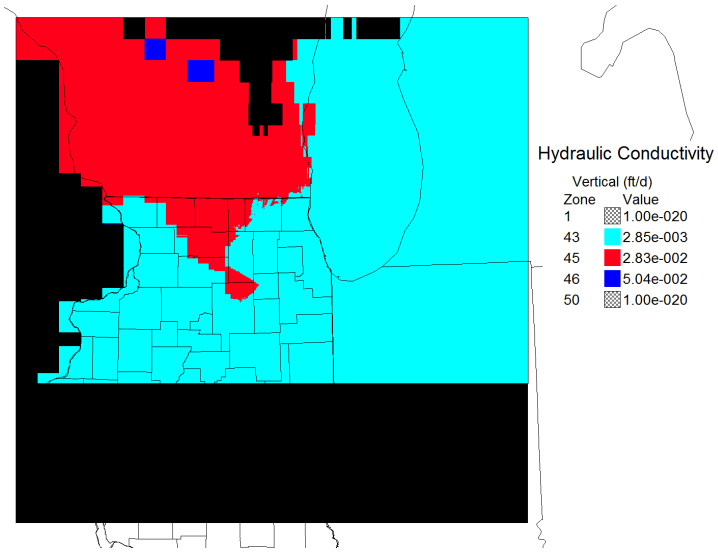

Figure 6.19: Vertical Hydraulic Conductivity in Layer 5 (Mt. Simon). Modified from Meyer et al., 2009

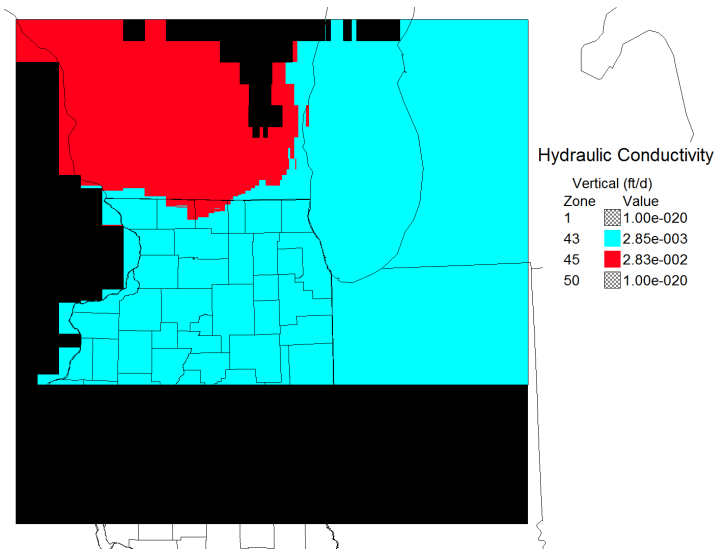

Figure 6.20: Vertical Hydraulic Conductivity in Layer 6 (Mt. Simon). Modified from Meyer et al., 2009

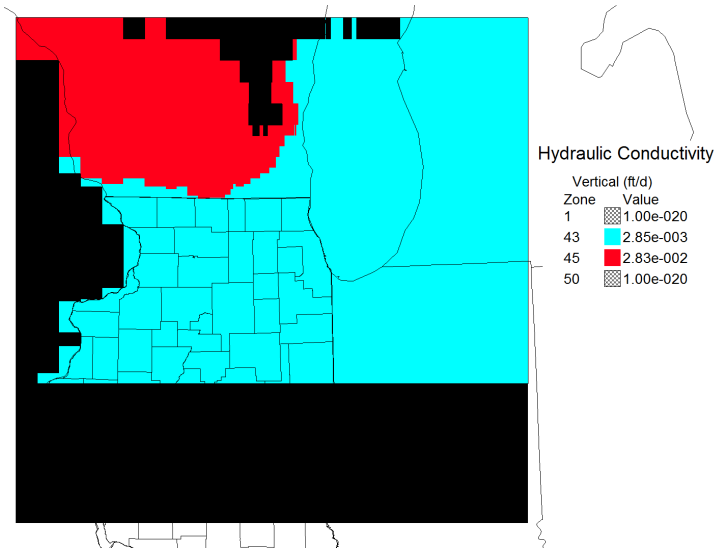

Figure 6.21: Vertical Hydraulic Conductivity in Layer 7 (Mt. Simon). Modified from Meyer et al., 2009

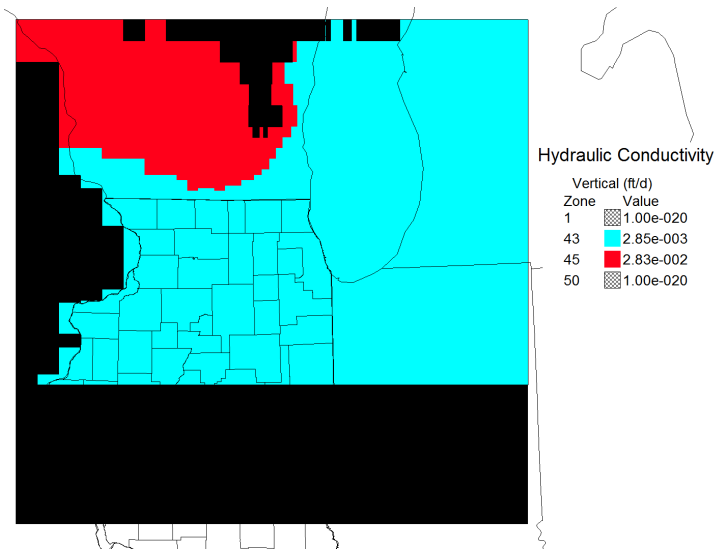

Figure 6.22: Vertical Hydraulic Conductivity in Layer 8 (Mt. Simon). Modified from Meyer et al., 2009

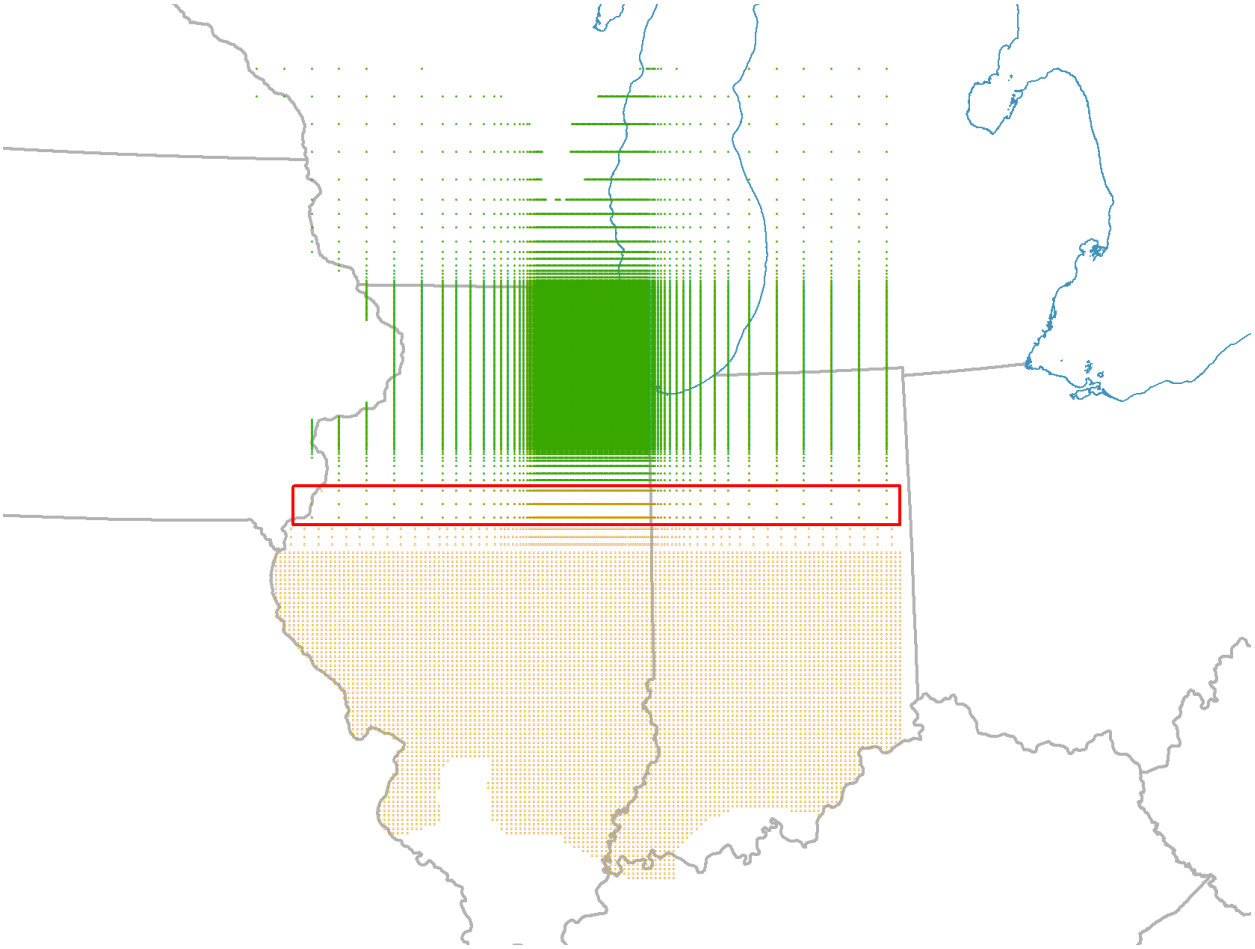

Figure 6.23: Nodes from Both Models with Overlapping Nodes in Red Rectangle

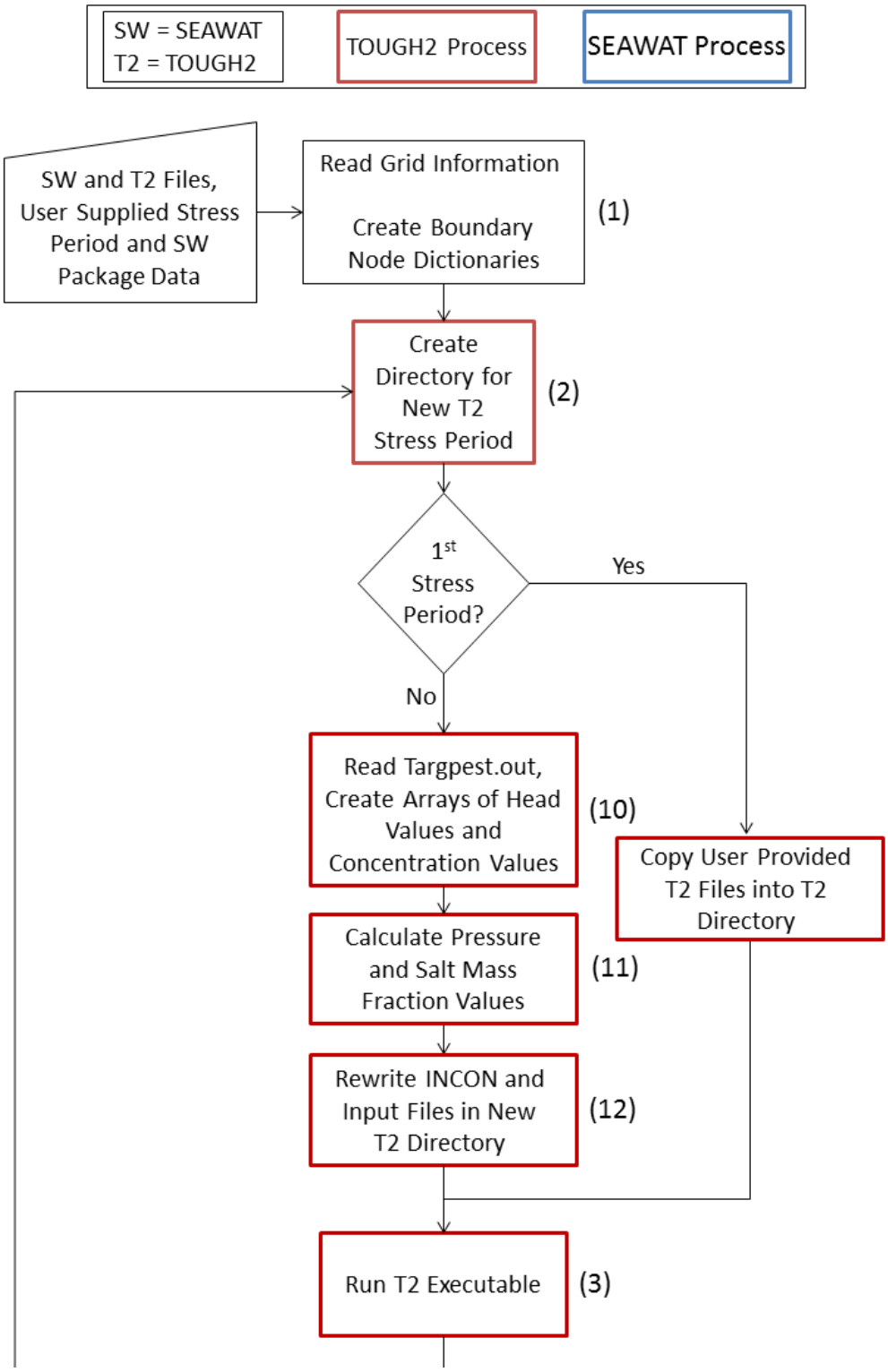

Figure 6.24: Flowchart of the Coupling Process

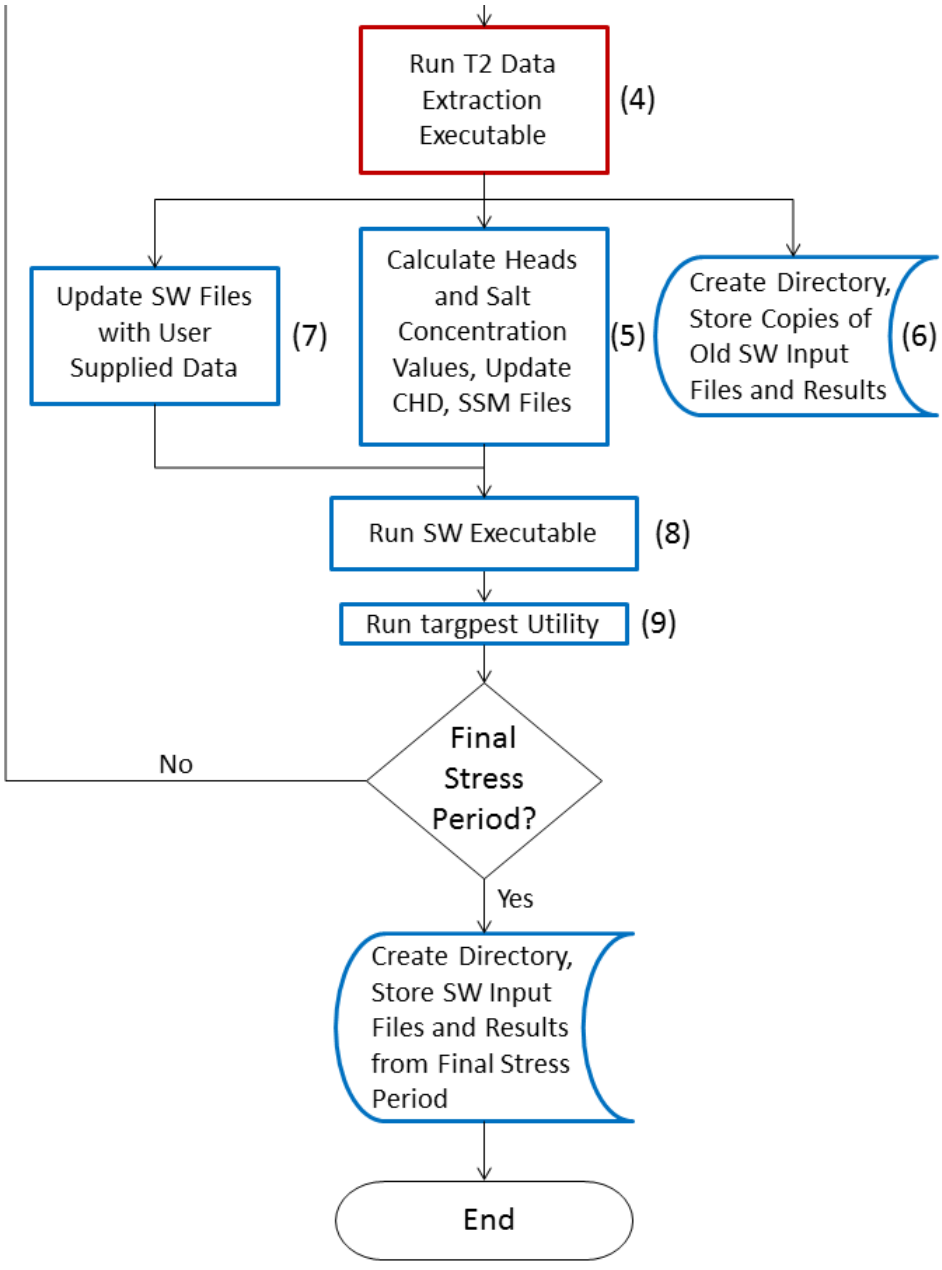

Figure 6.24 (Cont.)

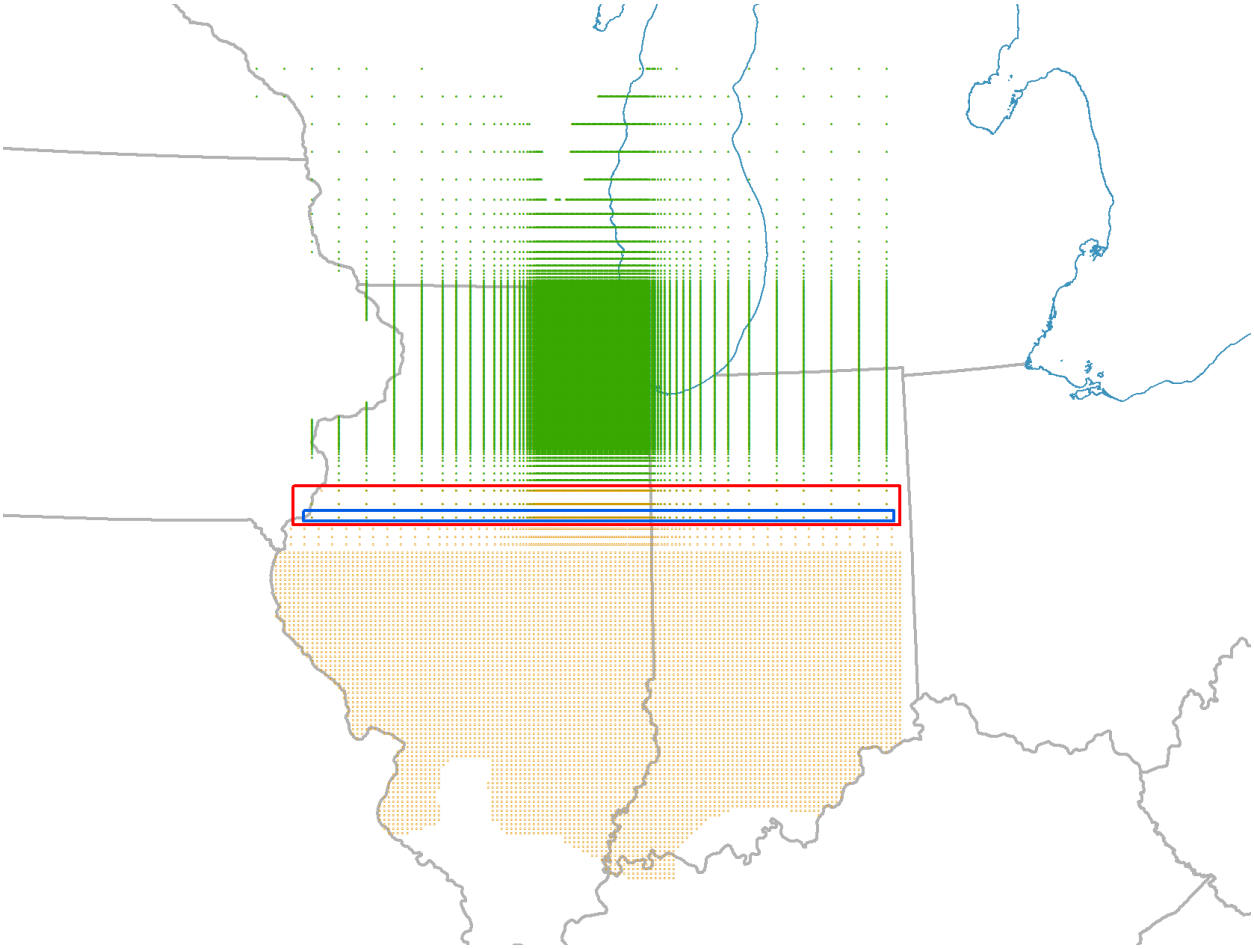

Figure 6.25: Interior TOUGH2 Model Nodes and Southern Boundary Nodes of SEAWAT Model (In Blue Rectangle)

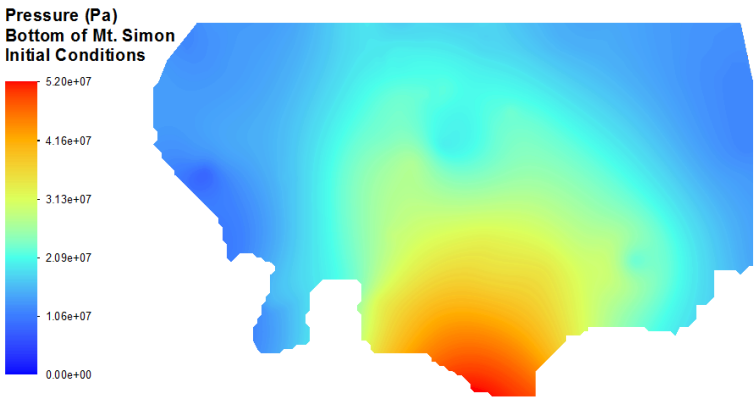

Figure 6.26: Initial Pressures at Bottom of Mt. Simon (Pa)

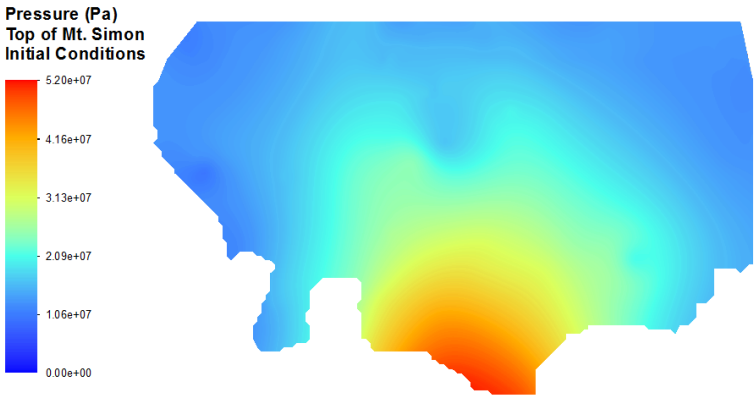

Figure 6.27: Initial Pressures at Top of Mt. Simon (Pa)

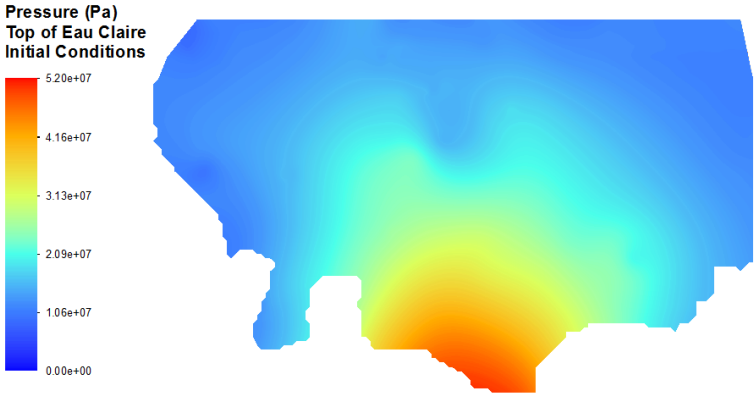

Figure 6.28: Initial Pressures at Top of Eau Claire (Pa)

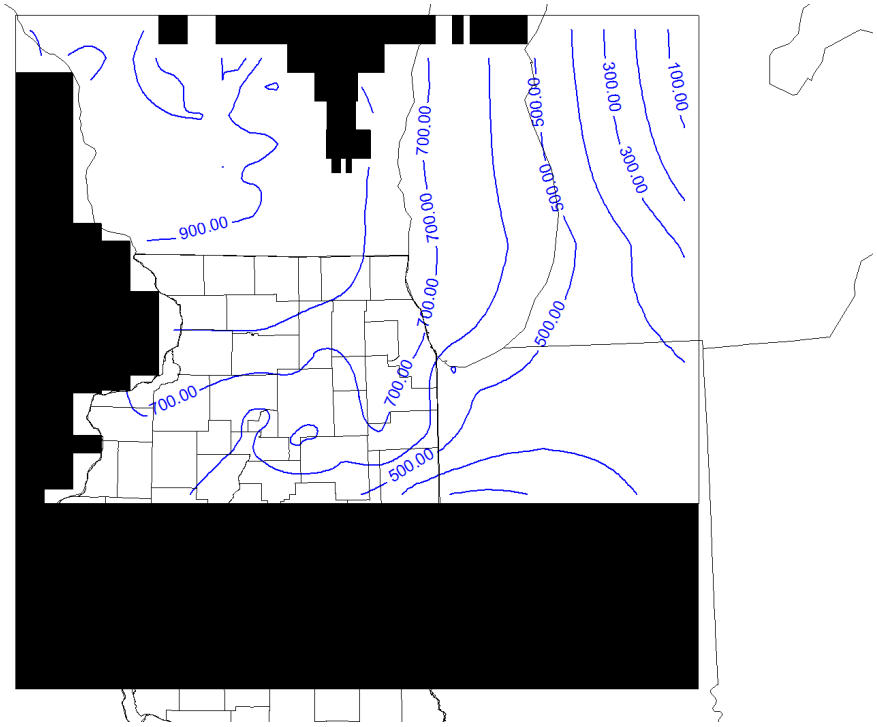

Figure 6.29: Initial Heads at Bottom of Mt. Simon (Above msl). Base map modified from Meyer et al., 2009

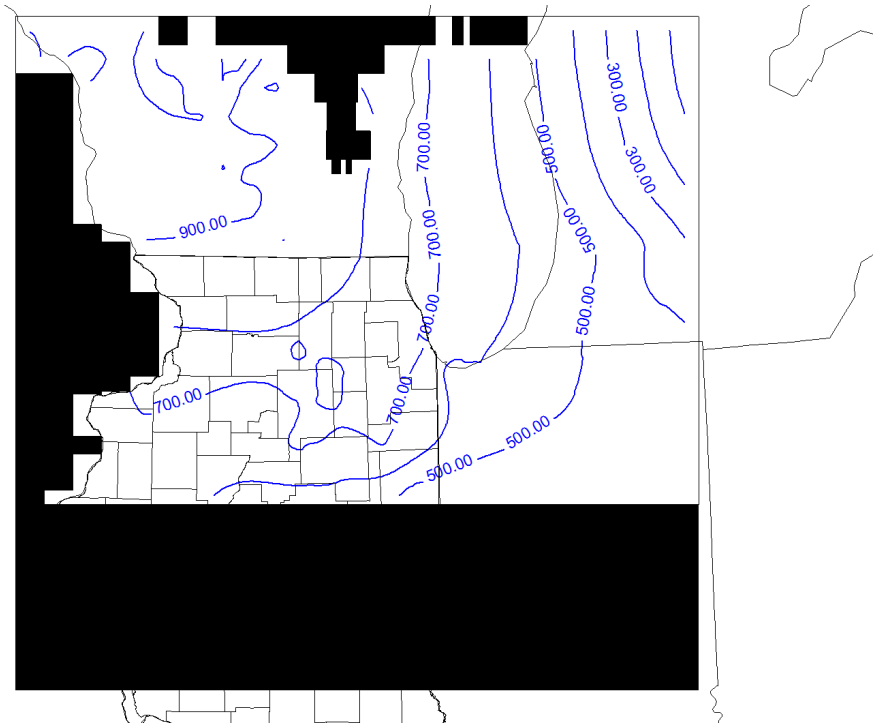

Figure 6.30: Initial Heads at Top of Mt. Simon (Above msl). Base map modified from Meyer et al., 2009

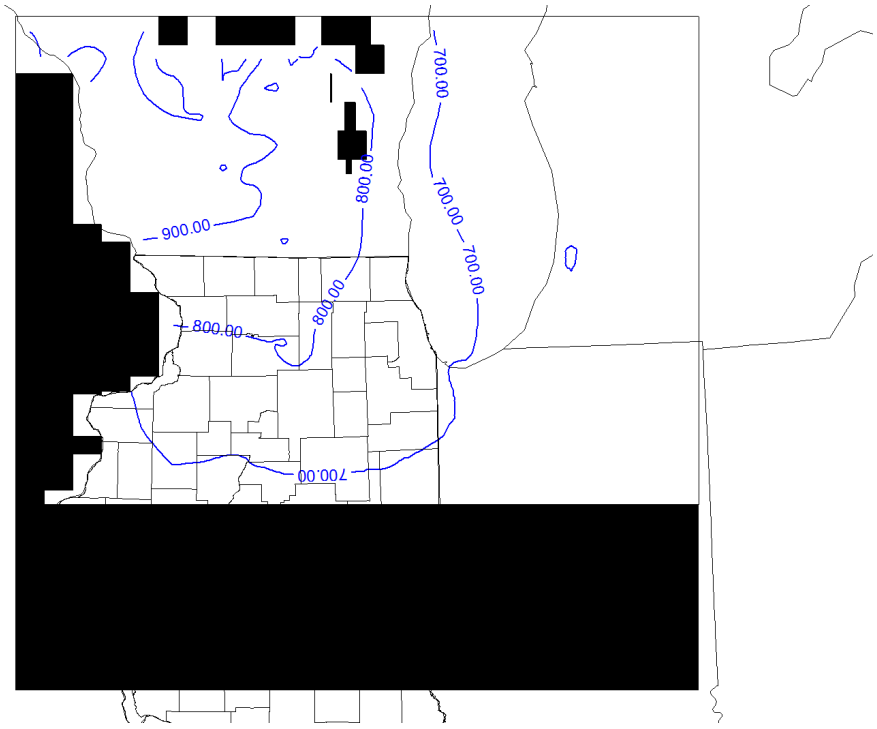

Figure 6.31: Initial Heads at Top of Eau Claire (Above msl). Base map modified from Meyer et al., 2009

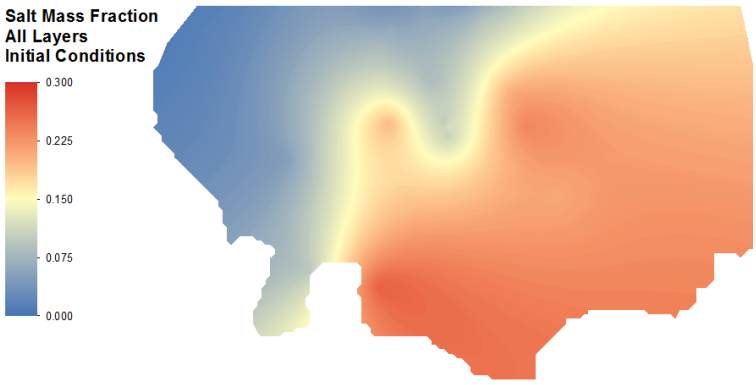

Figure 6.32: Initial Salt Mass Fraction In All Layers

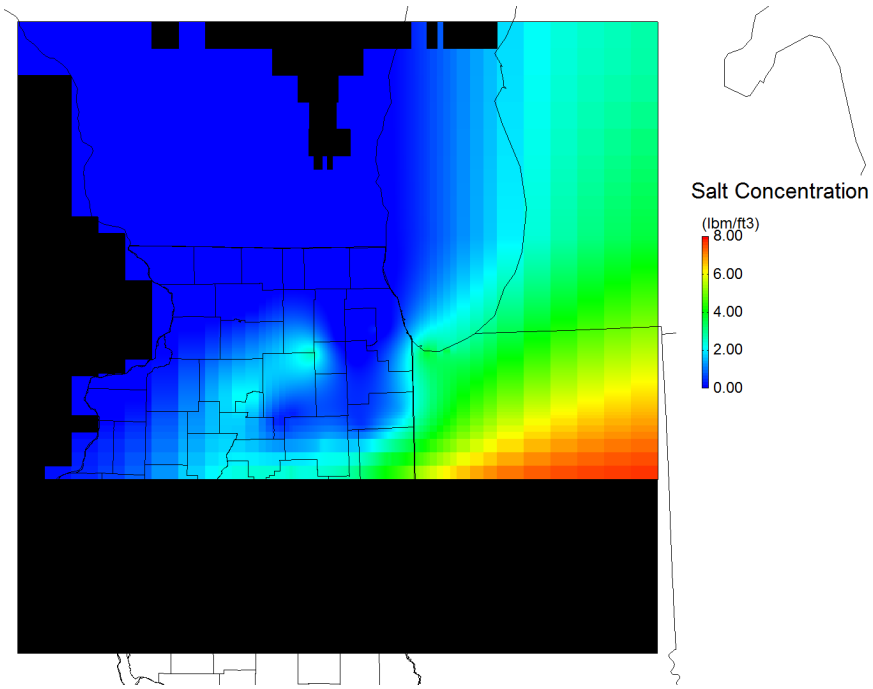

Figure 6.33: Initial Salt Concentration at Bottom of Mt. Simon (lbm/ft^3). Base map modified from Meyer et al., 2009

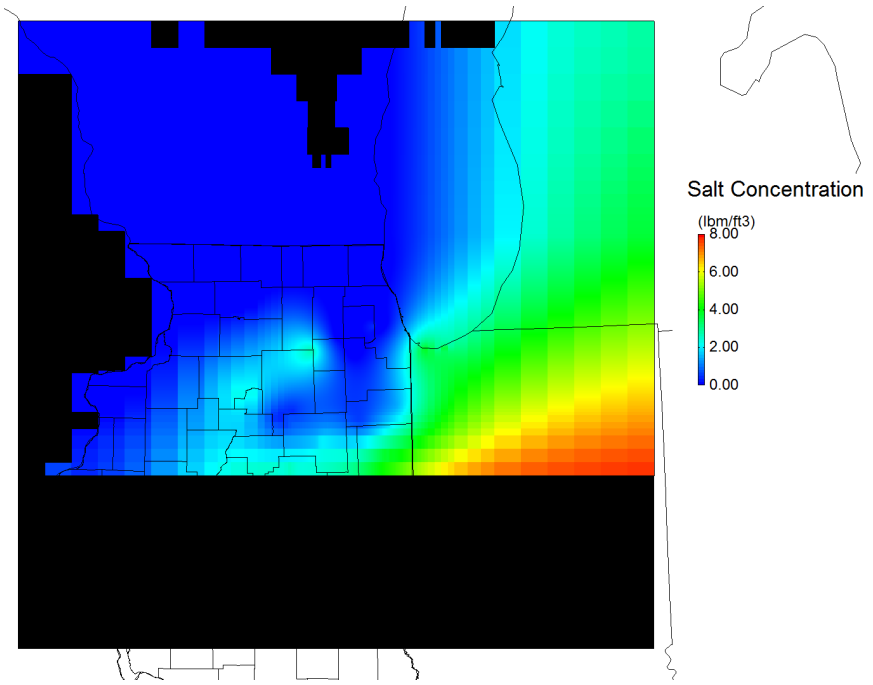

Figure 6.34: Initial Salt Concentration at Top of Mt. Simon (lbm/ft^3). Base map modified from Meyer et al., 2009

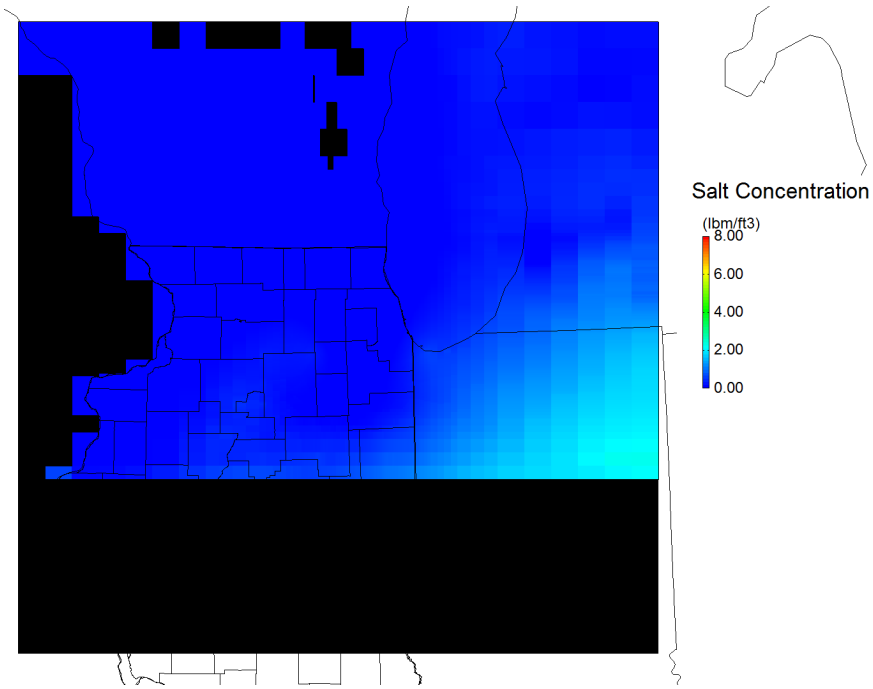

Figure 6.35: Initial Salt Concentration at Top of Eau Claire (lbm/ft^3). Base map modified from Meyer et al., 2009

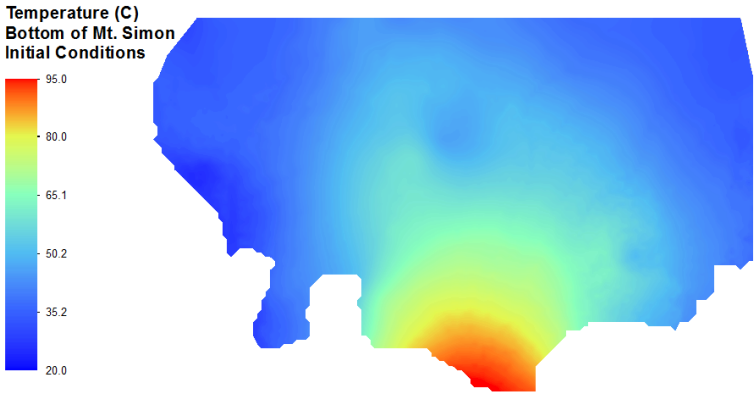

Figure 6.36: Initial Temperature at Bottom of Mt. Simon (°C)

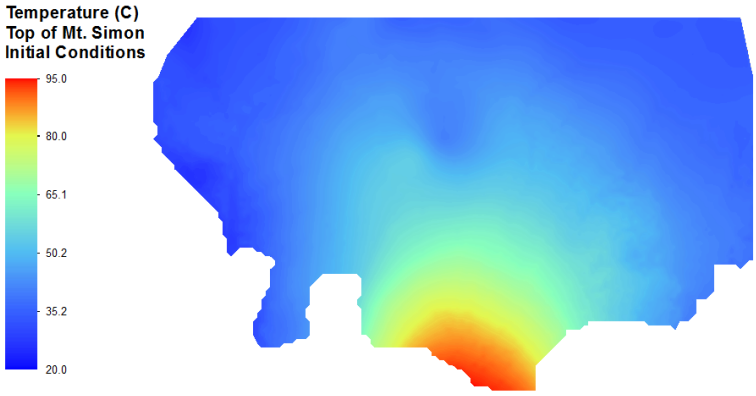

Figure 6.37: Initial Temperature at Top of Mt. Simon (°C)

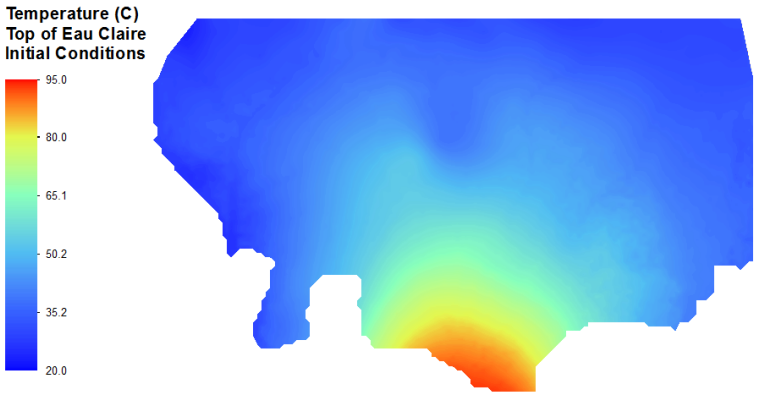

Figure 6.38: Initial Temperature at Top of Eau Claire (°C)

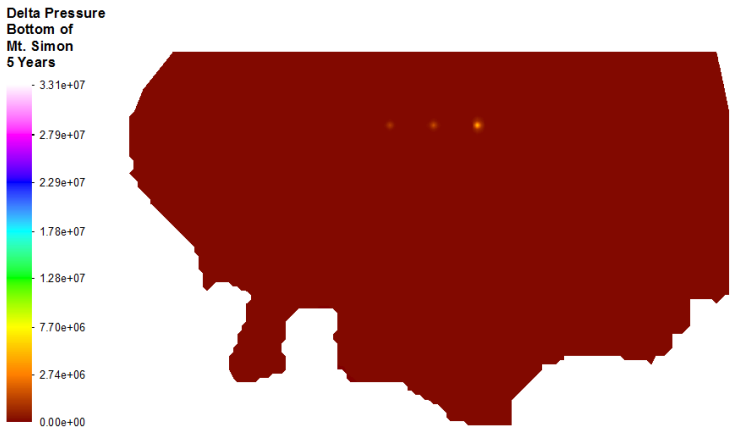

Figure 6.39: Change in Pressure (Pa) at Bottom of Mt. Simon After 5 Years of Pumping

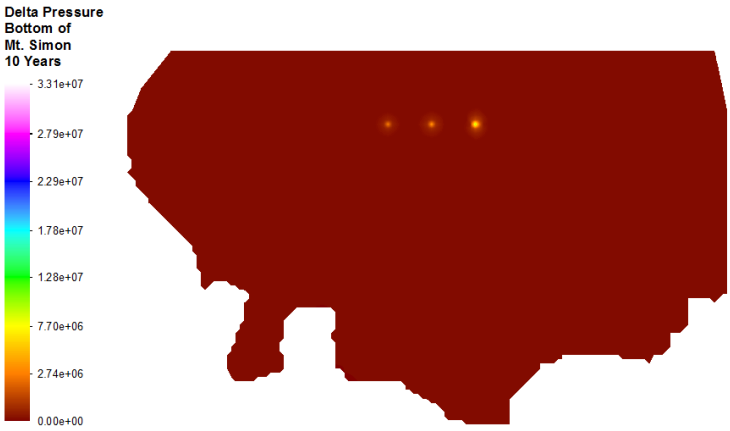

Figure 6.40: Change in Pressure (Pa) at Bottom of Mt. Simon After 10 Years of Pumping

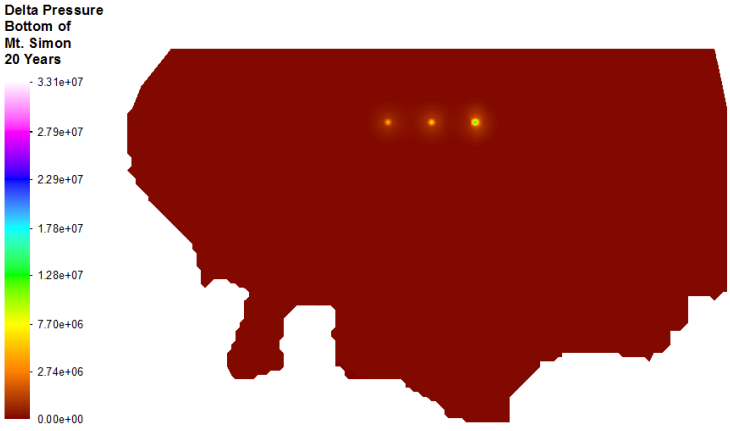

Figure 6.41: Change in Pressure (Pa) at Bottom of Mt. Simon After 20 Years of Pumping

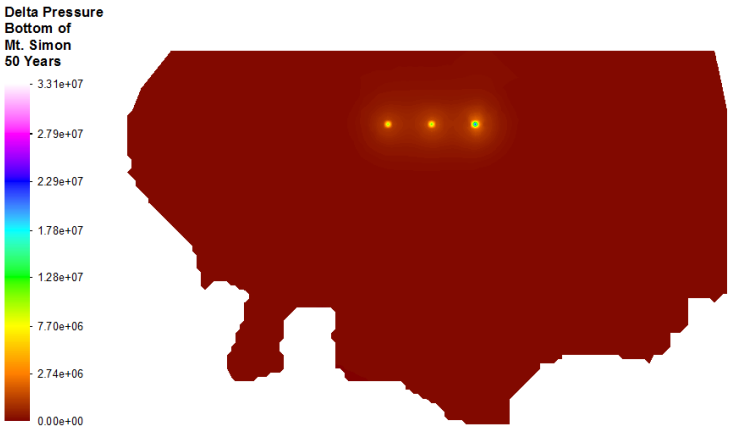

Figure 6.42: Change in Pressure (Pa) at Bottom of Mt. Simon After 50 Years of Pumping

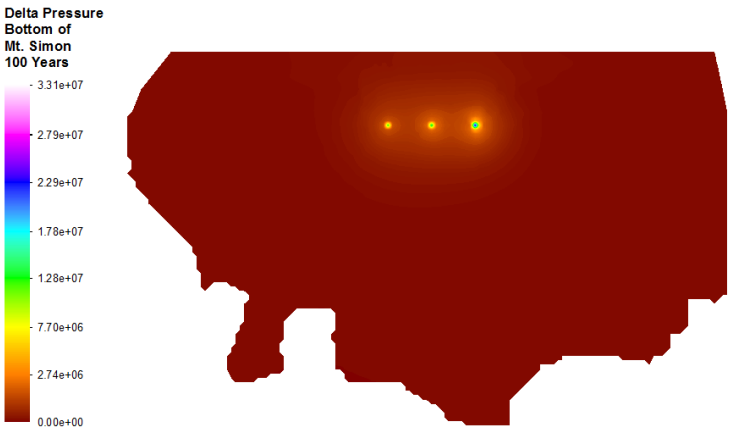

Figure 6.43: Change in Pressure (Pa) at Bottom of Mt. Simon After 100 Years of Pumping

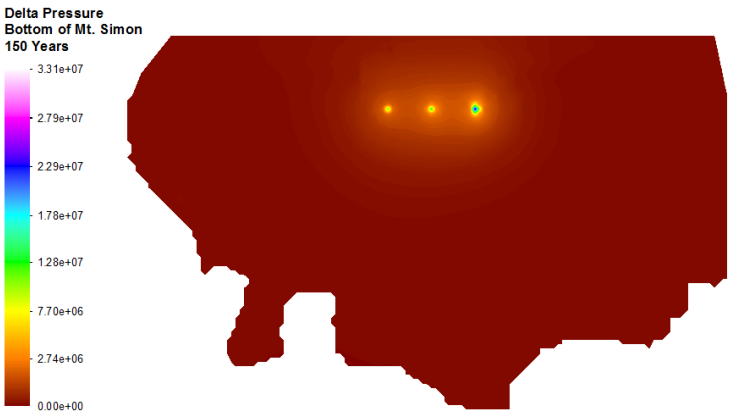

Figure 6.44: Change in Pressure (Pa) at Bottom of Mt. Simon After 150 Years of Pumping

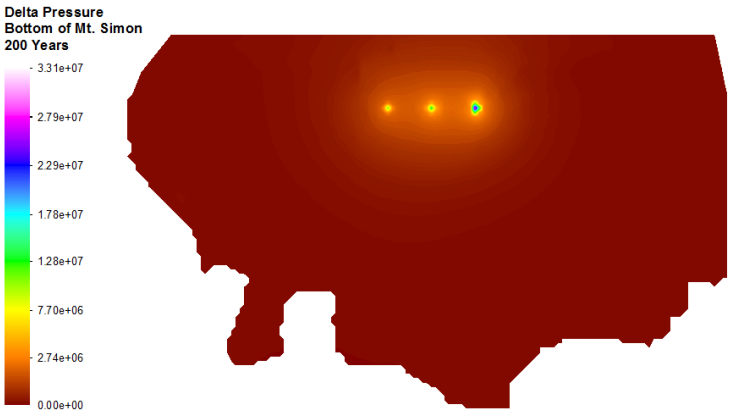

Figure 6.45: Change in Pressure (Pa) at Bottom of Mt. Simon After 200 Years of Pumping

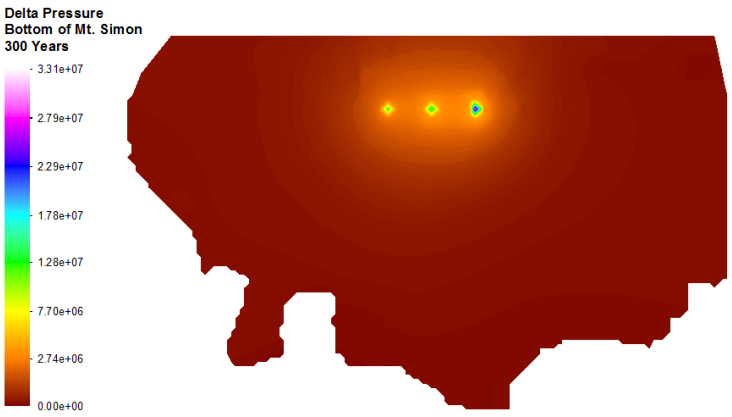

Figure 6.46: Change in Pressure (Pa) at Bottom of Mt. Simon After 300 Years of Pumping

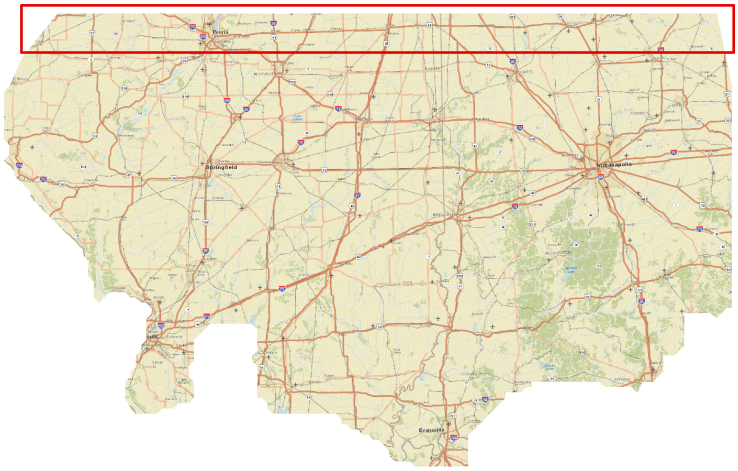

Figure 6.47: TOUGH2 Domain with Overlapping Region Outlined in Red

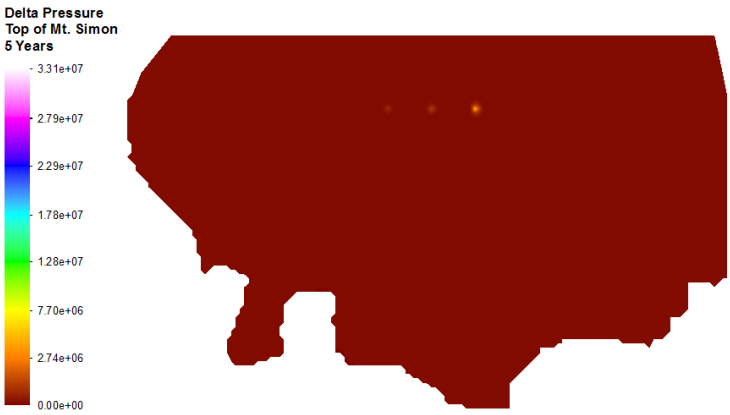

Figure 6.48: Change in Pressure (Pa) at Top of Mt. Simon After 5 Years of Pumping

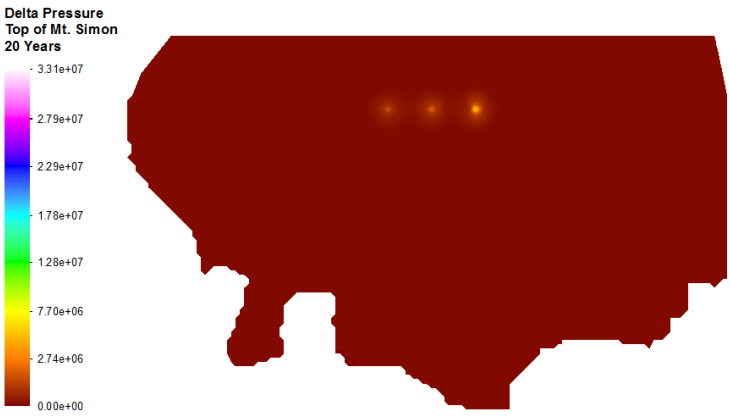

Figure 6.49: Change in Pressure (Pa) at Top of Mt. Simon After 20 Years of Pumping

Figure 6.50: Change in Pressure (Pa) at Top of Mt. Simon After 100 Years of Pumping

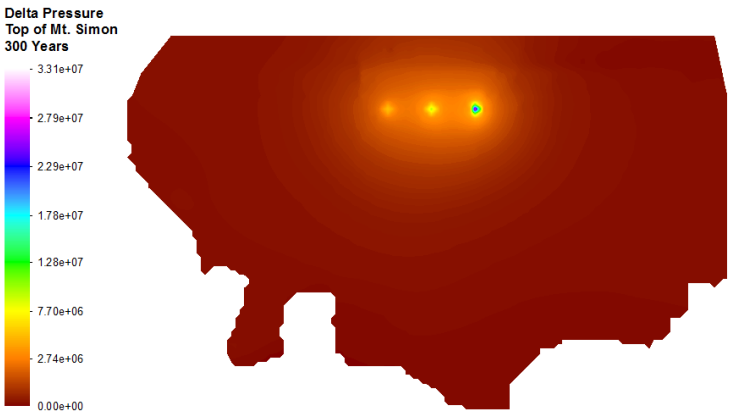

Figure 6.51: Change in Pressure (Pa) at Top of Mt. Simon After 300 Years of Pumping

Figure 6.52: Change in Pressure (Pa) at Top of Eau Claire After 100 Years of Pumping

Figure 6.53: Change in Pressure (Pa) at Top of Eau Claire After 200 Years of Pumping

Figure 6.54: Change in Pressure (Pa) at Top of Eau Claire After 300 Years of Pumping

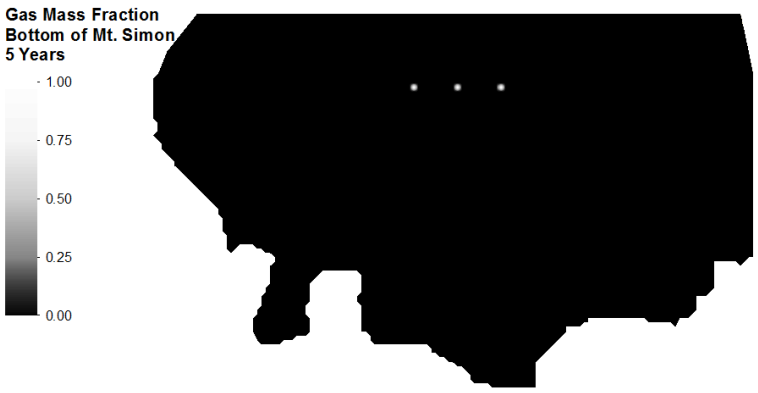

Figure 6.55: Gas Mass Fraction at Bottom of Mt. Simon After 5 Years of Pumping

Figure 6.56: Gas Mass Fraction at Bottom of Mt. Simon After 200 Years of Pumping

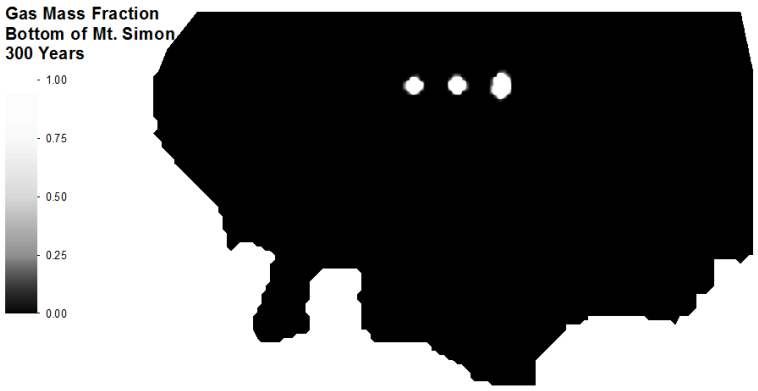

Figure 6.57: Gas Mass Fraction at Bottom of Mt. Simon After 300 Years of Pumping

Figure 6.58: Gas Mass Fraction at Top of Mt. Simon After 100 Years of Pumping

Figure 6.59: Gas Mass Fraction at Top of Mt. Simon After 300 Years of Pumping

Figure 6.60: Gas Mass Fraction at Top of Eau Claire After 300 Years of Pumping

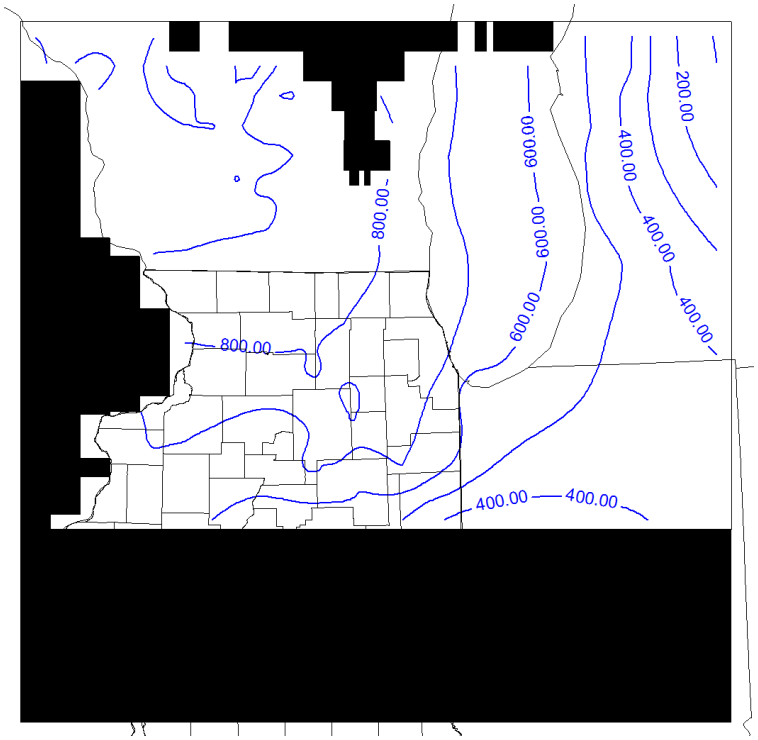

Figure 6.61: Heads at Bottom of Mt. Simon After 5 Years of Pumping (Heads in Feet Above msl). Base map modified from Meyer et al., 2009

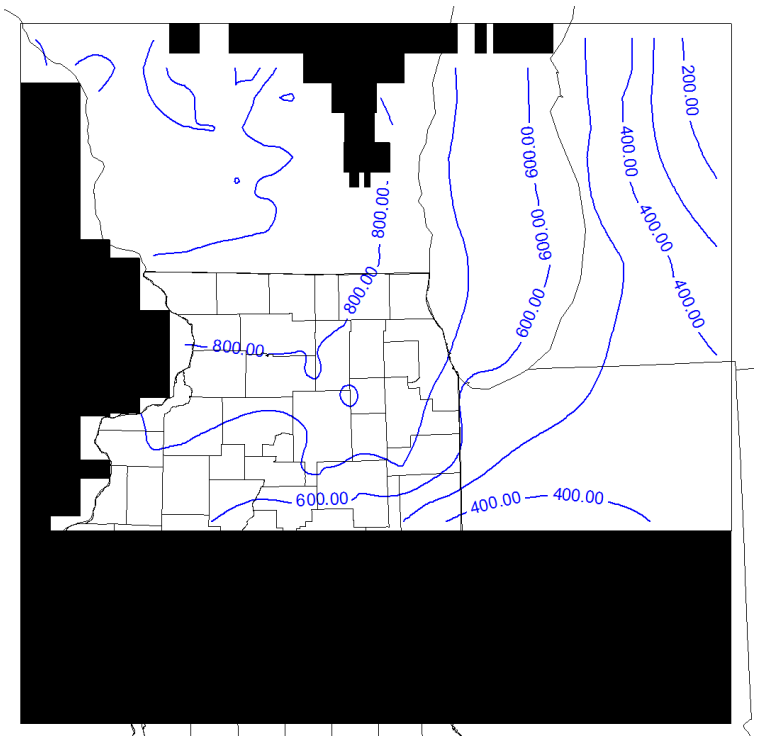

Figure 6.62: Heads at Bottom of Mt. Simon After 10 Years of Pumping (Heads in Feet Above msl). Base map modified from Meyer et al., 2009

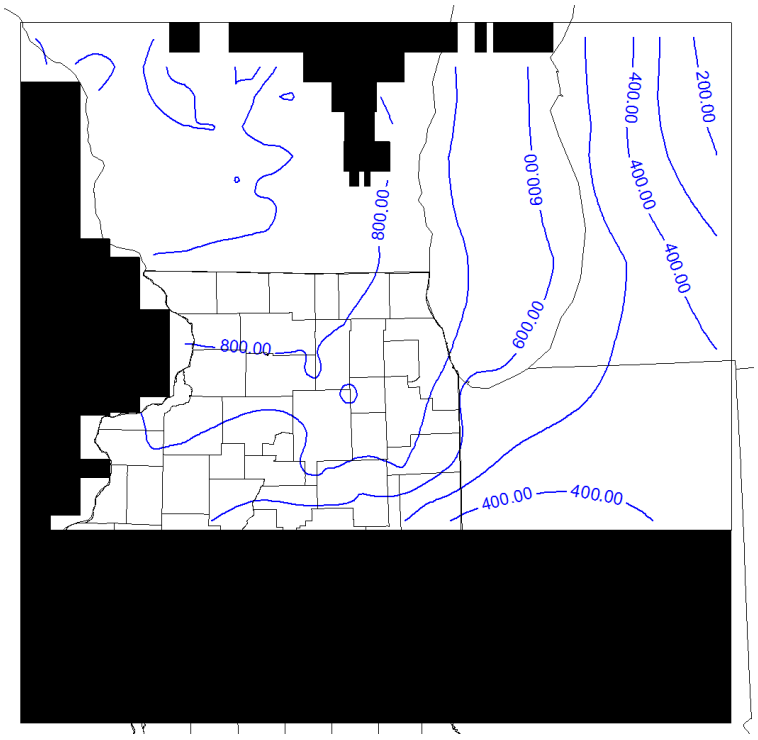

Figure 6.63: Heads at Bottom of Mt. Simon After 20 Years of Pumping (Heads in Feet Above msl). Base map modified from Meyer et al., 2009

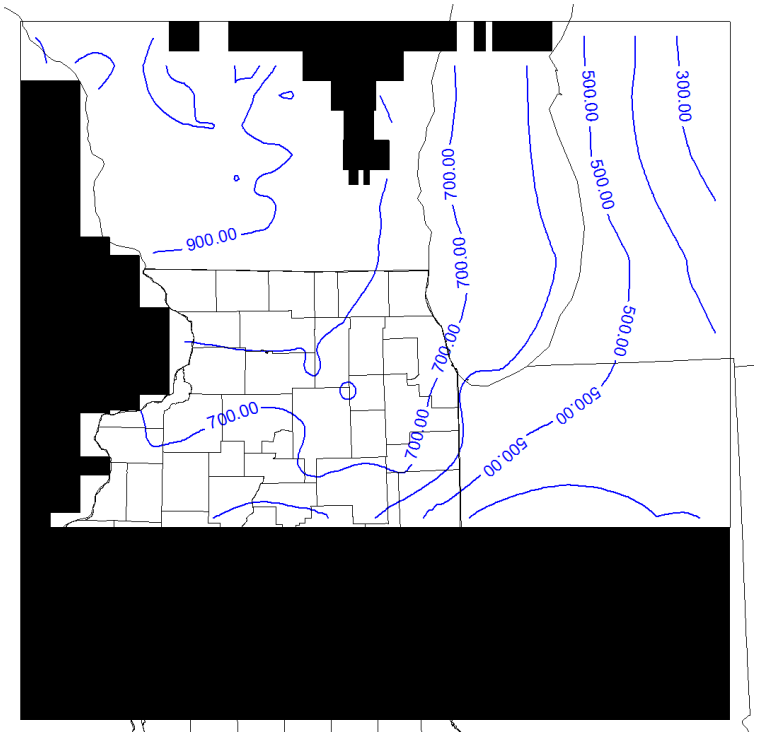

Figure 6.64: Heads at Bottom of Mt. Simon After 50 Years of Pumping (Heads in Feet Above msl). Base map modified from Meyer et al., 2009

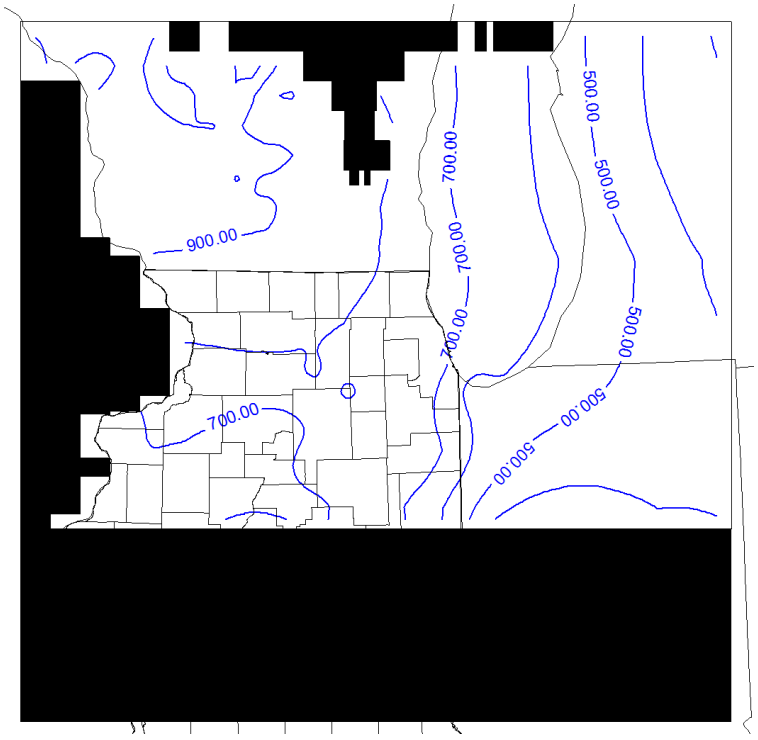

Figure 6.65: Heads at Bottom of Mt. Simon After 100 Years of Pumping (Heads in Feet Above msl). Base map modified from Meyer et al., 2009

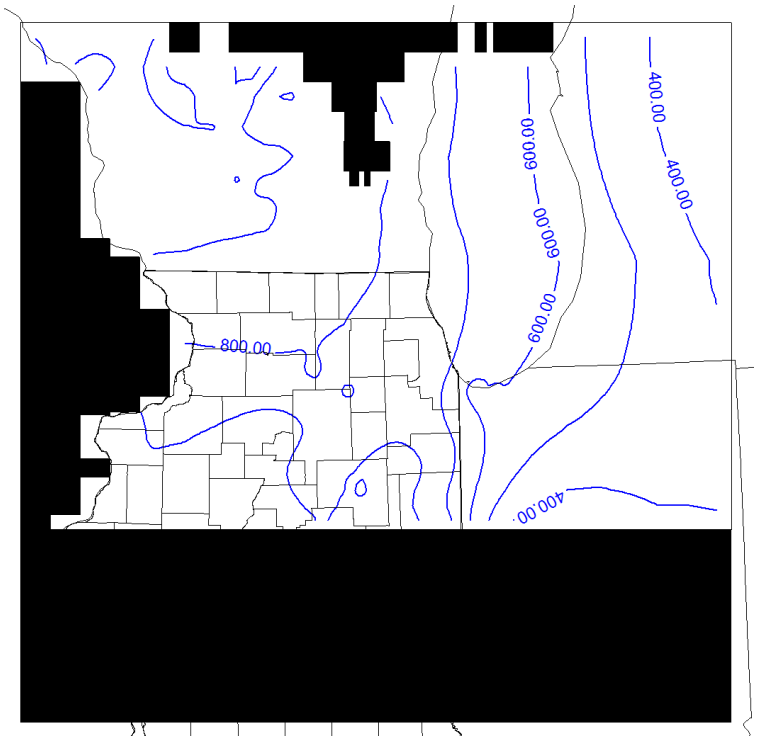

Figure 6.66: Heads at Bottom of Mt. Simon After 150 Years of Pumping (Heads in Feet Above msl). Base map modified from Meyer et al., 2009

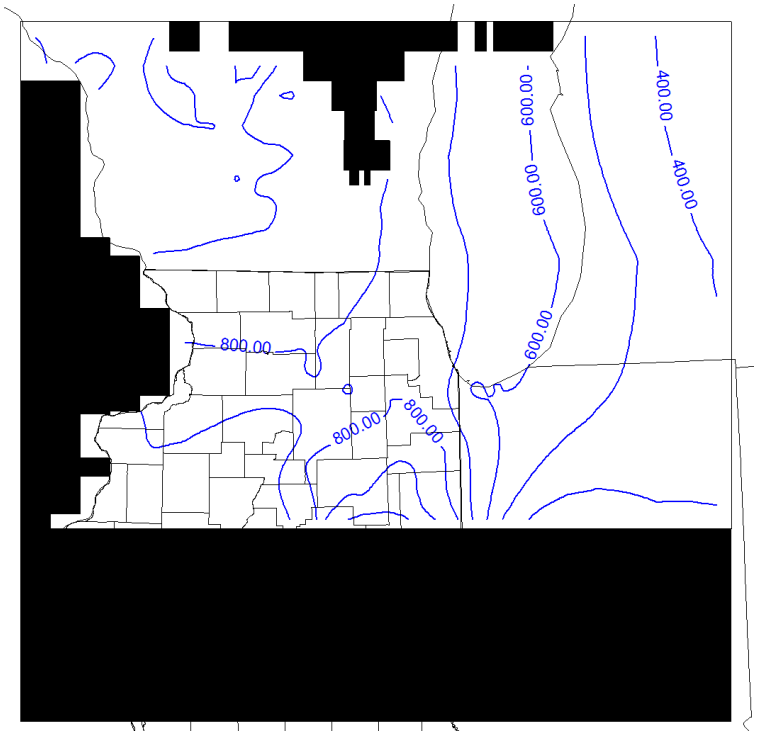

Figure 6.67: Heads at Bottom of Mt. Simon After 200 Years of Pumping (Heads in Feet Above msl). Base map modified from Meyer et al., 2009

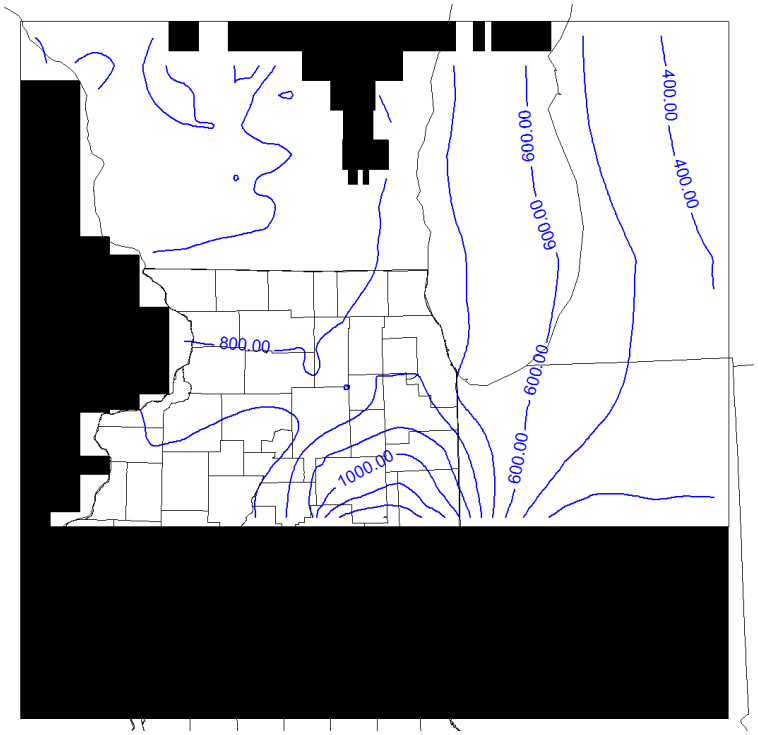

Figure 6.68: Heads at Bottom of Mt. Simon After 300 Years of Pumping (Heads in Feet Above msl). Base map modified from Meyer et al., 2009

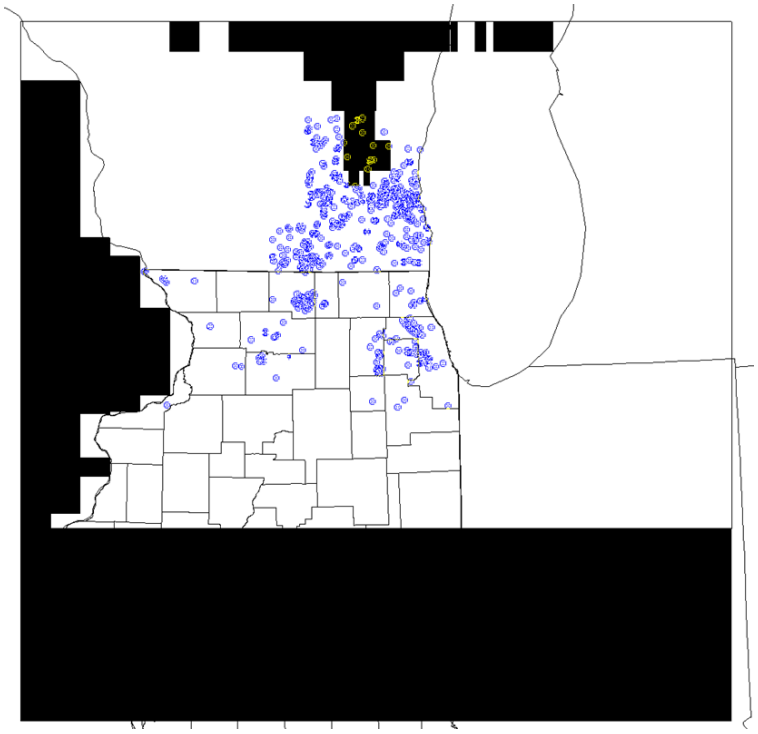

Figure 6.69: Location of Pumping Wells Open to the Mt. Simon Reservoir. Base map modified from Meyer et al., 2009

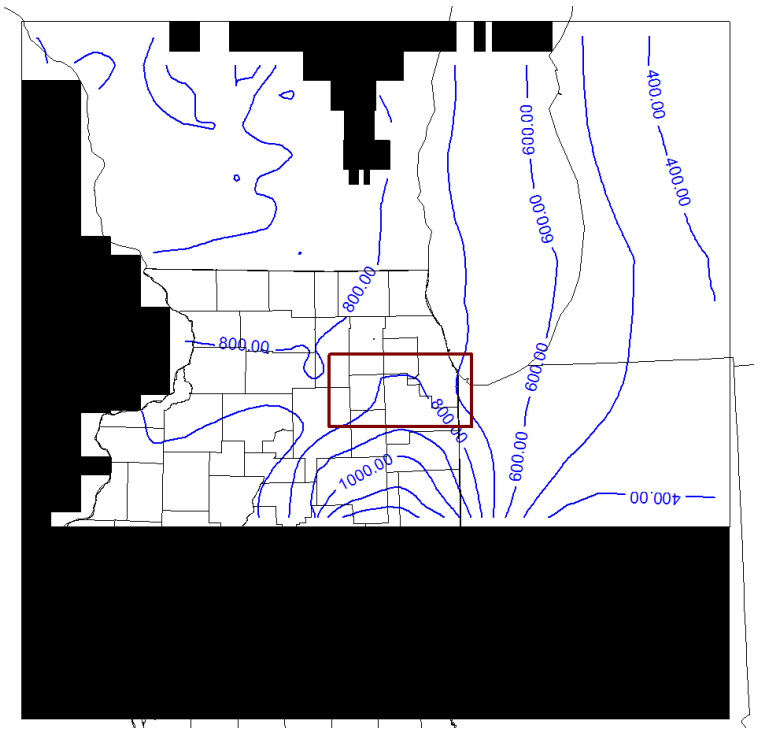

Figure 6.70: Maroon Box Outlining Net Flux Study Area. Base map modified from Meyer et al., 2009

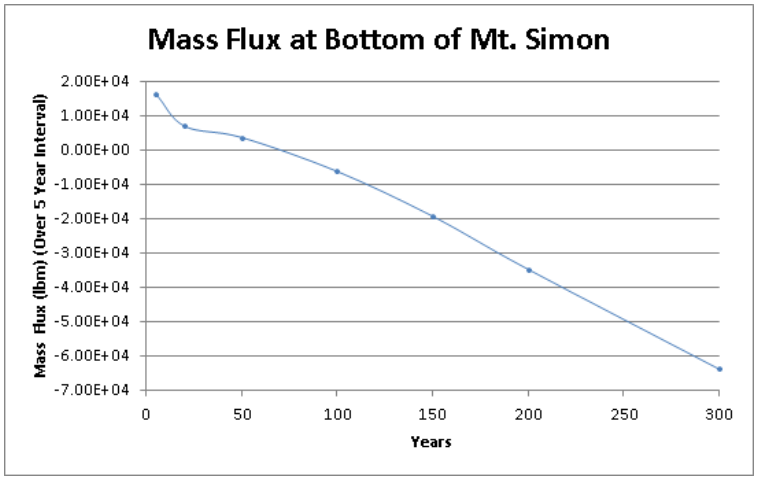

Figure 6.71: Net Flux in the Vertical Direction for a Section of the Mt. Simon

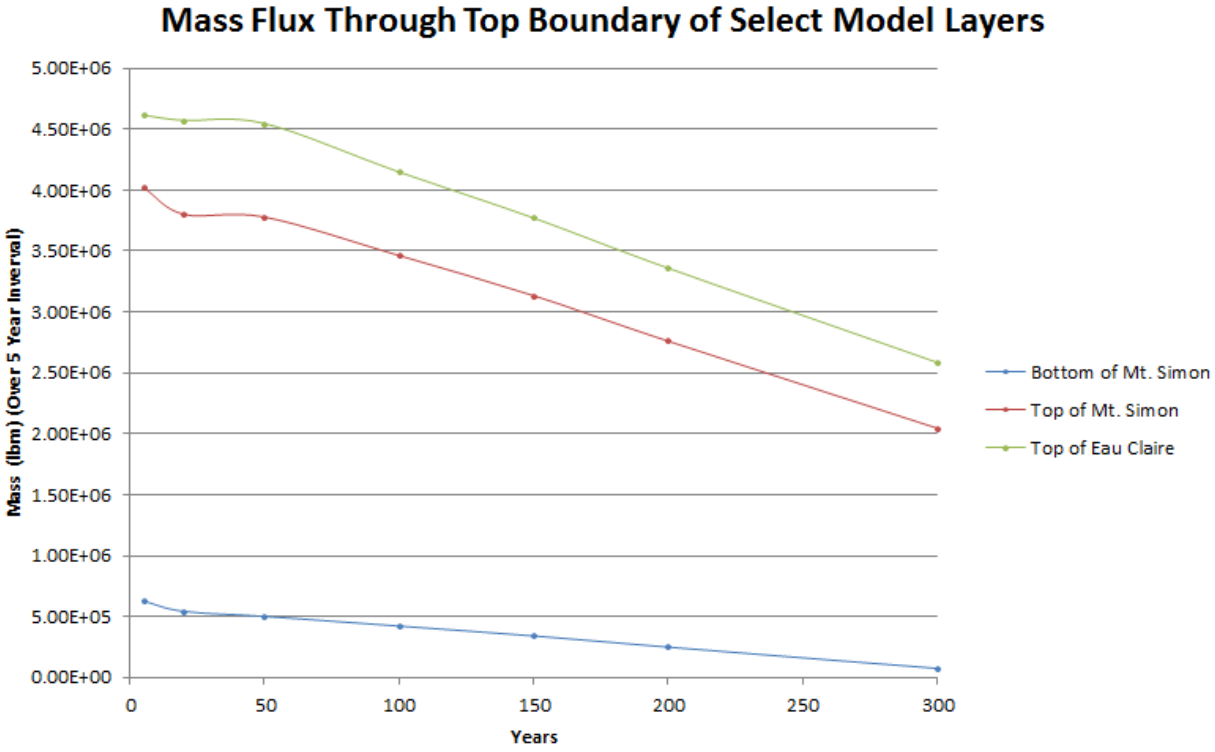

Figure 6.72: Mass Balance of Select Layers (Measured over 5 Yr Intervals)

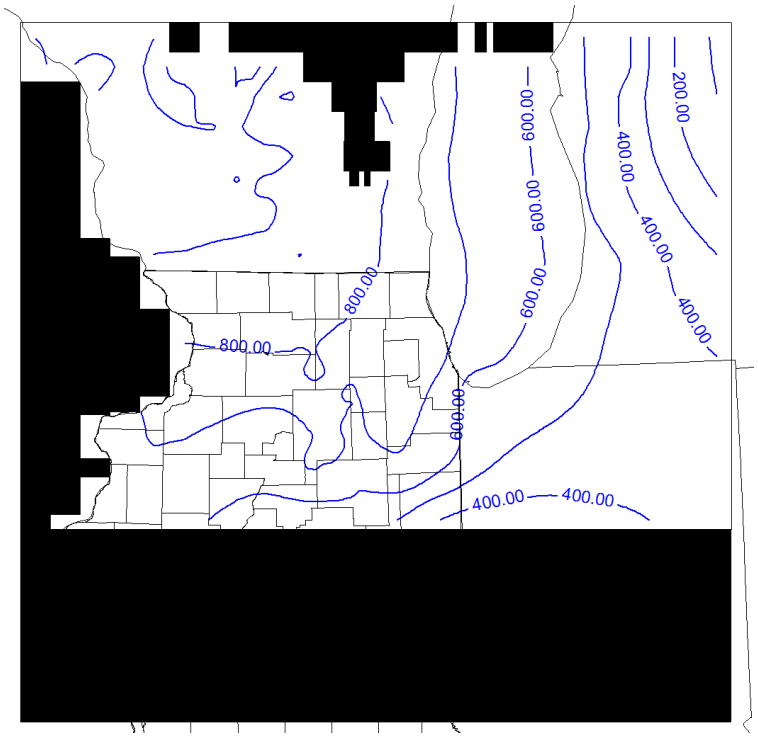

Figure 6.73: Heads at Top of Mt. Simon After 5 Years of Pumping (Heads in Feet Above msl). Base map modified from Meyer et al., 2009

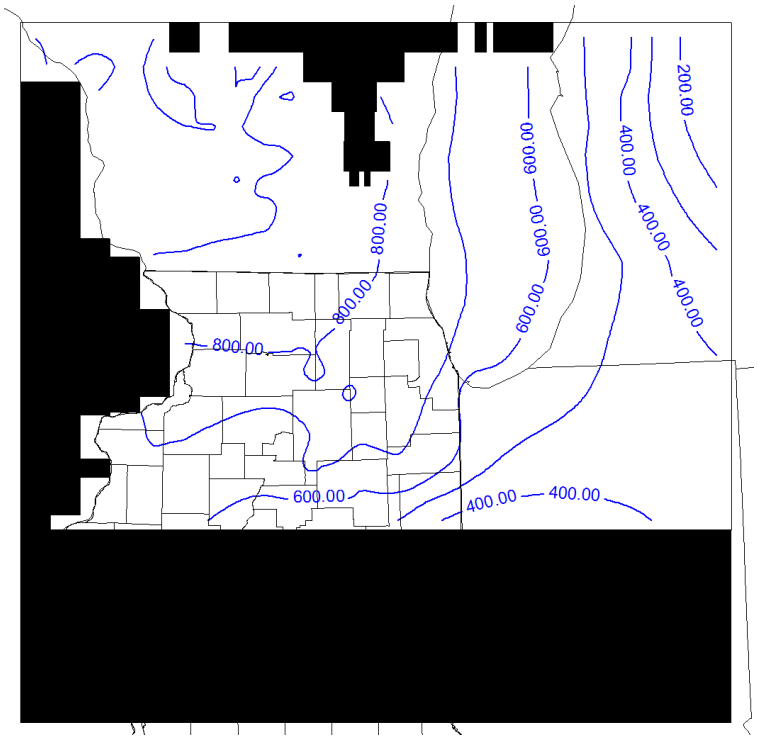

Figure 6.74: Heads at Top of Mt. Simon After 10 Years of Pumping (Heads in Feet Above msl). Base map modified from Meyer et al., 2009

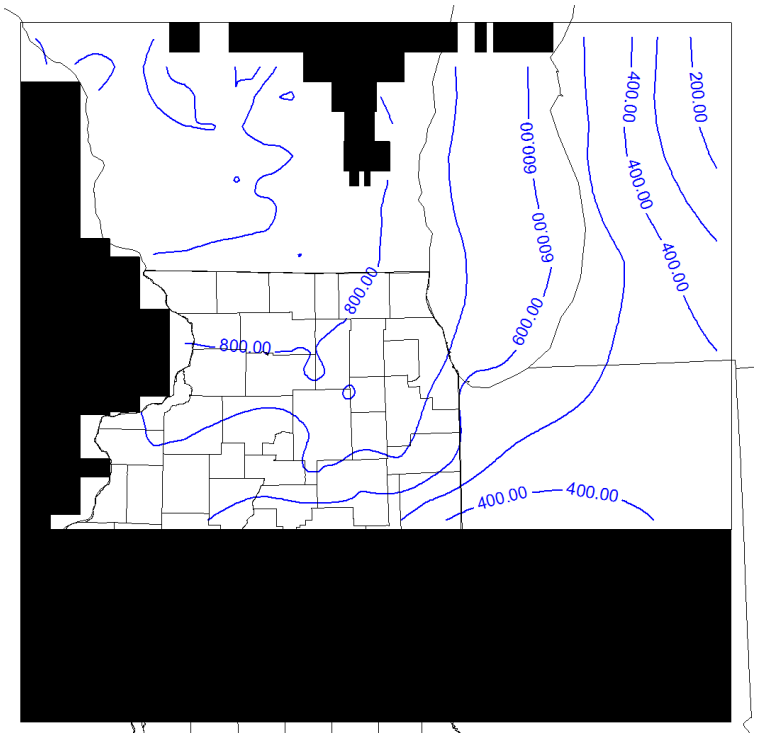

Figure 6.75: Heads at Top of Mt. Simon After 20 Years of Pumping (Heads in Feet Above msl). Base map modified from Meyer et al., 2009

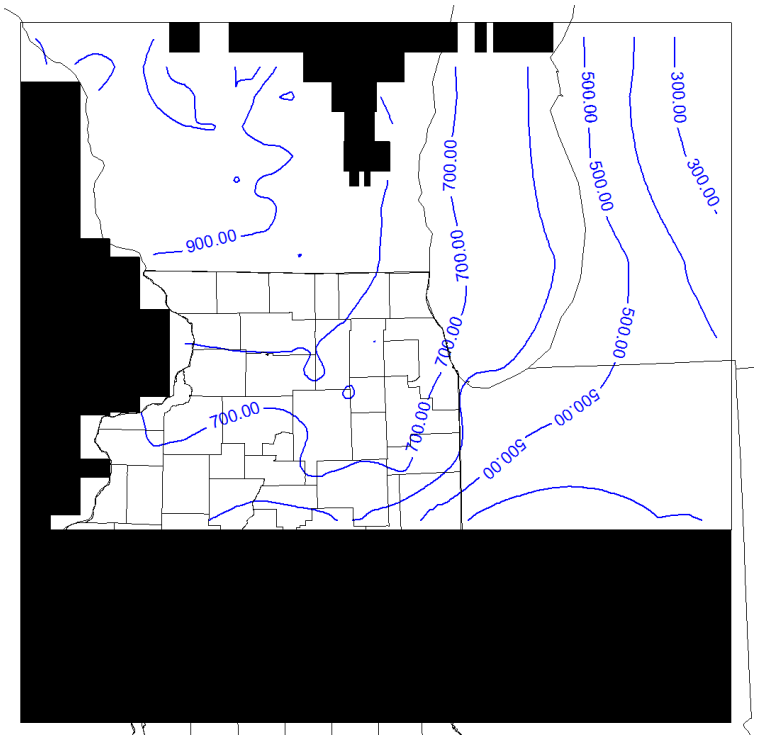

Figure 6.76: Heads at Top of Mt. Simon After 50 Years of Pumping (Heads in Feet Above msl). Base map modified from Meyer et al., 2009

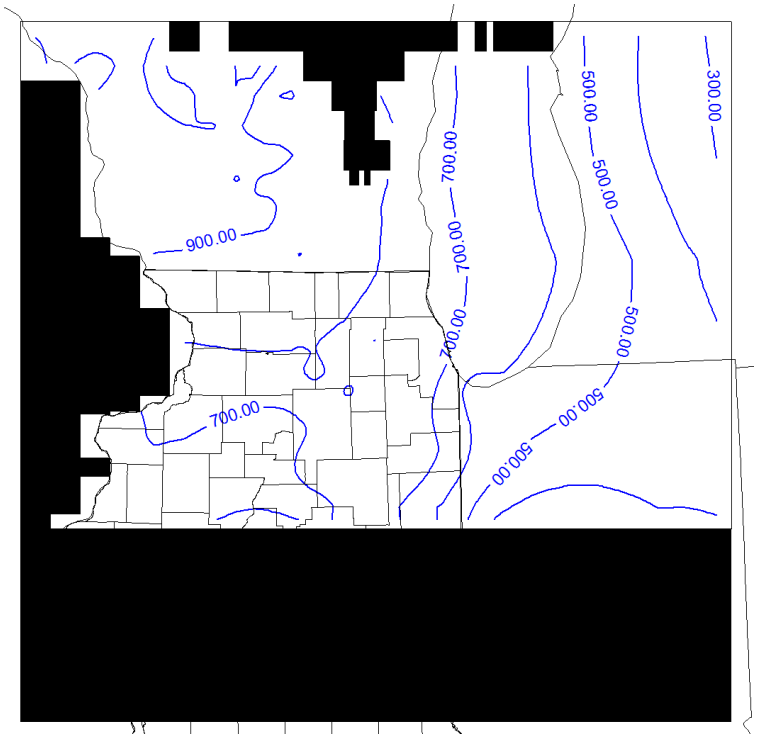

Figure 6.77: Heads at Top of Mt. Simon After 100 Years of Pumping (Heads in Feet Above msl). Base map modified from Meyer et al., 2009

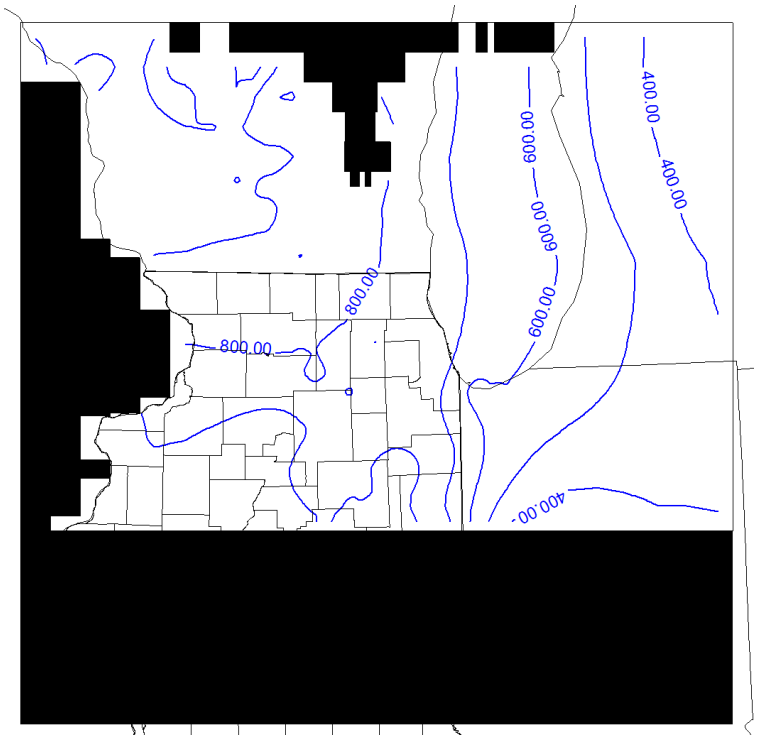

Figure 6.78: Heads at Top of Mt. Simon After 150 Years of Pumping (Heads in Feet Above msl). Base map modified from Meyer et al., 2009

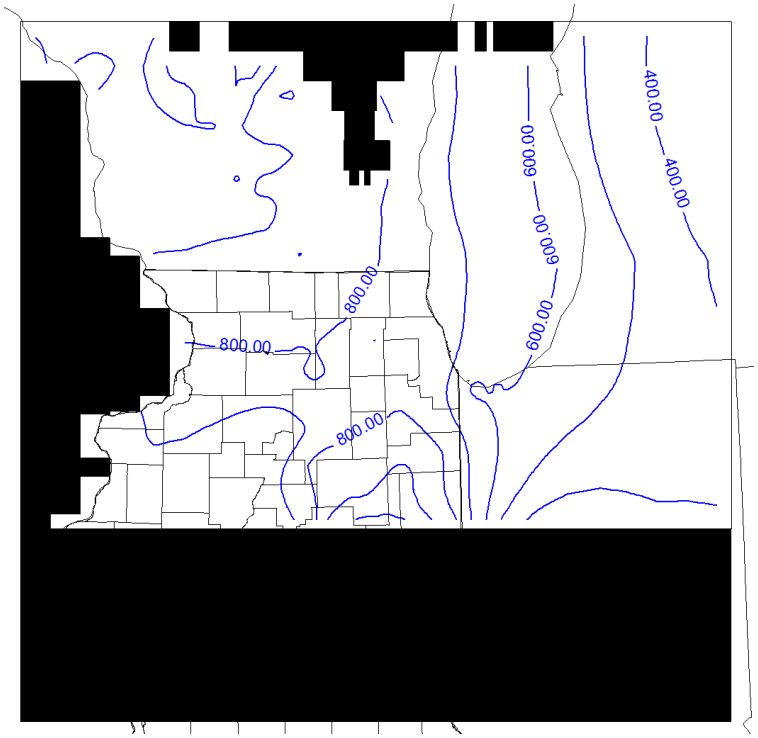

Figure 6.79: Heads at Top of Mt. Simon After 200 Years of Pumping (Heads in Feet Above msl). Base map modified from Meyer et al., 2009

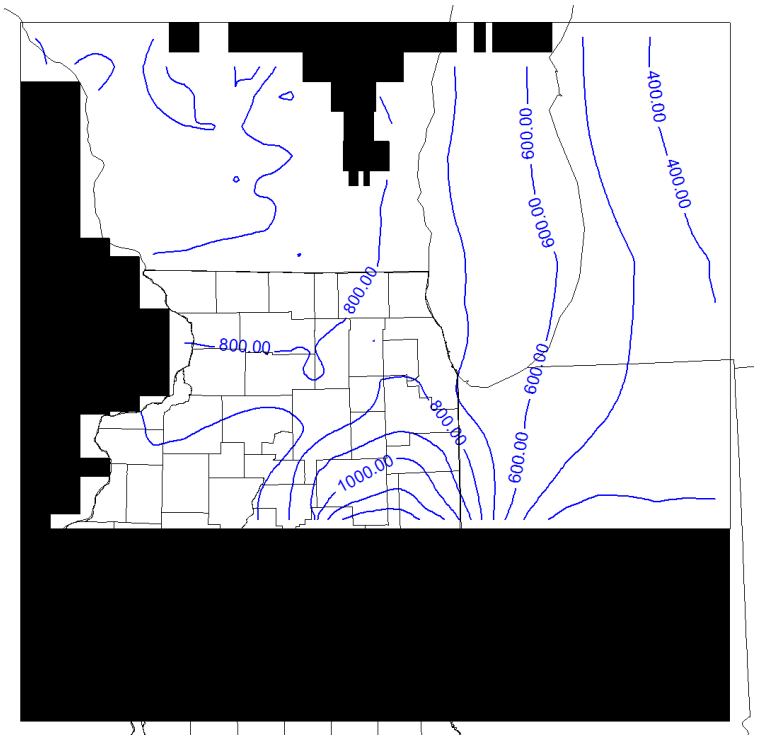

Figure 6.80: Heads at Top of Mt. Simon After 300 Years of Pumping (Heads in Feet Above msl). Base map modified from Meyer et al., 2009

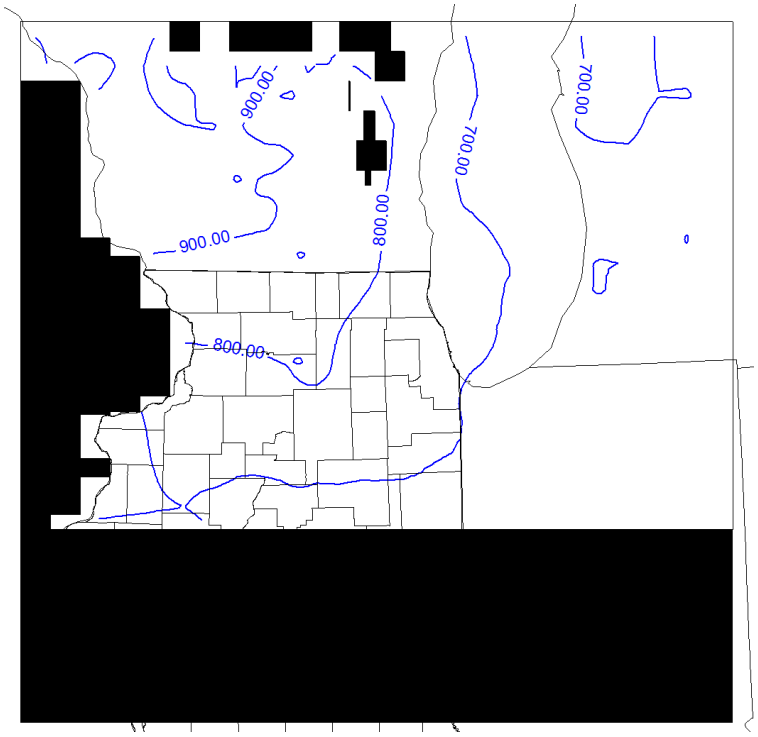

Figure 6.81: Heads at Top of Eau Claire After 5 Years of Pumping (Heads in Feet Above msl). Base map modified from Meyer et al., 2009

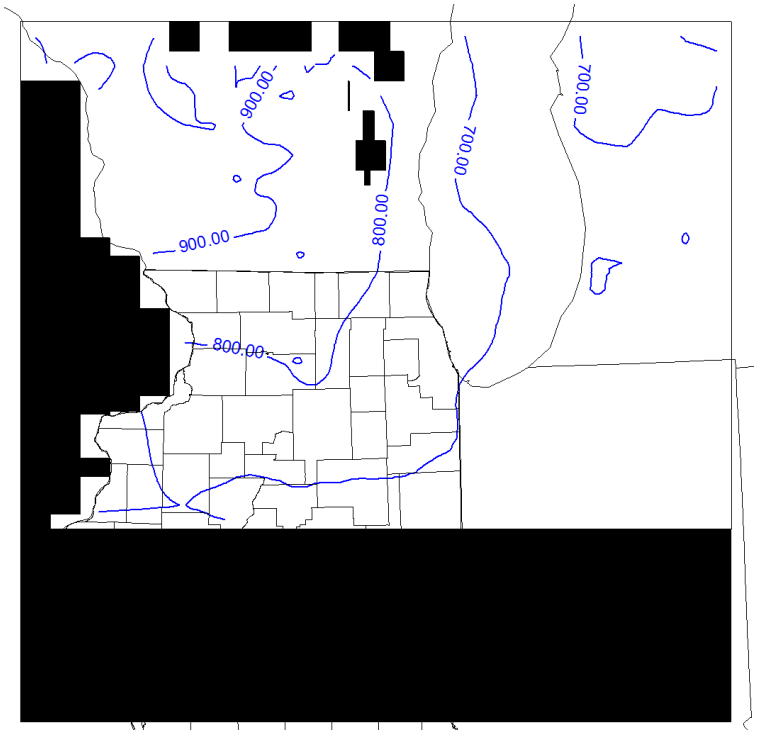

Figure 6.82: Heads at Top of Eau Claire After 10 Years of Pumping (Heads in Feet Above msl). Base map modified from Meyer et al., 2009

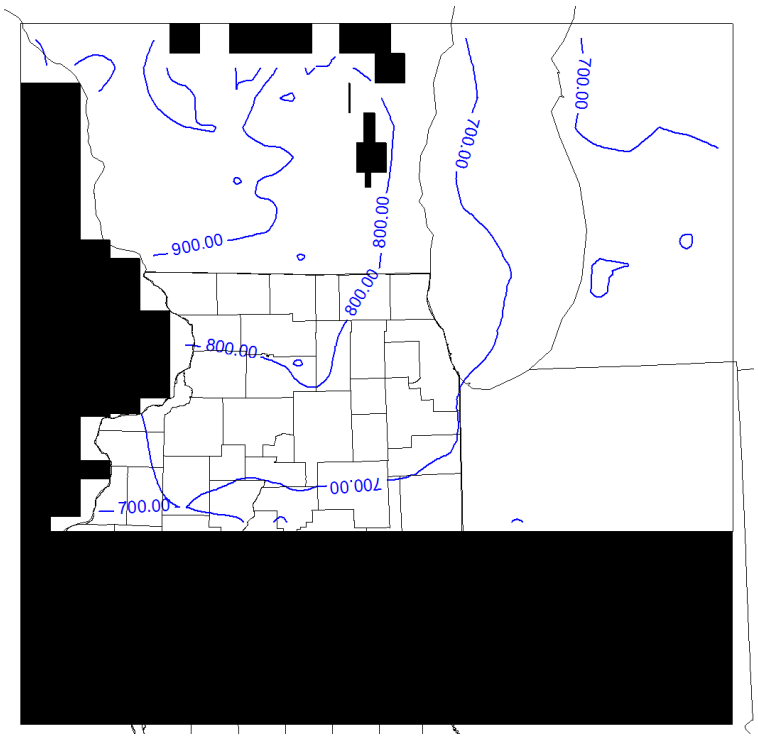

Figure 6.83: Heads at Top of Eau Claire After 20 Years of Pumping (Heads in Feet Above msl). Base map modified from Meyer et al., 2009

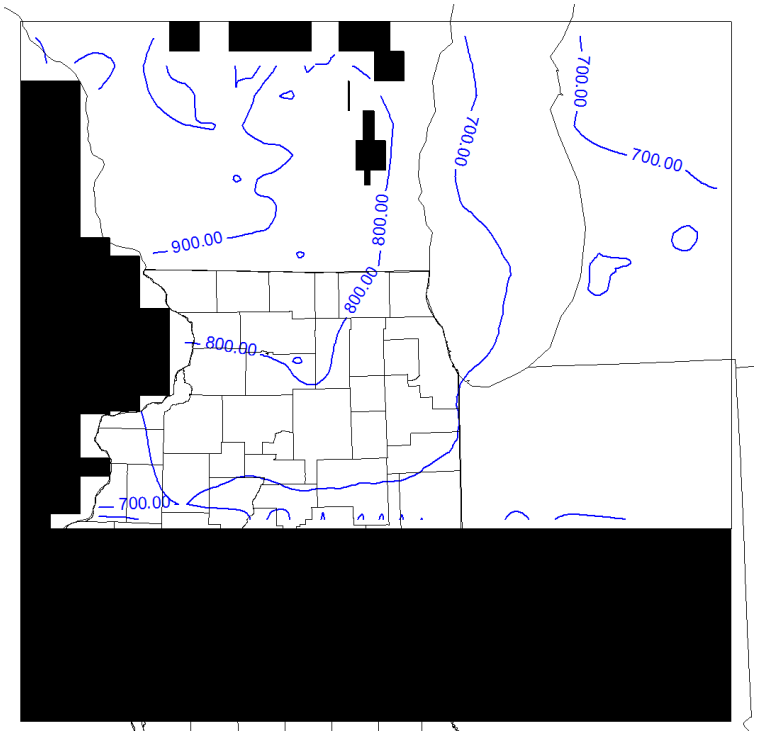

Figure 6.84: Heads at Top of Eau Claire After 50 Years of Pumping (Heads in Feet Above msl). Base map modified from Meyer et al., 2009

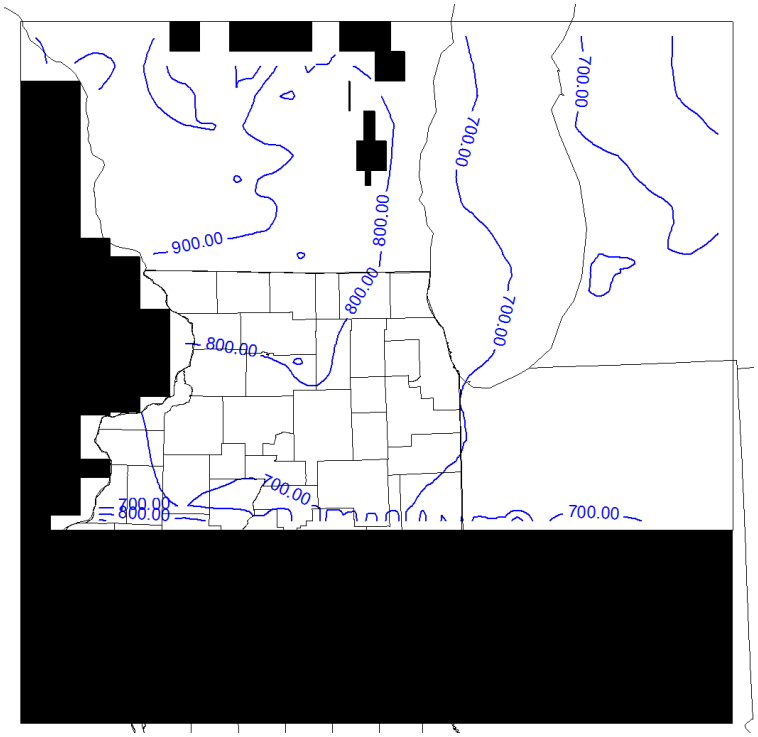

Figure 6.85: Heads at Top of Eau Claire After 100 Years of Pumping (Heads in Feet Above msl). Base map modified from Meyer et al., 2009

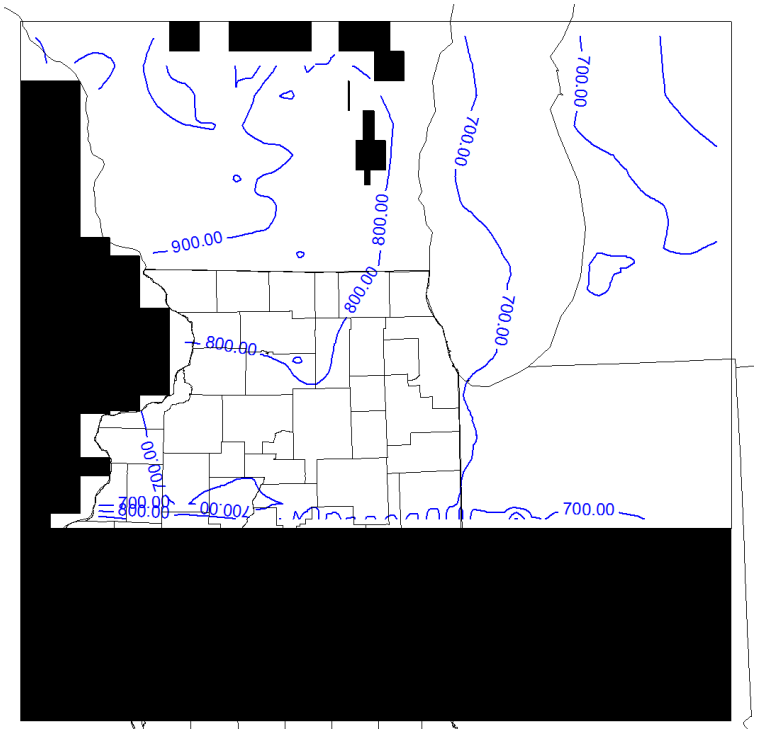

Figure 6.86: Heads at Top of Eau Claire After 150 Years of Pumping (Heads in Feet Above msl). Base map modified from Meyer et al., 2009

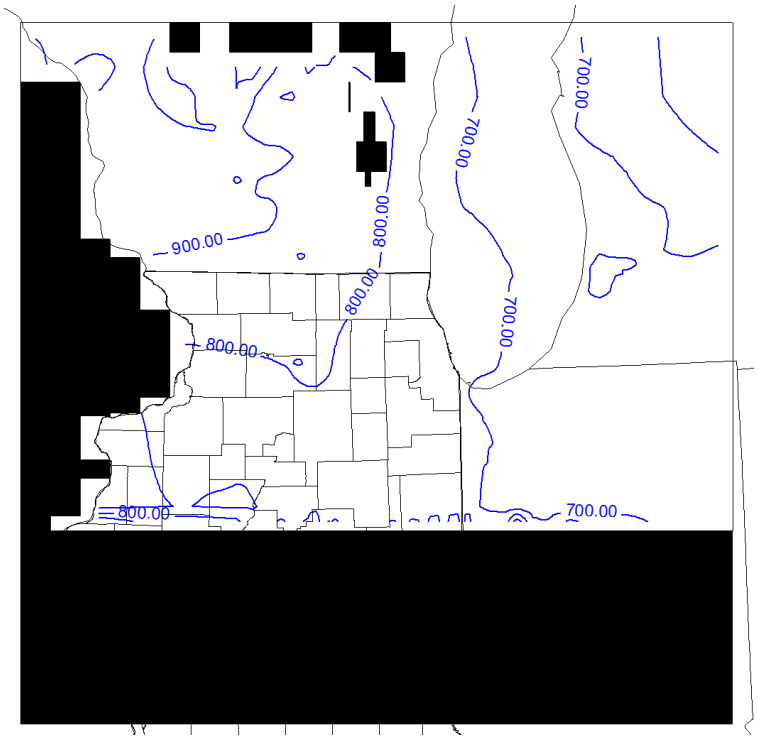

Figure 6.87: Heads at Top of Eau Claire After 200 Years of Pumping (Heads in Feet Above msl). Base map modified from Meyer et al., 2009

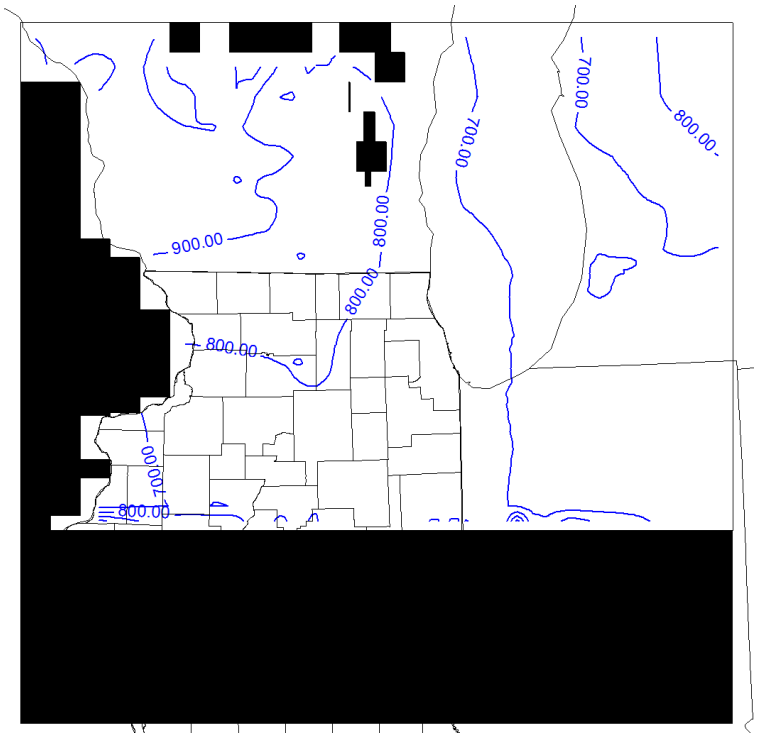

Figure 6.88: Heads at Top of Eau Claire After 300 Years of Pumping (Heads in Feet Above msl). Base map modified from Meyer et al., 2009

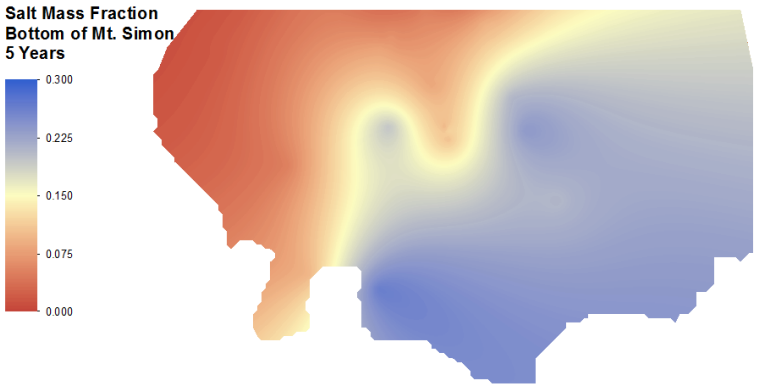

Figure 6.89: Salt Mass Fraction at Bottom of Mt. Simon after 5 Years of Pumping

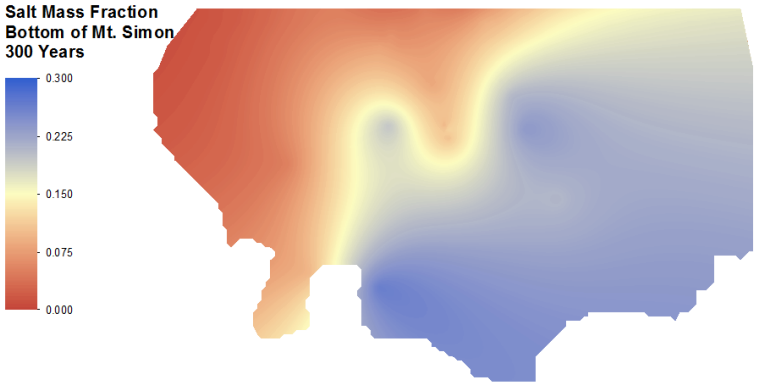

Figure 6.90: Salt Mass Fraction at Bottom of Mt. Simon after 300 Years of Pumping

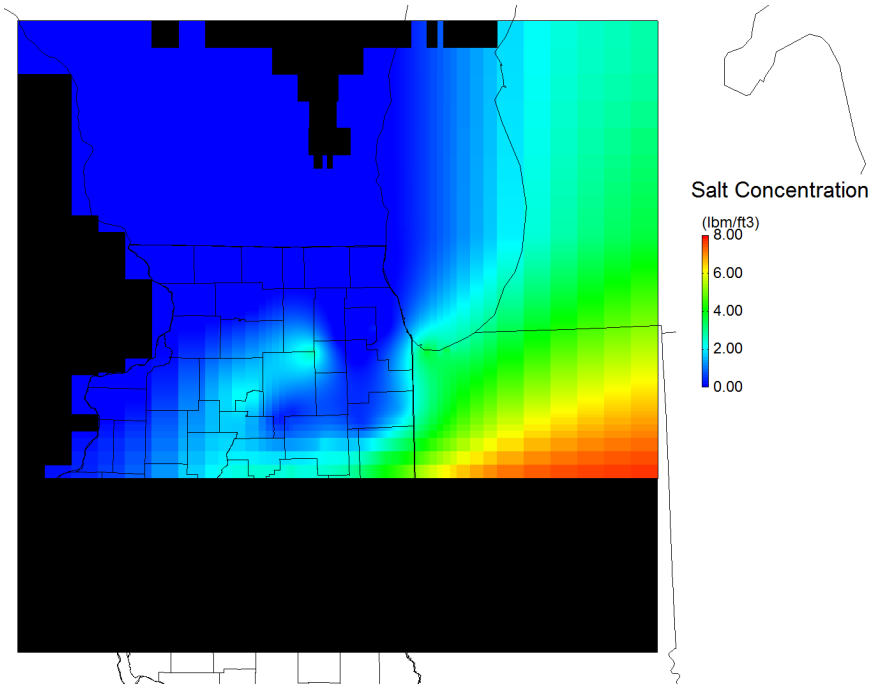

Figure 6.91: Salt Concentrations at Bottom of Mt. Simon After 5 Years of Pumping. Base map modified from Meyer et al., 2009

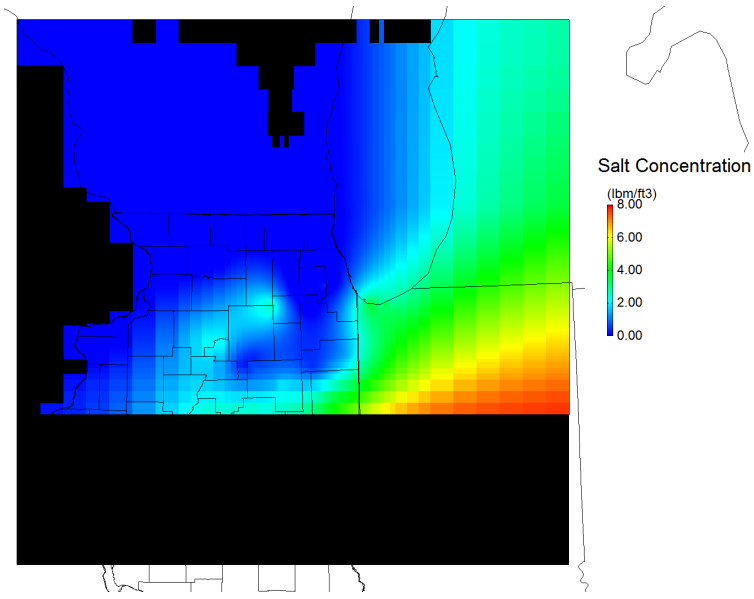

Figure 6.92: Salt Concentrations at Bottom of Mt. Simon After 200 Years of Pumping. Base map modified from Meyer et al., 2009

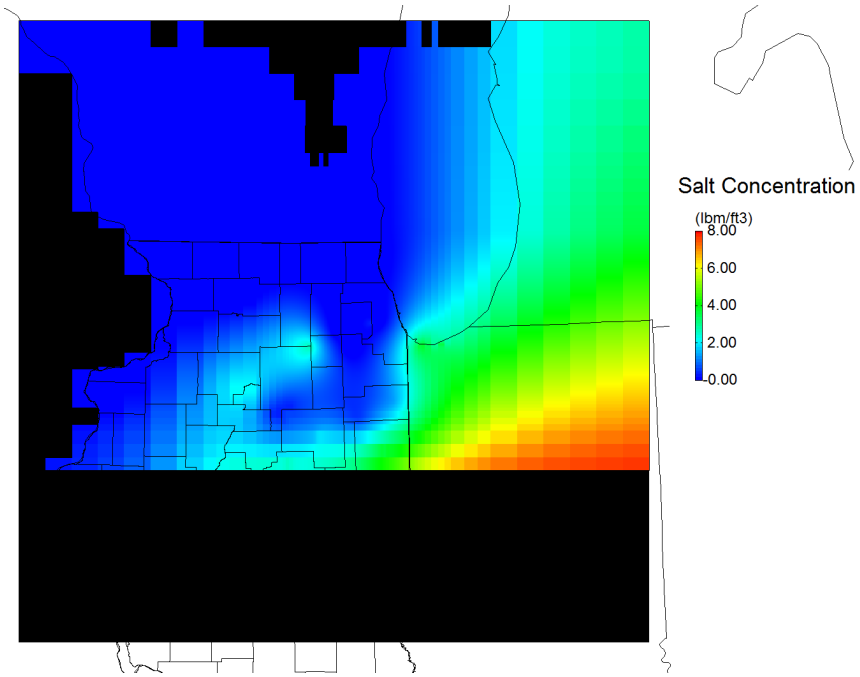

Figure 6.93: Salt Concentrations at Bottom of Mt. Simon After 300 Years of Pumping. Base map modified from Meyer et al., 2009

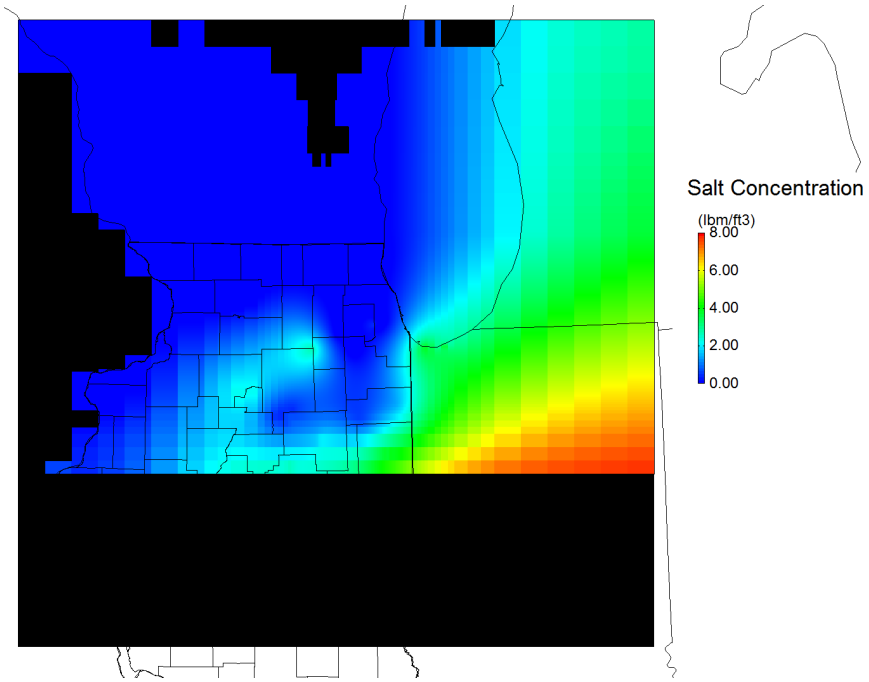

Figure 6.94: Salt Concentrations at Top of Mt. Simon After 5 Years of Pumping. Base map modified from Meyer et al., 2009

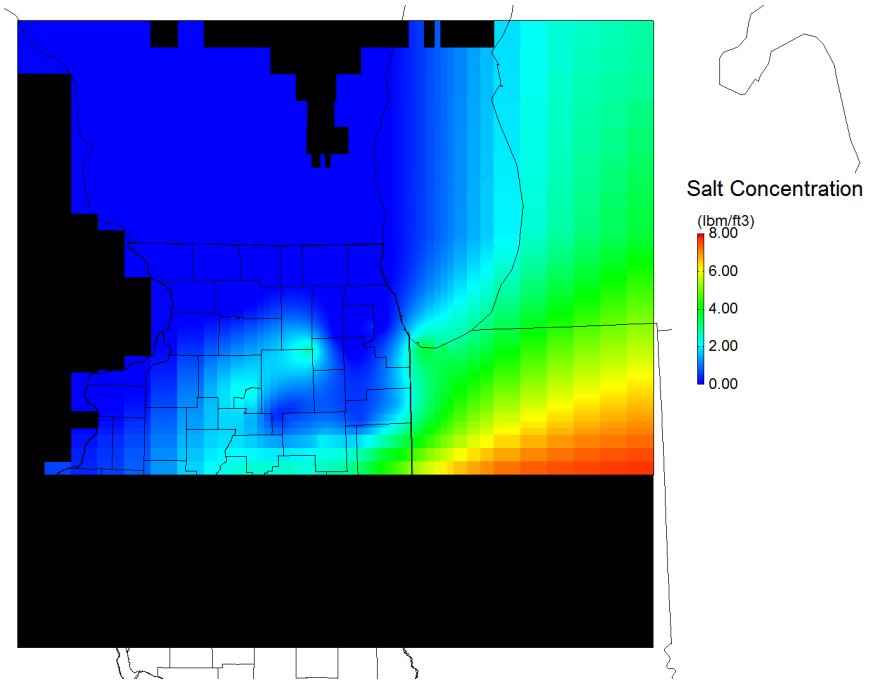

Figure 6.95: Salt Concentrations at Top of Mt. Simon After 200 Years of Pumping. Base map modified from Meyer et al., 2009

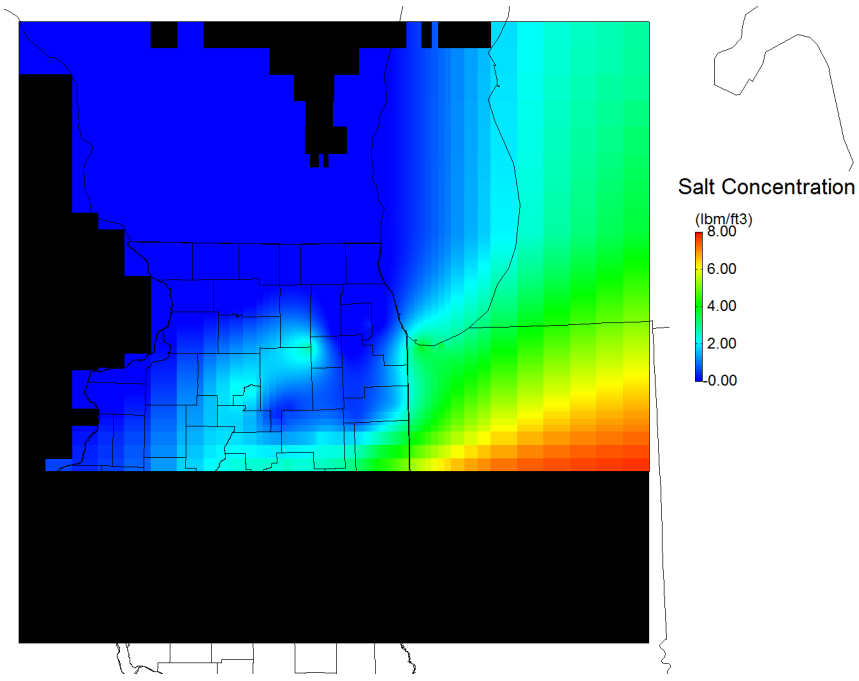

Figure 6.96: Salt Concentrations at Top of Mt. Simon After 300 Years of Pumping. Base map modified from Meyer et al., 2009

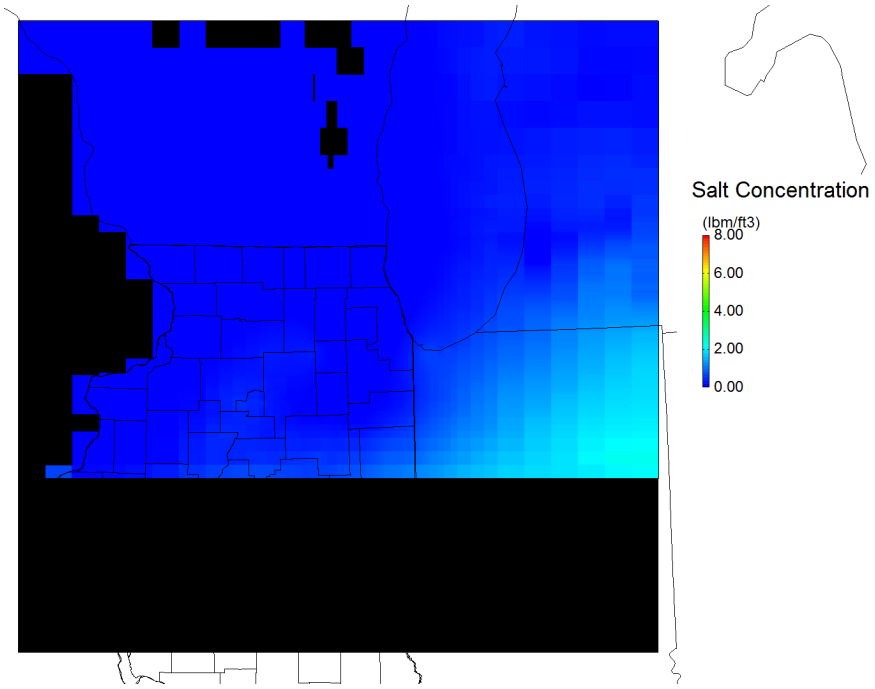

Figure 6.97: Salt Concentrations at Top of Eau Claire After 5 Years of Pumping. Base map modified from Meyer et al., 2009

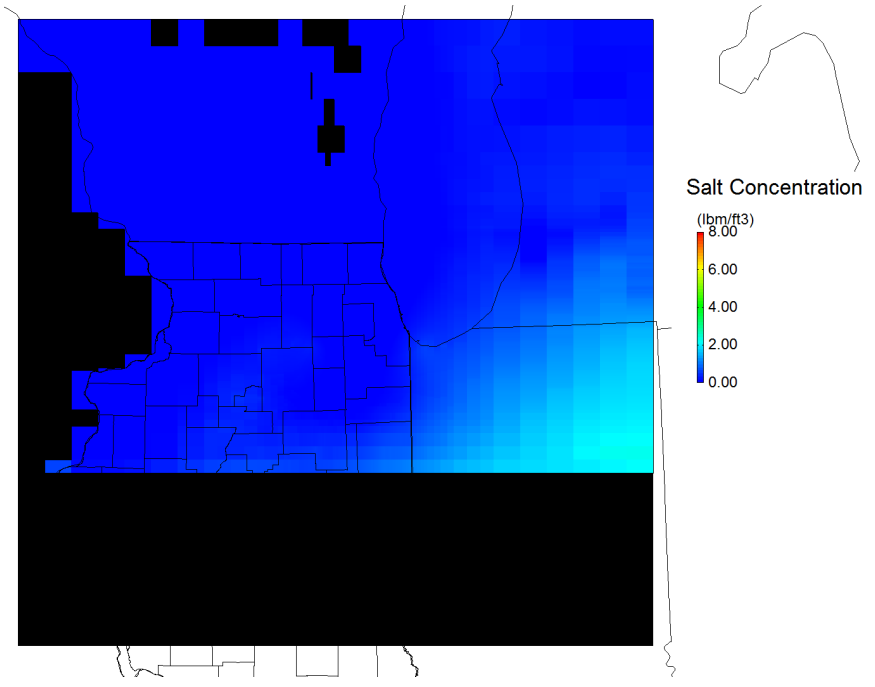

Figure 6.98: Salt Concentrations at Top of Eau Claire After 200 Years of Pumping. Base map modified from Meyer et al., 2009

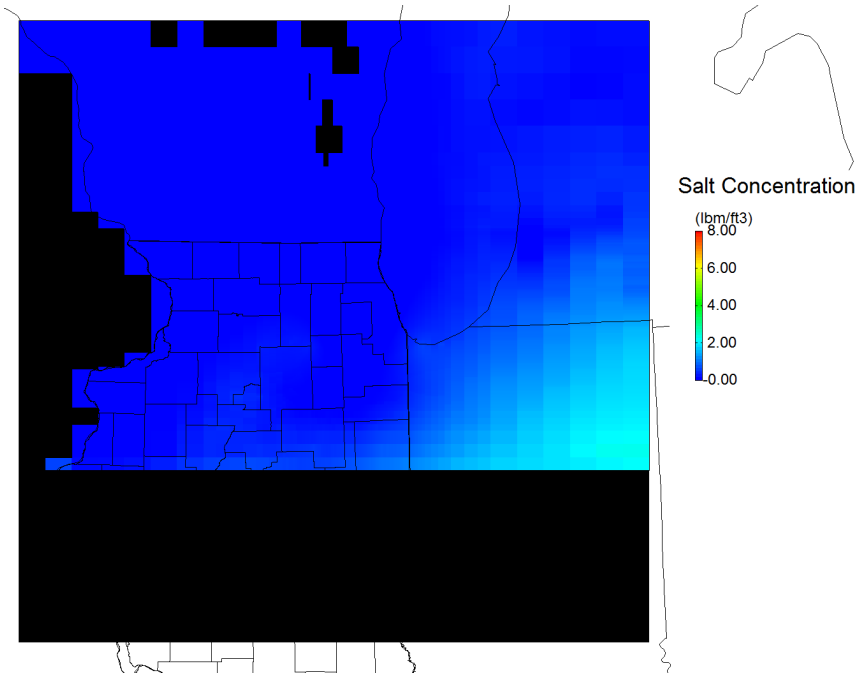

Figure 6.99: Salt Concentrations at Top of Eau Claire After 300 Years of Pumping. Base map modified from Meyer et al., 2009

APPENDIX

The pseudocode in this Appendix is given to provide a more thorough explanation of the details of the linking scheme. All formatting is done in a manner consistent with code written in the Python programming language. Arrows, such as in line 12, indicate that the line is too long for the page and continues below.

```
1  import modules
2
3  obtain working directory path from user
4
5  read user supplied input file:
6          read SEAWAT file base name
7          read number of rows, columns, and layers
8          read x and y offsets for SEAWAT
9          read reference density value
10         read density-concentration slope
11         read list of SEAWAT packages used (excluding CHD, SSM)
12         read locations of SEAWAT files containing package ↩
              information for all stress periods
13         read row/column number of SEAWAT exterior boundary ↩
              rows/column
14         read row/column number of SEAWAT interior boundary ↩
              rows/column
```

```
15          read location of .bas file for cell type information
16          read location of .dis file for discritization
17          read TOUGH2 exterior boundary node list
18          read TOUGH2 interior boundary node list
19          read location of TOUGH2 MESH file
20          read stress period discretization information with ↩
               TOUGH2 injection data
21
22  read TOUGH2 MESH:
23          T2_MESH dictionary[element names]= xyz locations
24          T2_MESH_rev dictionary[xyz locations]=element names
25
26  read .bas file:
27          create array of boundary cell types
28
29  read .dis file:
30          calculate cell location using x and y offsets
31          # create exterior and interior boundary cell ↩
               dictionaries
32          SW_ext dictionary[row, column, layer]= x,y,z
33          SW_int dictionary[row, column, layer]= x,y,z
34
35  T2_bound_SW dictionary[T2 boundary element names]= SEAWAT ↩
       boundary row, column, layer values
36  SW_bound_T2 dictionary[SEAWAT boundary row, column, layer ↩
       values]= T2 boundary element names
37
38  for i in number of stress periods:
```

```
39          current stress period = i + 1  #account for 0 indexing
40
41          calculate starting and ending times
42
43          create directory for new TOUGH2 stress period
44
45          read TOUGH2 INCON file:
46                  TOUGH2-INCON dictionary[boundary element ↩
                       names]= primary variables
47
48          if current stress period not equal to 1:
49                  read targpest.out file:
50                          # results must be in a known order: ↩
                               beginning at lowest row/column ↩
                               value in top layer,
51                          # progressing to highest row/column ↩
                               value before moving to next layer ↩
                               and repeating
52                          create array of locations, head values
53                          create array of locations, ↩
                               concentration values
54
55                  create empty SW-results dictionary
56                  # Convert SEAWAT output to TOUGH2 input
57                  for entry in head value array:
58                          density = reference density + ↩
                               (density-concentration slope * ↩
                               concentration)
```

```
59                  pressure = gravity * (head - x ↩
                       location) * density
60                  temperature = temperature value from ↩
                       TOUGH2-INCON dictionary
61                  salt mass fraction = salt mass ↩
                       fraction value from TOUGH2-INCON ↩
                       dictionary
62                  while pressure_difference > tol:
63                          new_density = F(temperature, ↩
                               salt mass fraction, density)
64                          new_pressure=gravity * (head ↩
                               - x location) * new_density
65                          pressure_difference = ↩
                               new_pressure - pressure
66                          adjust salt mass fraction ↩
                               estimate based on ↩
                               pressure difference
67                          density = new_density
68                  add element name with salt mass ↩
                       fraction and pressure values to ↩
                       SW-results dictionary
69
70              rewrite TOUGH2 input file using new times, ↩
                   new injection rates
71              rewrite SAVE file, using new pressure and ↩
                   salt mass fraction values, rename INCON
72              copy into new directory necessary ↩
                   user-prepared files
```

```
73          else:
74                  copy all user-prepared files into new T2 directory
75
76          if current stress period not equal to 1:
77                  move old SEAWAT results files into old SEAWAT directory
78
79          launch TOUGH2 executable, wait for termination
80
81          launch ext.exe to extract results, wait for termination
82
83          create empty TOUGH-results dictionary
84          read ext.exe output file:
85                  add each entry to TOUGH-results dictionary
86
87          create directory for old SEAWAT files and copy them into it
88
89          # Convert TOUGH2 output to SEAWAT input
90          for entry in list of SEAWAT packages:
91                  write new file using data from file containing data for all stress periods
92
93          # Write ssm and chd files
94          for SW_key in SW_ext dictionary:
95                  # ssm file
96                  TOUGH_key=SW_bound_T2 dictionary[SW_key]
```

```
97              salt mass fraction = TOUGH-results ↩
                   dictionary[TOUGH_key]
98              calculate density with salt mass fraction value
99              convert density results to english units
100             density=(density - reference density) / ↩
                   density-concentration slope
101             write line for SW_key with calculated ↩
                   density value
102
103             # chd file
104             pressure = TOUGH-results dictionary[TOUGH_key]
105             elevation = T2_MESH dictionary[TOUGH_key]
106             head = (pressure / (gravity * density_SI)) + ↩
                   elevation
107             convert head to english units
108             write line for SW_key with calculated head ↩
                   value
109
110         launch SEAWAT, wait for termination
111
112         move starting .UCN file into old directory
113
114         # old.UCN is name of starting concentrations in each ↩
               run
115         run savelast to extract last concentration values at ↩
               last step, name old.UCN
116
117         run targpest to extract desired head and ↩
```

```
            concentration values
118
119 create directory for files of the final SEAWAT run
120 move input files from last SEAWAT run into final stress ↩
    period's directory
121 copy results from last SEAWAT fun into final stress period's ↩
    directory
```

REFERENCES

[1] R. H. Socolow and S. W. Pacala, "A Plan to Keep Carbon in Check." *Scientific American*, vol. 295, no. 3, pp. 50 – 57, 2006. [Online]. Available: http://search.ebscohost.com.proxy2.library.illinois.edu/login.aspx?direct=true&db=aph&AN=21847999&site=ehost-live

[2] W. S. Han, B. J. McPherson, P. C. Lichtner, and F. P. Wang, "Evaluation of Trapping Mechanisms in Geologic CO2 Sequestration: Case Study of SACROC Northern Platform, a 35-Year CO2 Injection Site," *American Journal of Science*, vol. 310, pp. 282–324, April 2010.

[3] M. G. S. Consortium, "Geology of Deep Saline Sequestration," 2011, Midwest Geological Sequestration Consortium. [Online]. Available: http://sequestration.org/science/geologyofdeepsaline.html

[4] U. D. of Energy (USDOE), "United States Carbon Utilization and Storage Atlas (Atlas IV)," National Energy Technology Laboratory, Pittsburgh, PA, USA, Tech. Rep. 4th ed., 2012.

[5] M. A. Celia and J. M. Nordbotten, "Practical Modeling Approaches for Geological Storage of Carbon Dioxide," *Ground Water*, vol. 47, no. 5, pp. 627–638, 2009. [Online]. Available: http://dx.doi.org/10.1111/j.1745-6584.2009.00590.x

[6] K. Pruess, C. Oldenburg, and G. Moridis, *TOUGH2 User's Guide, Version 2*, Earth Sciences Division, Lawrence Berkeley National Laboratory, University of California, Berkeley, California 94720, September 2012.

[7] W. Guo and C. D. Langevin, *User's Guide to SEAWAT: A Computer Program for Simulation of Three-Dimensional Variable-Density Ground-Water Flow*, United States Geological Survey, 2002.

[8] C. D. Langeivn, W. B. Shoemaker, and W. Guo, *MODFLOW-2000, the U.S. Geological Survey Modular Ground-Water Model - Documentation of the SEAWAT-2000 Version with the Variable-Density Flow Process (VDF) and the Integrated MT3DMS Transport Process (IMT)*, United State Geological Survey, 2003.

[9] M. Karsten, S. Varma, and E. Bekele, "Challenges of modelling the impact of multi-purpose aquifer utilization on variable-density groundwater flow." *Les Rencontres scientifiques d'IFP Energies nouvelles*, 2011.

[10] E. A. Baidariko and S. P. Pozdniakov, "Simulation of Liquid Waste Buoyancy in a Deep Heterogeneous Aquifer," *Water Resources*, vol. 38, pp. 544–554, 2011.

[11] M. Sophocleous and S. P. Perkins, "Methodology and application of combined watershed and ground-water models in Kansas," *Journal of Hydrology*, vol. 236, pp. 185–201, 2000.

[12] N. W. Kim, I. M. Chung, Y. S. Won, and J. G. Arnold, "Development and application of the integrated SWAT-MODFLOW model," *Journal of Hydrology*, vol. 356, no. 1-2, pp. 1 – 16, 2008. [Online]. Available: http://www.sciencedirect.com/science/article/pii/S0022169408000991

[13] L. Galbiati, F. Bouraoui, F. Elorza, and G. Bidoglio, "Modeling diffuse pollution loading into a Mediterranean lagoon: Development and application of an integrated surface-subsurface model tool," *Ecological Modelling*, vol. 193, no. 1-2, pp. 4 – 18, 2006. [Online]. Available: http://www.sciencedirect.com/science/article/pii/S0304380005004539

[14] J. O. Rumbaugh and D. B. Rumbaugh, *Guide to Using Groundwater Vistas*, version 6 ed., Environmental Simulations Inc., P.O. Box 156, Reihnolds, PA, 17569.

[15] M. C. Hill and C. R. Tiedeman, *Effective Groundwater Model Calibration: With Analysis of Data, Sensitivities, Predictions, and Uncertainty.* Wiley-Interscience, 2007.

[16] J. Doherty, *PEST: Model-Independent Parameter Estimation*, 5th ed., Watermark Numerical Computing, July 2004.

[17] D. Feinstein, T. Eaton, D. Hart, J. Krohelski, and K. Bradbury, "Regional Aquifer Model for Southeastern Wisconsin; Report 1: Data Collection, Conceptual Model Development, Numerical Model Construction, and Model Calibration," U.S. Geological Survey, Tech. Rep., 2005.

[18] U. E. I. Administration, "Underground Natural Gas Storage," http://www.eia.gov/pub/oil_gas/natural_gas/analysis_publications/ngpipeline/undrgrnd_storage.html, U.S. Energy Information Administration.

[19] L. E. Yoksoulian, J. T. Freiburg, S. K. Butler, P. M. Berger, and W. R. Roy, "Mineralogical alterations during laboratory-scale carbon sequestration experiments for the Illinois Basin," *Energy Procedia*, vol. 37, no. 0, pp. 5601–5611, 2013.

[20] L. B. N. L. E. S. Division, "TOUGH: Suite of Simulators for Nonisothermal Multiphase Flow and Transport in Fractured Porous Media," August 2013, Lawrence Berkeley National Laboratory. [Online]. Available: http://esd.lbl.gov/research/projects/tough/

[21] E. Mehnert and P. Weberling, "Groundwater Salinity within the Mt. Simon Sandstone in Illinois and Indiana," illinois State Geological Survey Circular, in review.

[22] A. P. Visocky, M. G. Sherrill, and K. Cartwright, "Geology, Hydrology, and Water Quality of the Cambrian and Ordovician Systems in Northern Illinois," Illinois State Geological Survey, Champaign, IL, Tech. Rep., 1985, in cooperation with the United States Geological Survey.

[23] Q. Zhou, J. T. Birkholzer, E. Mehnert, Y.-F. Lin, and K. Zhang, "Modeling Basin- and Plume-Scale Processes of CO2 Storage for Full-Scale Deployment," *Ground Water*, vol. 48, no. 4, pp. 494–514, 2010. [Online]. Available: http://dx.doi.org/10.1111/j.1745-6584.2009.00657.x

[24] M. T. Van Genuchten, "A Closed-form Equation for Predicting the Hydraulic Conductivity of Unsaturated Soils," *Soil Science Society of America Journal*, vol. 44, pp. 892–898, 1980.

[25] S. Meyer, G. Roadcap, Y. Lin, and D. Walker, "Simulation of Groundwater Flow in Kane County and Northeastern Illinois," Ilinois State Water Survey, Tech. Rep., 2009.

[26] B. Dziegielewski, X. Yang, T. Bik, and M. Richey, "County-Level Forecasts of Water Use in Illinois: 2005-2025," Southern Illinois University Carbondale, Department of Geography, Tech. Rep., 2005.

[27] J. L. J. Haas, "Physical Properties of the Coexisting Phases and Thermochemical Properties of the H_20 Component in Boiling NaCL Solutions," *Geological Survey Bulletin*, vol. 1421-A, 1976.

[28] C. Zheng and G. D. Bennet, *Applied Contaminant Transport Modeling.* Van Nostrand Reinhold, 1995.

[29] Midwest Geological Sequestration Consortium (MGSC), "Thickness of the Mt. Simon Sandstone in the Illinois Basin [map]," December 2005, http://sequestration.org/resources/publish/saline_thick_map_dec05.pdf, scale 1:1,000,000.

[30] Midwest Geological Sequestration Consortium (MGSC), "Salinity of the Mt. Simon Sandstone in the Illinois Basin [map]," December 2005, http://sequestration.org/resources/publish/saline_salinity_map_dec05.pdf, scale 1:1,000,000.